Utilizing interspecies comparisons between *Toxoplasma gondii* and *Hammondia hammondi* to elucidate mechanisms driving life stage development, life cycle flexibility, and pathogenesis

by

Sarah Louise Sokol Borrelli

Bachelor of Science in Honors, Seton Hill University, 2015

Submitted to the Graduate Faculty of the

Dietrich School of Arts and Sciences in partial fulfillment

of the requirements for the degree of

Doctor of Philosophy

University of Pittsburgh

2021

UNIVERSITY OF PITTSBURGH

DIETRICH SCHOOL OF ARTS AND SCIENCES

This dissertation was presented

by

Sarah Louise Sokol Borrelli

It was defended on

July 7, 2021

and approved by

Andrea Berman PhD, Associate Professor, Department of Biological Sciences

Anne Carlson PhD, Assistant Professor, Department of Biological Sciences

Miler Lee PhD, Assistant Professor, Department of Biological Sciences

William Sullivan Jr. PhD, Showalter Professor of Pharmacology & Toxicology and Microbiology & Immunology, Indiana University School of Medicine

Jon Boyle PhD, Associate Professor, Department of Biological Sciences

Utilizing interspecies comparisons between *Toxoplasma gondii* and *Hammondia hammondi* to elucidate mechanisms driving life stage development, life cycle flexibility, and pathogenesis

Sarah Louise Sokol Borrelli, PhD

University of Pittsburgh, 2021

Multi-host life cycles of eukaryotic parasites are fundamentally important for their success because they are linked to the way that these parasites replicate, disseminate, transmit, and cause disease in each host. As parasites of this nature progress through their life cycle, they transition between different developmental stages that function to promote survival and transmission in a specific host environment. The transitions between these life stages are especially important for the parasites *Toxoplasma gondii* and *Hammondia hammondi*. *T. gondii* and *H. hammondi* are closely related Apicomplexans that share a large majority of their genes in near perfect synteny. Despite this genomic similarity, these parasites have stark differences in their life cycle flexibility and virulence. To begin to understand the mechanisms for these differences, we have compared the developmental programs of these parasite species in head-to-head experiments and identified critical differences in the timing of stage conversion and response to stress. We were able to exploit this knowledge to produce the first ever transgenic *H. hammondi* line. We also used the developmental differences between *T. gondii* and *H. hammondi* and thorough transcriptional comparisons to identify new factors driving life stage conversion in *T. gondii.* Specifically, we identified the gene *Regulator of Cystogenesis 1 (ROCY1)*, which encodes a zinc finger CCCH motif containing protein that plays a critical role in *in vitro* tissue cyst formation and is required

for tissue cyst formation *in vivo*. Our data also suggest that ROCY1 is regulated, at least in part, by a *T. gondii* transcription factor that serves as a regulator of differentiation, Bradyzoite-Formation Deficient 1 (BFD1). Together, our findings begin to elucidate the regulatory networks driving stage conversion in *T. gondii* and *H. hammondi.*

Table of contents

List of tables

List of figures

Preface

Earning a PhD has been something I have dreamed of for well over a decade. The journey to get here has been far from easy and would not have been remotely possible without the support of so many people. First, I would like to thank my husband, Tim, for listening to my problems, dealing with my crazy schedule, riding with me (or most likely driving me) to lab on the weekends, sitting through all my practice talks, being my personal IT consultant, and always supporting my dreams. I would also like to thank my parents, Tish and Tony, for their unconditional love and support, for teaching me the value of hard work, and for always encouraging me to do my best. I would also like to thank my best friend, Cortney, for always listening to me and encouraging me to be my best self, especially after a difficult day in the lab. I would not be here today without the love and support of my family members.

I would also like to thank my advisor, Jon Boyle, for teaching me how to be both a better scientist and a better person, supporting my passion for designing large, challenging experiments, listening to my crazy hypotheses, and always valuing my opinions and treating me with respect. I feel so lucky to be a member of the Boyle lab, and am so thankful that I have been able to learn from all the amazing lab members. I would also like to thank all my current and former lab members for all their support and help throughout this journey. I would especially like to thank Dr. Matt Blank, Dr. Rachel Coombs, Dr. Sheen Wong, and Abby Primack for everything that they have done to support me and my project over the years.

I would also like to thank the members of my committee, Dr. Andrea Berman, Dr. Anne Carlson, Dr. Miler Lee, and Dr. Bill Sullivan for their guidance and insight as this project has developed throughout the years. I have learned so much from each of them and greatly appreciate

their commitment to my success. I would also like to thank Cathy Barr for everything she has done to keep me on track and for making the details of being a graduate student much easier.

1.0 Introduction

Portions of this chapter have been previous published: Sokol-Borrelli S.L., Coombs R.S., Boyle J.P. 2020. A Comparison of Stage Conversion in the Coccidian Apicomplexans Toxoplasma gondii, Hammondia hammondi, and Neospora caninum. Front. Cell. Infect. Microbiol. 10, 608283. Additional information has been added.

Eukaryotic parasites with multi-host life cycles have the unique challenge of persisting in a variety of environments. Parasites of this nature must exist in a life form that is permissible and optimized for growth, survival, and transmission in a given host. The ability to adopt these specific life forms is critical for *Toxoplasma gondii* and *Hammondia hammondi*, members of the Sarcosystidae family coccidia. These mammalian parasites follow heteroxenous, two-host life cycles (*1*–*5*) where they must survive in a variety of cell types and experience an array of host-derived immune pressures. To deal with changing environments, these parasites undergo stage conversion where they transition to life forms that each serve an important function for survival and fitness (ultimately defined as transmission). Stage conversion is essential for the success of both *T. gondii* and *H. hammondi*, however the mechanisms and networks underlying this process are only starting to be understood. Investigating and comparing how both parasites transition between their shared life stages has the potential to improve our understanding of stage conversion and reveal novel factors involved in the mechanisms driving such a critical process for *T. gondii* and *H. hammondi.*

1.1 *Toxoplasma gondii*

Toxoplasma gondii is an obligate, intracellular, eukaryotic parasite belonging to the phylum Apicomplexa. *T. gondii* was discovered in 1908 in the tissue of the rodent *Ctenodactylus gundi* by Nicolle and Manceaux in Tunisia (*6*) and by Splendor in the tissues of a rabbit in Brazil (*7*). Nicolle and Manceaux named this newly discovered organism *Toxoplasma gondii* after its morphology, with *toxo* meaning bow and *plasma* meaning life, and the host organism from which they believed it was originally identified, *Ctenodactylus gondi (8)*, which was misidentified at the time of naming (*9*, *10*). *T. gondii* follows a complicated two-host life cycle (described below) where it transitions between varying life forms optimized for success in a given host or environment (*1*, *2*, *11*). *T. gondii* is a zoonotic pathogen capable of infecting all warm-blooded animals and can cause severe disease in humans, especially in individuals with a compromised immune system (*12*) and in the developing fetus (*13*). *T. gondii* infects approximately one third of humans worldwide (*14*, *15*), and in the United States, it is estimated that congenital infection with *T. gondii* ranges from 1 in 3,000 to 1 in 10,000 live births (*13*). *T. gondii* can also cause severe disease in other animals including but not limited to cats, dogs, monkeys, and sheep (*16*). All in all, *T. gondii* is a global health concern for both humans and other animals.

1.1.1 Life cycle of *T. gondii*

Toxoplasma gondii follows a facultative homoxenous/heteroxenous two-host life cycle (Figure 1A). Sexual reproduction of *T. gondii* occurs in its definitive hosts which includes members of the *Felidae* genus. This specific developmental process produces millions of orally infectious, environmentally stable oocysts. Each oocyst contains 8 sporozoites contained within 2

sporocysts that are surrounded by an oocyst wall (*1*, *2*, *11*). When oocysts are ingested by an intermediate host, the sporozoites will excyst within the host digestive system and invade the intestinal epithelium. Once in the intestinal epithelium, sporozoites differentiate into tachyzoites, which are the fast-growing life stage responsible for acute infection. Eventually, *T. gondii* tachyzoites differentiate into bradyzoites, the slow growing life stage associated with chronic infection. Bradyzoites are found within tissue cysts which typically reside in the central nervous system or in skeletal and cardiac muscle (*17*). Bradyzoite tissue cysts are orally infectious to the definitive host. When ingested by a definitive host, tissue cysts will differentiate into the sexual stages resulting in the production of oocysts, thus completing the life cycle (*18*). Additionally, cats have been described as complete hosts for *T. gondii,* meaning that they can support the entire life cycle, because they support proliferation of tachyzoites and bradyzoites in tissues outside of the intestine in addition to supporting sexual life stages and sexual reproduction in intestinal tissues (*19*). One of the most unique components of the *T. gondii* life cycle is that its life cycle is flexible because it can bypass both asexual and sexual reproduction The bypass of sexual reproduction allows *T. gondii* to continually persist in only its intermediate hosts (*11*) and likely underlies its broad host range.

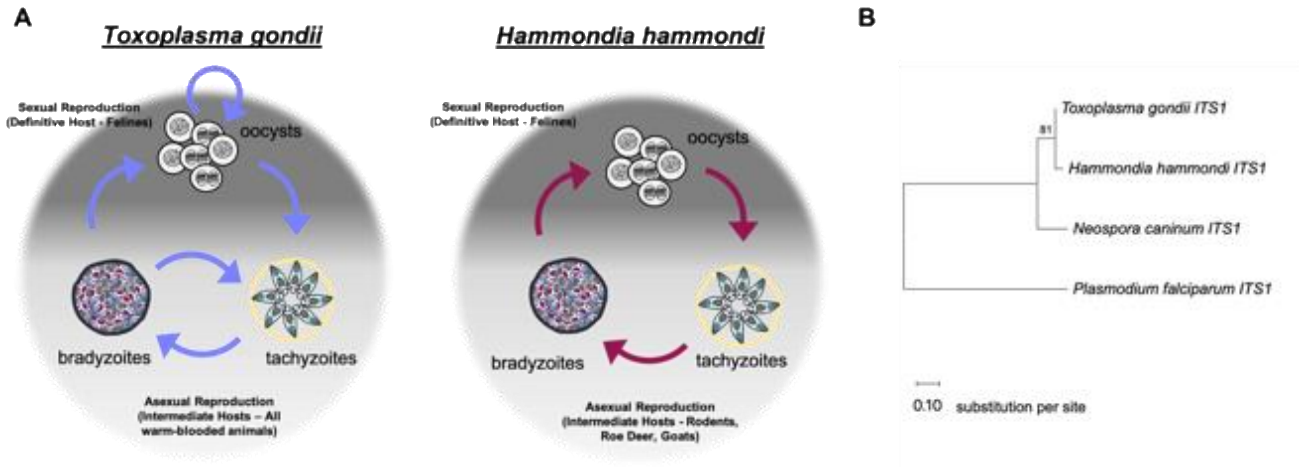

Figure 1. Life cycle of *Toxoplasma gondii* and *Hammondia hammondi*.

A) *T. gondii* follows a facultative heteroxenous/homoxenous life cycle where during a given cycle it can bypass both sexual or asexual replication. *H. hammondi* follows a strict obligate heteroxenous life cycle and lacks bypasses found in the *T. gondii* life cycle. Sexual reproduction for both *T. gondii* and *H. hammondi* occurs in members of the *Felidae* genus. B) Neighbor-joining tree depicting relationship between ITS1 (Internal transcribed spacer 1) sequences of *T. gondii*, *H. hammondi*, and *N. caninum*. *P. falciparum* is used as an outgroup. Sequences were obtained from GenBank. Bootstrap values for 1000 replicates are indicated. Scale bar represents the substitutions per site.

1.1.2 *Toxoplasma gondii* - host range, transmission, and pathogenesis

Toxoplasma gondii has a broad intermediate host range and can infect all warm-blooded animals including birds (*12*). Transmission of *T. gondii* occurs through the fecal-oral route, when oocysts, shed in cat feces, are ingested by an intermediate host. Transmission can also occur when an intermediate host consumes tissues infected with bradyzoite-containing tissue cysts (*9*). Additionally, vertical transmission of *T. gondii* can occur during primary infection of a mother, as tachyzoites are able to cross the placenta (*13*). Although infections are often asymptomatic, *T. gondii* infections persist in the host in the form of tissue cysts, the life stage that contributes to chronic infection (*20*). Tissue cysts cannot be cleared by the host immune response nor can they be eliminated by known antiparasitic drugs (*21–24*). *T. gondii* infections are thought to be long term, as bradyzoite containing tissue cysts reside in host tissue for extended periods of time and can reactivate causing clinical disease (*12*, *25*, *26*). Reactivation can occur when 1) a chronically infected host becomes immunocompromised which results in rapid proliferation and dissemination of tachyzoites, 2) when a naïve intermediate host ingests *T. gondii* tissue cysts, the bradyzoites contained within these tissue cysts are released during digestion and transition back to tachyzoites which then disseminate and cause acute infection in the host before encysting during chronic infection, or 3) as a result of transplantation of an organ that was previously infected with *T. gondii*.

Reactivation results in expanded transmission for *T. gondii*, as it allows for the parasites to be continually propagated through asexual reproduction in intermediate hosts and underlies disease progression in immunocompromised hosts (*17*). To date, the molecular determinants of this unique ability have not been elucidated, but this ability has likely had a dramatic impact on the global distribution and broad host range of *T. gondii*.

1.1.3 *Toxoplasma gondii* in humans – global prevalence, disease, and treatment

T. gondii is the causative agent for the human disease toxoplasmosis, has a worldwide distribution, and is estimated to have infected 2 billion people (*27*). It is estimated to infect 1 million new individuals in the United States each year (*28*). Recent studies have calculated the global seroprevalence of *T. gondii* infection to be 25.7%, with estimated seroprevalence ranging from 16.4% in Asia to 61.4% in Africa (*14*).

T. gondii is one of the leading causes of hospitalization and the second leading cause of death caused by a food borne illness in the United States (*29*). Typically, infections with *T. gondii* are asymptomatic or results in fever, muscle aches, malaise, headache, sore throat, and mild lymphadenopathy (*16, 30*). However, as previously mentioned, infection with *T. gondii* can become problematic for individuals with compromised immune systems, such as HIV/AIDS patients or organ transplant patients, when latent infections reactivate into highly replicative life forms and result in tissue damage (*23, 30–36*). Infection with *T. gondii* can also be problematic when infection occurs for the first time in pregnant women. Congenitally acquired toxoplasmosis can result in spontaneous abortion or severe birth defects, typically impacting the central nervous system. The effects of congenitally acquired toxoplasmosis can develop in utero or months to years

after birth (*13*). Additionally, *T. gondii* is capable of invading and replicating in the retina, resulting in ocular toxoplasmosis, which can cause severe retinal damage that can lead to blindness (*37*).

Following infection with oocyst-derived sporozoites or bradyzoites, *T. gondii* disseminates to its host's lymph nodes and distant organs by traveling through the blood stream and the lymphatic system. Typically, disease associated with toxoplasmosis is caused by the intracellular replication of tachyzoites (either during primary infection or from a ruptured tissue cyst) that ultimately lead to tissue necrosis. Necrosis is usually followed by inflammation (*16*) that leads to killing of tachyzoites, primarily by interferon-γ and tumor necrosis factor activated macrophages and cytotoxic T cells (*38*). Typically, necrosis and associated abscesses give rise to the disease processes caused by *T. gondii*, including encephalitis and retionochoroiditis (*16, 38*).

There are a variety of treatments for toxoplasmosis that target tachyzoites. Some of the most common treatments include sulfonamides, such as sulfadiazine, dapsone, and pyrimethamine, (*24, 39, 40*) which inhibit parasite folate metabolism (*16, 24*). Other treatments include macrolides (such as spiramycin and azithromycin) (*24*), clindamycin (*41*), minocycline, and rifabutin (*24*). However, there are no FDA approved antimicrobials that are able to target bradyzoite containing tissue cysts (*16, 23, 24*). The lack of antimicrobials targeting bradyzoites in combination with the sheer number of individuals infected with *T. gondii* make understanding the developmental processes needed to form bradyzoites fundamentally important for the development of novel therapeutics that can specifically act on these life stages to eliminate chronic infection.

1.2 *Hammondia hammondi*

Hammondia hammondi is also an obligate, intracellular eukaryotic parasite and is the closest extant relative of *T. gondii (42, 43)*. *H. hammondi* was first discovered in cats by J. K. Frenkel and J. P. Dubey in 1975 and is named in honor of Professor Datus M. Hammond for his contributions to the knowledge about coccidian parasites (*5*). Unlike its close relative, *T. gondii*, *H. hammondi* is thought to be avirulent as it is not known to cause disease in humans (*42*).

1.2.1 Life cycle of *H. hammondi*

Hammondia hammondi follows a strict obligate heteroxenous life cycle (Figure 1A). Sexual reproduction only occurs within the intestinal epithelium of the definitive host, which includes felids. *H. hammondi* oocysts, which are morphologically indistinguishable for *T. gondii* oocysts, are orally infectious to intermediate hosts (*3*, *5*). *H. hammondi* oocysts, like *T. gondii* oocysts, excyst within the host digestive system and release sporozoites that invade the intestinal epithelium and differentiate into tachyzoite and bradyzoite life stages as infection progresses. Unlike *T. gondii* infections, feline hosts can only support *H. hammondi* enteroepithelial stages and do not support extraintestinal infections (*42*). Furthermore, during asexual reproduction *H. hammondi* tachyzoites remain infectious to intermediate hosts until they terminally differentiate into bradyzoite/tissue cyst life stages (*42*, *44*) that are only orally infectious to definitive feline hosts. It is hypothesized that terminally differentiated *H. hammondi* parasites are incapable of reactivation, however, this has yet to be tested in head-to-head comparisons with *T. gondii*.

1.2.2 *Hammondia hammondi* - host range, transmission, and pathogenesis

H. hammondi has a restricted host range, as its only known natural intermediate hosts are rodents (*45*), roe deer (*46*), and goats (*47*). Despite having a limited known natural host range, *H. hammondi* has been shown experimentally to infect monkeys (*48*), dogs (*49*), rabbits, and pigs (*42*), yet is unable to infect birds (*50, 51*). Despite this slight expansion in experimental host range, nonmurine animals are considered poor hosts for *H. hammondi* as infections do not result in robust chronic infection as *H. hammondi*-infected tissues from these animals lead to poor oocyst production when fed to cats compared to *H. hammondi*-infected murine tissues (*51*). *H. hammondi* is only transmitted by oocysts through the fecal-oral route (*42*) and is not known to be capable of horizontal (*42*) or vertical transmission (*51*). In rodents, *H. hammondi* is avirulent in comparison to *T. gondii*. *H. hammondi* is not known to infect humans and is not known to cause natural disease in any animal model (*42*). However, experimental oral infection with a high dose of 10^5 or 10^6 oocysts can result in morbidity and mortality in mice during acute infection (*5*). While the true prevalence of *H. hammondi* is difficult to determine as it can only be accurately detected through assays analyzing DNA (see section 1.3.1 below), a study of feces from cats in Germany found that a similar number of cats shed *H. hammondi* oocysts in their feces as compared to *T. gondii*, suggesting that both parasite species occur similarly in the environment (*52*). Considering the similar environmental prevalence combined with the antigenic similarity between *T. gondii* and *H. hammondi* (discussed in section 1.3.1 below), it is possible that the natural host range for *H. hammondi* is broader than its current description, and it is possible that *H. hammondi* is capable of infecting humans. New serological based methods of distinguishing between these two parasites species are needed to thoroughly address this possibility. Appendix A describes the work that we have done to begin to develop assays of this nature.

1.3 Comparison between *T. gondii* and *H. hammondi*

1.3.1 Parasite biology, morphology, and antigenicity

Even though *H. hammondi* is now recognized as its own species (*42*), *H. hammondi* was previously described as a strain of *T. gondii (53)* and was even referred to as *Toxoplasma hammondi (54)* due to the extensive similarities between species. Morphologically, the various life stages of *T. gondii* and *H. hammondi* are highly similar. These parasites both contain the same classes of organelles (rhoptries, dense granules, micronemes, a conoid, a single mitochondrion, and a nucleus) and are indistinguishable by light microscopy (*42*). However, there are minor species-specific differences that can be observed with electron microscopy. *H. hammondi* rhoptries are electron-dense rhoptries and their sporozoites contain a crystalloid body. Conversely, *T. gondii* have electron-lucent rhoptries and their sporozoites lack a crystalloid body (*42*, *55*). *T. gondii* tachyzoites, bradyzoites, and sporozoites are also slightly smaller (0.2-0.7µm) in length than the corresponding life stage in *H. hammondi*. There are no morphological differences in oocysts or in bradyzoite containing tissue cysts between parasite species. However, *H. hammondi* tissue cysts are rarely found in the brains of infected mice whereas tissue cysts are commonly found in the brains of mice infected *T. gondii (42).*

Another similarity between *T. gondii* and *H. hammondi* is that both parasite species are antigenically similar. While there are antibodies that can be identified that are specific for *H. hammondi (56),* the majority of antibodies raised against either *T. gondii* or *H. hammondi* demonstrate cross reactivity with parasite lysates and/or organelles to varying degrees (*42*, *57–61*). These likenesses suggest that these parasites also have extensive similarities in their antigenic protein repertoire. While these antigenic similarities are useful for immunostaining assays in *H.*

hammondi, the similarities with regards to antigenicity make serological distinctions between *T. gondii* infection and *H. hammondi* infection very challenging. The ideal method for determining if an infection is caused by *T. gondii* or *H. hammondi* is through PCR analysis of genomic parasite DNA. Various primers sets have been identified that are species-specific and can be used to distinguish between infection with these two parasites (*62, 63*). However, obtaining parasite DNA from infected hosts can be challenging, especially during the chronic stage of infection. PCR based diagnostic methods are not commonly used for detection (*64*).

1.3.2 Life cycle differences between *H. hammondi* and *T. gondii*

Despites sharing all life stages (sexual stages including schizonts, gamonts, and merozoites; oocysts; sporozoites; tachyzoites; and bradyzoites) with *T. gondii* that are morphologically indistinguishable with light microscopy, *H. hammondi* and *T. gondii* have important differences in their life cycle (Figure 1A). The main distinguishing factor is that *H. hammondi* follows a strict obligate heteroxenous life cycle where it must initiate infections in intermediate hosts from sporozoites contained within oocysts (the product of sexual replication), progress through its asexual life stages (tachyzoite to bradyzoite) in the intermediate host, and then only bradyzoites can initiate an infection in its definitive feline hosts to induce sexual reproduction. *H. hammondi* bradyzoites are not known to cause infection in other intermediate hosts, a common mode of transmission for *T. gondii*, and feline definitive hosts are not complete host (complete hosts are able to support both sexual and asexual replication) for *H. hammondi* as they are for *T. gondii (3, 42).*

Unlike *T. gondii*, *H. hammondi* cannot be continuously propagated in tissue culture. A variety of cell types, including bovine monocytes, African Green monkey kidney cells, primary

rhesus monkey kidney cells, WI-38 human fibroblasts, feline kidney cells, and bovine kidney cells can be infected with oocyst-derived sporozoites or tachyzoites obtained from mesenteric lymph nodes of an orally infected mouse. All these host cells can support parasite replication. However, as infection progresses, the *H. hammondi* parasites form cyst like structures and eventually disappear from culture. (*42*, *55*, *65*). Furthermore, the cyst structure that form during *in vitro* cultivation of *H. hammondi* are only infectious to cats (*55*). The life cycle differences exhibited by *H. hammondi*, specifically its obligate nature, likely determine *H. hammondi's* inability to continuously grow in *in vitro* tissue culture. Understanding the progression and timing of *H. hammondi's* development *in vitro* is essential for facilitating studies in the parasite species designed to elucidate the mechanistic factors that determine its obligate life cycle.

1.3.3 Genetic comparisons between *T. gondii* and *H. hammondi*

In addition to the morphological and life cycle features described above, genetic comparisons between *H. hammondi* and *T. gondii* demonstrate that these two parasites species are very closely related (*43*, *66*–*68*) (Figure 1B). Comparisons in the internal transcribed spacer 1 sequences of *T. gondii* and *H. hammondi* revealed differences in less than 5% of nucleotide positions (*43*, *67*). Furthermore, the overall genomic divergence between *H. hammondi* (HhCatGer041) and *T. gondii* (GT1) is predicted to be 4.9% and only 96 of 8,993 *T. gondii* genes queried had no significant reciprocal blast hits when compared to *H. hammondi*, demonstrating that these species share many of the same genes. Moreover, most of these genes (>95%) are found in the same order and orientation (*68*), suggesting that overall gene content and gene arrangement is highly similar between both species. Additional work has also found extensive genomic synteny (29 long syntenic blocks that contain >80% of genes, ~1 megabase reciprocal translocation with

chromosomes Ia and IX, and a few rearranged blocks) when comparing *T. gondii and H. hammondi*. This study identified 7,095 shared orthologs using OrthoMCL analysis of shared proteomes between *H. hammondi* and *T. gondii* (*43*). The genomic similarities combined with the life cycle similarities (same life stages, yet *T. gondii* life cycle has bypasses and flexibility that is not a part of the *H. hammondi* life cycle) displayed by both parasite species makes it unlikely that gene content plays a major role in the phenotypic differences between these parasite species. Overall, *H. hammondi* and *T. gondii* have a very similar genetic tool kit but likely use those tools in different ways to support their distinct life cycles. Comparing how these two parasites use their shared genes is a promising approach for identifying the genetic components contributing to the development and life cycle restrictions in both parasites.

1.3.4 Shared virulence factors

Comparisons between different strains of *T. gondii* have revealed several genes that have differing impacts on *T. gondii* virulence *in vivo* (*69–71*), making it possible that virulence differences between *H. hammondi* and *T. gondii* could be explained by species-specific differences in key virulence factors. If true, this would mean that differences in these virulence factors are some of the major contributors to the phenotypic differences observed between *T. gondii* and *H. hammondi.* However, studies have revealed that the *H. hammondi* orthologs of critical virulence factors rhoptry protein (ROP) 18, ROP5, ROP16 and dense granule protein (GRA)15 are all functional when expressed in *T. gondii* (*68, 72*), suggesting that these virulence factors do not contribute to the differences displayed by *T. gondii* and *H. hammondi.* This finding is important because it further demonstrates that the genetic factors contributing to the developmental

difference between these species is likely the major driver for the virulence and life cycle differences observed between *T gondii* and *H. hammondi.*

1.3.5 Transcriptional profile comparison

While *T. gondii* transcriptomes at varying life stages have been extensively studied (*73*), transcriptional studies in *H. hammondi* are only beginning to be investigated, as working with *H. hammondi* is inherently more challenging because of its obligate two-host life cycle and terminal differentiation phenotype. The first of these studies used microarray analysis of *T. gondii* (VEG) and *H. hammondi* (HhCatGer041) sporulated oocysts to investigate transcriptional differences. This study revealed highly distinct transcriptional profiles between each species and found that several genes upregulated in *H. hammondi* are also upregulated in the bradyzoite life stage in *T. gondii (72)*, suggesting that transcriptional differences may underlie the developmental differences identified between both species. These transcriptional differences, especially the early emergence of bradyzoite genes, could be fundamentally important for the life cycle differences observed between parasites. The transcriptional changes that occur during *H. hammondi* development represent a critical knowledge gap. Characterizing these transcriptional changes and comparing them to what we currently know about the transcriptional changes that occur between various stages of *T. gondii* will be useful for uncovering the mechanisms controlling development and the life cycle differences observed between these two parasites.

1.4 Biology of bradyzoite life stages in *T. gondii*

Despite the fundamental phenotypic differences that exist between *T. gondii* and *H. hammondi*, the formation of bradyzoites is a critical step in the transmission of *T. gondii* and *H. hammondi*. Bradyzoites are necessary for transmission as their cyst wall provides protection during passage through the mammalian gut (*74*), and they are also required for sexual reproduction which dramatically expands the number of infectious oocysts available to infect new hosts. Even though the definitive hosts for *T. gondii* are complete hosts (hosts that can support both sexual and asexual replication), bradyzoite formation within these animals is still needed for sexual reproduction to occur. Bradyzoite-containing tissue cysts also allow the parasites to remain in a host for an extended period of time as it has been hypothesized that they cannot be cleared by the host immune system. However, recent studies suggest that tissue cysts are cleared from murine brains 20 months post-infection (*75*), however it is unclear if tissue cyst remain in other tissues. Finally, interconversion that occurs in *T. gondii* allows for these parasites to be transmitted independently of the definitive host, a remarkable trait given the vastly different species that can serve as intermediate hosts for these parasites. For these reasons, understanding the mechanisms driving the conversion of tachyzoites to bradyzoites and how it compares between species is necessary to manage the many manifestations of disease caused by these organisms. While few studies have directly compared *H. hammondi* and *T. gondii (42, 72)*, the *T. gondii* bradyzoite has been extensively studied through intraspecies comparisons of varying life stages (*22*, *26*, *76*, *77*). These studies have broadened our understanding of the *T. gondii* bradyzoite and are beginning to uncover the mechanisms governing stage conversion associated gene expression.

1.4.1 Triggers of bradyzoite formation

While signals derived from the environment, such as from an infected host cell, are likely at the heart of stage conversion in *T. gondii* and its near relatives, the precise mechanisms used to respond to these signals have remained elusive. However, the effect of various signals on inducing life stage development, specifically tissue cyst formation, has been well studied in *T. gondii.*

An important but underappreciated fact is that most strains of *T. gondii* are capable of spontaneously converting into bradyzoites when grown *in vitro* in a variety of different host cells (*78*, *79*). When *T. gondii* infections are initiated with parasites derived from sporozoites or low-passage tachyzoites or bradyzoites, the parasites will first grow as tachyzoites but will later form tissue cysts that express bradyzoite markers and/or are able to induce oocyst shedding when fed to cats (*78*, *80*). This phenomenon of spontaneous stage conversion in *T. gondii* was most thoroughly studied in *T. gondii* strain VEG. When infections are initiated with *T. gondii* VEG sporozoites, the parasites transition into a rapidly growing tachyzoite stage resembling many lab-adapted strains like *T. gondii* RH, and after ~20 divisions they begin to differentiate into slower growing parasites that express bradyzoite markers, suggesting that there may be a developmental clock controlling this spontaneous conversion (*80*). Taken together, these findings suggest that there is a parasite intrinsic factor that enables sporozoite-derived tachyzoites to transition to bradyzoites following initial tachyzoite expansion, at least for the VEG strain. This parasite intrinsic factor could potentially be playing the same role in *H. hammondi.* Characterizing the developmental differences during this time period in *T. gondii* and *H. hammondi* is important for understanding this phenotype and how such a factor contributes to development.

Host factors, specifically the differentiation state of a given host cell, can also impact *T. gondii* cystogenesis. *T. gondii* forms tissue cysts when grown in mouse primary skeletal muscle

cells that have been differentiated into polynucleated myotubes, which are withdrawn from cell cycle progression (*81*, *82*). When these host cells are genetically manipulated to knock-down Testis-specific Y-encoded-like protein 2 (Tspyl2), a negative cell cycle regulator that contributes to withdrawal from host cell cycle progression in these myotubes, *T. gondii* fails to form tissue cysts in these cells (*82*). Additionally, expression levels of the host gene human cell division autoantigen-1 (CDA1) have been shown to be important for bradyzoite development. *T. gondii* grows slower and expresses bradyzoite-specific genes when grown in host cells treated with the trisubstituted pyrrole small molecule compound 1, which induces the expression of host CDA1 (*83*). CDA1 is a negative regulator of cell growth and has regions with homology to testis protein TSPY (*84*). Additionally, *T. gondii* forms tissue cysts when grown in HeLa cells that overexpress a transgene encoding CDA1 (*83*). Moreover, *T. gondii* forms tissue cysts when grown in neuronal cells, which like polynucleated myotubes are withdrawn from the cell cycle (*85*–*87*). The ability of cells that have withdrawn from their cell cycle to promote tissue cyst formation in *T. gondii* is a likely contributor to the preference *T. gondii* shows for muscular tissue and tissues of the central nervous system.

Several well characterized stressors are known to induce *T. gondii* tachyzoite-to-bradyzoite stage conversion *in vitro* (summarized in Table 1). Perhaps the most well-known stressor that leads to robust formation of *T. gondii* tissue cysts *in vitro* is alkaline pH (pH ~8 as compared to the standard pH growth conditions of 7.2-7.4). Multiple groups have shown that alkaline pH induces *T. gondii* cyst development either when applied to host cells after infection (*88*) or when applied to extracellular parasites prior to infection (*89*). Alkaline pH induces known bradyzoite markers, such as bradyzoite antigen 1 (BAG1) (*80*) and also induces cyst wall formation (*90*, *91*). Despite robust induction of *T. gondii* tissue cyst development, the exact mechanism of pH-induced cyst

formation in *T. gondii* remains unknown. Increases in extracellular pH can result in accelerated cell movements and cytoplasm contraction (*92*). Increased intracellular pH has been demonstrated to increase certain cellular processes, such as DNA and protein synthesis, mitotic events, and glycolysis, in mammalian cells (*93*, *94*). However, it is not clear if alkaline pH treatment used to induced bradyzoite development results in increased intracellular pH. It is possible that alkaline pH-derived stress induces a myriad of both host- and parasite-derived signals that are needed in order to initiate bradyzoite development. Investigating the changes in gene expression that occur in the host in response to these bradyzoite conditions would be useful for understanding how alkaline pH induces bradyzoite development in *T. gondii.*

Another inducer of bradyzoite development includes acidic pH stress. Treatment of infected host cells with pH 6.8 media induces the expression of bradyzoite markers, such as BAG1 (*95*). In addition to changes in pH, heat shock (43°C as opposed to 37°C) and sodium arsenite treatment of infected host cells have also been shown to induce expression of bradyzoite genes in *T. gondii.* However, heat shock is not an optimal method for inducing bradyzoite development as it often results in decreased parasite invasion, parasite killing, and loss of host cell viability (*88*). Moreover, endoplasmic reticulum (ER) stress derived from treatment with tunicamycin has been shown to induce expression of bradyzoite transcripts as a result of both translational and transcriptional control derived from an unfolded protein response (*96*).

Nutrient starvation can also induce stage conversion in *T. gondii*. Pyrimidine starvation achieved via deletion of the uracil phosphribosyl transferase (UPRT) gene in combination with growth in atmospheric CO_2 (0.03% compared to 5%) also leads to a parasite growth reduction and expression of bradyzoite markers (*97*). Arginine starvation also decreases the replication of *T. gondii* and induced tissue cyst formation (*98*). Cholesterol depletion via growth in media

supplemented with lipoprotein-depleted serum (as compared to growth in 5% fetal bovine serum) has also been shown to induce bradyzoite gene expression (*99*).

Additionally, interferon gamma (IFN-γ) treatment of *T. gondii* infected macrophages results in expression of bradyzoite specific antigens (*100*), however IFN-γ is not capable of inducing expression of bradyzoite specific antigens in human fibroblasts (*88, 95, 101, 102*). Other *in vitro* stressors that may mimic IFN-γ driven immune pressure also induce *T. gondii* cystogenesis, such as the production of nitric oxide. Exogeneous nitric oxide produced from sodium nitroprusside (SNP) treatment can induce expression of the bradyzoite marker BAG1 (*100*). Exogenous nitric oxide likely inhibits proteins involved in the electron transport chain, thus treatment with mitochondrial inhibitors oligomycin, antimycin A (*100*), and atovaquone (*21*) can also induce expression of bradyzoite antigens in *T. gondii.* Overall, the numerous and diverse exogenous stressors capable of inducing bradyzoite development in *T. gondii* suggest that multiple signals can be used as triggers to induce the fundamental process of bradyzoite formation. It is critical to compare these methods in terms of gene expression and tissue cyst formation to fully understand their function in cystogenesis.

In comparison to *in vitro* systems, the *in vivo* factors required to induce cystogenesis are much less clear. One of the most well-studied potential inducers of cyst formation is IFN-γ. It is also thought that IFN-γ may play a critical role in cystogenesis. It is hypothesized that IFN-γ contributes to the initiation of tissue cyst formation *in vivo*, as it can induce cystogenesis *in vitro* (described above). However, IFN-γ knockout mice fail to control acute proliferation of parasites and succumb to acute infection (*101, 103*) even when infected with avirulent strains of *T. gondii (104)* making it difficult to determine if IFN-γ induces cystogenesis *in vivo*. It is also possible that *T. gondii* spontaneously forms tissue cysts during *in vivo* infections, but this spontaneous

development is again challenging to observe experimentally due to the lethality of *T. gondii* infections in mice with disrupted immune systems.

In vivo factors have also been implicated in suppressive roles for cytogenesis. Tumor necrosis factor-alpha (TNF-α) and inducible nitric oxide synthase (iNOS) may play a role in restricting cystogenesis, as TNF receptor p55- and p75-deficient mice and iNOS deficient mice develop more tissue cyst in the brain compared to wild type mice despite relatively equivalent parasite burden in peritoneal cells early in infection. Interestingly, mice deficient for TNF-α receptors or iNOS succumb to chronic infection while the WT mice survive (*105*, *106*). It is challenging to determine if the increase in tissue cysts in the brains of these mice is a result of TNF-α and iNOS restricting tissue cyst development, or if more parasites make it to the brain prior to tissue cyst formation. Future experiments using live imaging that quantifies parasite burden could be useful to test these hypotheses. Additionally, CD4+ and CD8+ T-cells are important for the maintenance of chronic infection characterized by the bradyzoite/tissue cyst life stage. Depletion of these cells with neutralizing antibodies leads to reactivation of *T. gondii* infection resulting in parasite proliferation (*107*). Linking what is known about *in vitro* cyst development in *T. gondii* to what happens *in vivo* is a significant, but important, knowledge gap. Understanding how spontaneous development occurs in *T. gondii* and how immunity factors alter development in the context of an *in vivo* infection is important for understanding the pressures that result in the establishment of a chronic infection in natural settings.

Table 1. Summary of exogenous stressors that induce bradyzoite development in *T. gondii*

Stressor	Parasite Life Stage used for infection	Parasite Strain	Host Cell	Method used to determine bradyzoite formation	Citation
Alkaline pH (treatment of infected host cells)	Sporozoites	VEG	Human foreskin fibroblasts (HFFs)	bradyzoite-specific antibodies	(*80*)
	In vivo tachyzoites	RH	HFFs; Vero cells	bradyzoite-specific antibodies	(*88*)
Alkaline pH (extracellular parasites)	*In vitro* tachyzoites	ME49	HFFs	bradyzoite-specific antibodies	(*89*)
Heat Shock (43 degrees C)	*In vivo* tachyzoites	RH	Vero cells	bradyzoite-specific antibodies	(*88*)
Tunicamycin (ER Stress)	*In vitro* tachyzoites	--	HFFs	bradyzoite-specific transcripts	(*96*)

Sodium arsenite	*In vivo* tachyzoites	RH	Vero cells	bradyzoite-specific antibodies	(*88*)
Sodium nitroprusside (SNP) (extracellular parasites)	*In vitro* tachyzoites	ME49	HFF	bradyzoite-specific antibodies	(*89*)
SNP (infected host cells)	*In vitro* tachyzoites	NTE	Murine bone marrow-derived macrophages (BMDM)	bradyzoite-specific antibodies	(*100*)
Interferon gamma	*In vitro* derived tachyzoites	NTE	Murine peritoneal macrophages	bradyzoite-specific antibodies	(*102*)
	In vitro tachyzoites	NTE	Murine BMDM	bradyzoite-specific antibodies	(*100*)
Antimycin A	*In vitro* tachyzoites	NTE	Murine BMDM	bradyzoite-specific antibodies	(*100*)
Oligomycin	*In vitro* tachyzoites	NTE	Human fibroblasts	bradyzoite-specific antibodies	(*100*)

Atovaquone	*In vitro* tachyzoites	PLK	HFFs	bradyzoite-specific antibodies	(*21*)
Arginine starvation	*In vitro* tachyzoites	RH; PLK	HFFs	Dolichos biflorus agglutinin	(*98*)
Pyrimidine starvation	*In vitro* tachyzoites	RHdletaUPRT	HFFs	bradyzoite-specific antibodies	(*97*)
Cholesterol depletion (Lipoprotein depleted serum)	*In vitro* tachyzoites	ME49	Chinese hamster ovary cells	Bradyzoite-specific antibodies	(*99*)
Compound 1	*In vitro* tachyzoites	ME49B7; Pru; VEG; CTG	HFFs	bradyzoite-specific antibodies; Dolichos biflorus agglutinin	(*83*)

1.4.2 Critical bradyzoite genes in *T. gondii*

Studies investigating *T. gondii* bradyzoites have begun to identify parasite factors that may play a role in altering gene expression during stage conversion. Thus far, the parasite factors that

have been identified include signaling proteins, chromatin modifiers, transcription factors, and RNA-binding proteins involved in transcript stability and/or translation control, all of which play important roles in the tachyzoite to bradyzoite transition. Furthermore, several bradyzoite genes have also been identified that have functional roles in the bradyzoite/tissue cyst and can serve as markers for bradyzoite development and tissue cyst formation.

1.4.2.1 Protein kinase A signaling and *T. gondii* bradyzoite development

Cyclic nucleotide signaling, including cyclic adenosine monophosphate (cAMP) and cyclic guanosine monophosphate (cGMP) have been implicated in bradyzoite development in *T. gondii.* Transient levels of cAMP are able to induce bradyzoite development, while sustained levels of cAMP prevent bradyzoite formation and promotes tachyzoite growth *(108–110)*. Generally, cAMP is a second messenger in signaling pathways and can interact with several proteins, including the effector protein kinase A (PKA) (*111*). *T. gondii* encodes three PKA catalytic subunits. When TgPKAc3 is deleted, parasites grow slower and have increased levels of spontaneous bradyzoite formation. Furthermore, parasites lacking TgPKAc3 are able to maintain tachyzoite growth when exposed to bradyzoite inducing growth conditions when cAMP levels are artificially elevated (*112*). These findings suggest that signaling through TgPKAc3 plays a critical role in bradyzoite formation in *T. gondii* and may be involved in transducing an external stress signal to induce changes in gene expression needed to induce bradyzoite formation.

1.4.2.2 Chromatin associated gene products involved in bradyzoite development

Stage conversion in eukaryotic parasites is accompanied by significant changes in patterns of gene expression (*113, 114*). The chromatin landscape of a given life stage plays a large role in what genes are expressed, therefore playing a critical role in stage conversion. Several chromatin

remodeling factors have been identified in *T. gondii* that play a role in altering the chromatin landscape during different life stages. One such factor is Histone Deacetylase 3 (HDAC3), which is a component of *T. gondii's* corepressor complex. HDAC3 is associated with bradyzoite-specific promoters (*115*) and when its activity is inhibited with the compound FR235222, expression of bradyzoite genes increases (*116*). These findings suggest that histone deacetylation via HDAC3 functions to repress the expression of bradyzoite genes and keeps *T. gondii* in a tachyzoite life form. HDAC3 has been shown to work with the recently discovered *T. gondii* microrchidia (MORC) protein. MORC interacts with several Apetala2 (AP2) transcription factors (described below) (*117*) (including AP2IX-4 and AP2XII-2 discussed below (*118*)) and recruits HDAC3 to chromatin, enabling the generation of hypo-acylated chromatin which represses gene expression. When MORC is depleted in *T. gondii*, the parasites begin to express transcripts typically expressed in other life stages, such as merozoite and oocysts specific genes, that are restricted to the *T. gondii* sexual stages (*117*). These findings suggest that MORC functions as a repressor of sexual development associated gene expression through chromatin modification in *T. gondii*.

Another histone remodeling enzyme found in *T. gondii* is GCN5-A, a lysine histone acetyltransferase. This enzyme plays an oppositional role to HDAC3. GCN5-A is found at tachyzoite promoters when *T. gondii* is grown under tachyzoite growth conditions (*115*). Additionally, ChIP qPCR experiments have shown that when *T. gondii* is exposed to alkaline pH stress conditions, GCN5-A occupancy is enriched in the promotors of bradyzoite specific genes that are upregulated in response to stress. When GCN5-A is knocked out in *T. gondii*, the parasites are unable to upregulate 74% of known bradyzoite genes in response to alkaline pH induced stress (*119*). Together, these findings demonstrate that GCN5-A plays a critical role in *T. gondii's* ability to alter its gene expression in response to alkaline pH stress.

Additional chromatin remodeling enzymes that play a role in the alteration of stage conversion associated gene expression have also been identified in *T. gondii*. These include TgCARM1 (*115*), TgSCRAP (*120*), and TgRSC8 (*121*, *122*). TgCARM1 is a histone arginine methyltransferase protein that is essential for parasite replication. When N-methyltransferase activity is inhibited with the small molecule AMI-1 via pretreatment of extracellular parasites, *T. gondii* forms significantly more bradyzoites compared to a vehicle control (*115*). TgSCRAP, a Snf2-related CBP activator protein and SNF/SWI chromatin remodeler, upregulates the expression of the known bradyzoite gene BAG1 during alkaline pH induced stress, and has been shown to enhance CREB (cAMP response element binding protein) mediated transcription, which may suggest a role in the protein kinase A signaling pathway (see above) that has also been implicated in bradyzoite development for *T. gondii* (*120*). Another chromatin remodeling complex that contributes to bradyzoite development is TgRSC8, a homolog of the nucleosome remodeling complex Rsc8p protein in *Saccharomyces cerevisiae*. When this protein is mutated in *T. gondii*, some bradyzoite genes show a significant reduction in transcript abundance when exposed to alkaline pH stress conditions. However, these mutants did not show reduced *Dolichos biflorus agglutinin* (DBA) staining (*122*), which specifically recognizes the glycosylated cyst wall protein CST1 (*91*). In addition to chromatin remodelers, histone variants have also been implicated in stage conversion in *T. gondii*. The histone variant H2AZ transcript is expressed in mature, *in vivo* bradyzoites. H2AX transcript is also expressed in mature, *in vivo* bradyzoites and displays increased expression *in vitro* during alkaline pH stress. H2AX is typically enriched in silent regions of DNA, suggesting that histone variants are important for altering gene expression during differentiation (*123*). All together, these findings suggest that the alteration of chromatin is an important contributor to stage conversion associated gene expression in *T. gondii*.

1.4.2.3 Transcription factors implicated in bradyzoite development

Transcription factors are an important class of proteins that play a significant role in the control of stage conversion specific gene expression and have long been investigated for their role in stage conversion associated gene expression in *T. gondii.* One of the first major classes of transcription factors investigated for their role in stage conversion in *T. gondii* were the AP2 transcription factors. AP2 factors were first identified in Apicomplexans in 2005. These transcription factors share the Apetala2 (AP2) integrase DNA binding domain typically found in transcription factors of numerous plant species (*124*). AP2 transcription factors are known to play a major role in stage conversion in *Plasmodium* species (*125*). There are currently 67 AP2 factors (66 annotated as AP2 domain transcription factors and 1 annotated as an AP2 domain-containing protein) annotated in the *T. gondii* ME49 genome (*126*). However, only 6 of these AP2 transcription factors have been tied to bradyzoite development in *T. gondii* to date. The AP2 transcription factor AP2IX-9 functions mainly as a repressor of bradyzoite development, maintaining parasites in an intermediate, pre-bradyzoite state. AP2IX-9 binds to the CAGTGT motif and functions to repress transcription (*127*). Furthermore, deletion of AP2IX-9 results in increased tissue cyst formation in parasites cultivated in normal growth conditions (*128*). Another AP2 factor, AP2XII-2, has been shown to interact with the MORC protein and results in increased tissue cyst formation *in vitro* upon knockdown in *T. gondii,* suggesting that this factor may be important for maintaining tachyzoites (*118*). Additionally, AP2 transcription factors have been identified in *T. gondii* that are involved in promoting bradyzoite development. These include AP2IV-4 (*129*), AP2IV-3 (*128*), and AP2IX-4 (*130*), and AP2XI-4 (*131*). When these AP2 transcription factors are deleted, parasites have a decreased ability to form tissue cysts *in vitro*

and/or *in vivo*. Furthermore, alteration (either deletion or overexpression) of these factors result in significant differences in transcript abundance of known bradyzoite genes (*128–131*).

In addition to AP2 transcription factors, *T. gondii* has additional transcription factors that are critical for stage conversion. Once such transcription factor is Bradyzoite Formation Deficient 1 (BFD1). BFD1 was recently identified as a master transcriptional regulator of bradyzoite development in *T. gondii* using a large-scale genetic screen. BFD1 is a nuclear localized Myb-like DNA binding protein that binds to the CACTGG motif near that transcriptional start site of differentially regulated genes. When BFD1 is deleted in *T. gondii*, these parasites fail to form tissue cysts both *in vitro* in response to alkaline pH derived stress and treatment with Compound 1. These knockout parasites also fail to form tissue cysts *in vivo*. Furthermore, BFD1 knockout parasites fail to express several bradyzoite specific genes when treated with alkaline pH, suggesting that BFD1 plays a major role in initiating stage conversion associated gene expression (*132*).

Additional *T. gondii* proteins that may play a role in stage conversion are the glycolytic enzymes, Enolase1 (ENO1) and Enolase 2 (ENO2). ENO1 is specifically expressed in bradyzoites and is a known bradyzoite specific gene. ENO2 is expressed in tachyzoites and can be found localized in the cytoplasm and nucleus (*133*). When ENO1 is deleted in *T. gondii*, the ability of the parasite to form *in vivo* cysts is impaired. Both ENO1 and ENO2 have been shown to bind promoters in ChIPseq and ChIP qPCR experiments and ENO1 has been shown to bind the ENO2 promoter. Furthermore, analysis of the ENO1 promoter revealed a stress response element that could be activated with nuclear extracts purified from bradyzoites (*134*). Together, these data demonstrate that ENO1 and ENO2 could have a role as transcription factors implicated in stage conversion.

1.4.2.4 Translational control involved in bradyzoite development

Translational control also plays a critical role in stage conversion associated gene expression in *T. gondii.* Phosphorylation of eukaryotic initiation factor-2 (eIF2) inhibits its guanine exchange factor (eIF2B) which results in repression of general translation. Proteins involved in the translation control pathway in *T. gondii* include Eukaryotic initiation factor 2 alpha (TgIF2α/eIF2) and initiation factor 2 kinase -A (TgIF2K-A), which can phosphorylate TgIF2α, and TgIF2K-B. TgIF2α is phosphorylated in response to stress derived from both alkaline pH, heat shock, sodium arsenite treatment, calcium ionophore treatment, and tunicamycin treatment. TgIF2α phosphorylation is maintained in bradyzoites and is accompanied by a global decrease in protein synthesis. When dephosphorylation of TgIF2α is inhibited, parasites both increase the transcriptional abundance of known bradyzoites genes as well as form DBA-positive tissue cysts (*135*, *136*). Furthermore, when the activity of TgIF2K-A is inhibited in *T. gondii,* thus decreasing TgIF2α phosphorylation, these parasites form significantly fewer tissue cysts when exposed to alkaline pH stress (*137*). These findings suggest that translational control is critical for the maintenance of bradyzoites.

Furthermore, *T. gondii* encodes two RNA binding proteins related to Alba proteins in archaea, TgAlba1 and TgAlba2. In response to alkaline pH derived stress, both TgAlba1 and TgAlba2 colocalize with RNA granules. These proteins bind greater than 30 RNAs, including their own. TgAlba1 bind to the promoter of TgAlba2. Upon deletion of TgAlba1, TgAlba2 is no longer translated. Moreover, deletion of TgAlba1 in *T. gondii* also leads to decreased tissue cyst formation *in vitro* (in response to alkaline pH stress) and *in vivo* (*138*). Together, these examples of RNA binding proteins found in *T. gondii* further demonstrate that translational control plays a critical role in stage conversion associated gene expression.

1.4.2.5 Other bradyzoite-specific genes

In addition to the work described above, there has also been extensive research performed using *T. gondii* bradyzoites generated using various forms of bradyzoite induction (described above) to identify bradyzoite-specific genes along with their function (*73*, *76*, *139*). The majority of the most well-known bradyzoite genes that have been identified include surface proteins belonging to the SAG-family, components of the tissue cyst wall, heat shock proteins (HSP), and metabolic proteins. *T. gondii* bradyzoites express several genes encoding surface antigens that are bradyzoite-specific in addition to genes that give rise to components that comprise the tissue cyst wall. Some of the most notable of these bradyzoite markers include SAG-related surface protein (SRS) SRS35B/SAG4 (*140*), SRS9 (*141*, *142*), SRS44/CST1 (*91*, *143*), matrix antigen 1 (MAG1) (*144*), bradyzoite pseudokinase 1 (BPK1) (*145*), BAG1/HSP30 (*146*), and HSP60 (*147*). Common bradyzoite-specific genes encoding metabolic proteins, include lactate dehydrogenase 2 (LDH2) (*148*) and enolase 1 (ENO1) (*149*), that are needed to support metabolic processes that likely rely on a different carbon source stored in amylopectin granules (*150*). Many of these bradyzoite-specific factors are commonly used for identifying bradyzoites and serving as markers of bradyzoite development or tissue cysts. They also play important roles for bradyzoites, such as forming a functional tissue cyst wall or functioning in metabolic processes. However, these types of bradyzoite specific genes are likely not genes that drive the global changes in stage conversion associated gene expression, with the exception of ENO1 (discussed above). Instead, the expression of these genes are likely controlled by regulatory factors in the network of stage conversion associated gene expression.

1.5 Conclusions

Despite sharing extensive genomic and morphological features, *T. gondii* and *H. hammondi* display several phenotypic differences with regards to their life cycle flexibility and virulence. However, the tachyzoite to bradyzoite transition is a fundamental developmental process for the success of *T. gondii* and *H. hammondi* as it is necessary for the survival and transmission of these parasite species. Despite extensive knowledge about the *T. gondii* bradyzoite generated through intraspecies comparisons or varying life stages, the genetic components involved in the mechanisms governing stage conversion between tachyzoite and bradyzoite life stages are only starting to be uncovered. Comparative studies investigating how these developmental processes occur and compare using interspecies comparisons between *T. gondii* and *H. hammondi* have the potential to uncover novel factors that drive bradyzoite formation. These comparisons can also reveal the mechanisms parasites like *T. gondii* and *H. hammondi* use to initiate the global changes associated with stage conversion on a mechanistic level.

2.0 Dissection of *in vitro* developmental program of *Hammondia hammondi* reveals a link between stress sensitivity and life cycle flexibility in *Toxoplasma gondii*

The contents of this chapter have been previously published: Sokol S.L., Primack A.S., Nair S.C., Wong Z.S., Tembo M., Verma S.K., Cerqueira -Cezar C.K., Dubey J.P., Boyle J.P. 2018. Dissection of the in vitro developmental program of Hammondia hammondi reveals a link between stress sensitivity and life cycle flexibility in Toxoplasma gondii. elife 7. I am responsible for the experimentation and writing in sections 2.1, 2.2.1, 2.2.2, 2.2.4, 2.2.5, 2.2.6, 2.2.7, and 2.3. I have included section 2.2.3 as it is fundamental component of this work which my future work has built upon.

2.1 Introduction

Toxoplasma gondii, the causative agent of toxoplasmosis, is a globally ubiquitous Apicomplexan parasite capable of infecting all warm-blooded animals, including approximately one-third of the human population (*42*, *151–153*). Although generally asymptomatic in immunocompetent individuals, *T. gondii* is capable of causing disease in the immunocompromised (including HIV/AIDS patients), developing neonates, and occasionally healthy individuals (*154–157*). The global ubiquity of *T. gondii* is due, at least in part, to its broad host range and ability to persist undetected in an immunocompetent host where it is either capable of being transmitted to a new intermediate host or recrudescing in the original host (*158*, *159*). These characteristics are

lacking in the nearest extant relative of *T. gondii*, *Hammondia hammondi*. Despite sharing the vast majority of their genes in near perfect synteny (*68*) and the same definitive felid host (*42*), *H. hammondi* is known to infect rodents, goats, and roe deer (*42, 43*), and at least in mice it is naturally avirulent compared to *T. gondii*. Unlike *T. gondii*, *H. hammondi* has an obligately heteroxenous life cycle (*42*), where intermediate host stages (i.e., tissue cysts) are only capable of infecting the definitive host, and definitive host stages (i.e., oocysts) are limited to infection of an intermediate host.

In addition to these life cycle differences, these two parasite species have *in vitro* behaviors that mirror their *in vivo* differences. Specifically, when *T. gondii* sporozoites (VEG strain (*80*)) are used to initiate infections in human host cells *in vitro*, they undergo a period of rapid replication, after which their growth rate slows and a subpopulation of parasites spontaneously convert to bradyzoite (e.g., cyst-like) stages (*160*). However, *T. gondii* parasites cultivated in this manner still undergo multiple cycles of replication, egress and reinvasion, and indefinite propagation (*80*). In contrast, when *H. hammondi* sporozoites are put into tissue culture they replicate slower than *T. gondii* (*55, 80*) and do not appear to be capable of subculture (either via passage of culture supernatants or after scraping and trypsinization. Ultimately *in vitro* cultivated *H. hammondi* form bradyzoite cyst-like stages that are infectious only to the definitive host (*55, 65*).

While the molecular determinants that control these dramatic phenotypic differences are unknown, the fact that life cycle restriction in *H. hammondi* occurs *in vitro* provides a unique opportunity to identify key aspects of *H. hammondi* biology that underlie its restrictive life cycle. By contrast, the life cycle restrictions in *H. hammondi* will allow for elucidation of the cellular and molecular differences in *T. gondii* that determine its comparatively flexible life cycle. It is important to note that with respect to other Apicomplexans (including *N. caninum* and *Plasmodium*

spp.), it is the *T. gondii* life cycle that is atypical; the majority of coccidian Apicomplexans are obligately heteroxenous (*11, 42, 161*). The most parsimonious explanation is that the obligately heteroxenous life cycle of *H. hammondi* is the ancestral state, and that during speciation *T. gondii* acquired novel traits linked to any number of key parasite processes (regulation of development, stress sensitivity, interactions with the host environment) that underlie its life cycle flexibility.

The obligately heteroxenous life cycle of *H. hammondi* makes experimentally characterizing and manipulating this parasite species difficult in comparison to other closely related apicomplexan parasites. We have characterized the invasion and replication rates of *T. gondii* (VEG strain (*162, 163*)) and *H. hammondi* (HhCatEth1 and HhCatAmer (*43, 164*)) from sporozoite-initiated infections, representing the most thorough head-to-head comparison of the intermediate host life stages of these distinct parasite species. Using sporozoite derived infections, we have also compared the timing and frequency of *in vitro* differentiation and report the first ever transcriptome from replicating *H. hammondi.* Together, these data reveal previously unknown features of *H. hammondi* development. Using information gleaned from these experiments, we were able to successfully subculture *H. hammondi* both *in vitro* and in a murine model during a highly predictable window of infectivity and replicative capacity. Additionally, we generated the first ever transgenic *H. hammondi,* opening up the door to future molecular and genetic studies in this poorly understood parasite species. These data provide fundamental insight for understanding how virulence and pathogenicity have evolved in *T. gondii* through interspecies comparisons with its closest extant relative. Finally, we found that *H. hammondi* is resistant to alkaline pH-induced tissue cyst formation and determined that the *H. hammondi* transcriptome is refractory to alkaline pH exposure. Our data indicate that *H. hammondi* exists as a unique zoite life stage and follows a developmental path that is distinct from the canonical tachyzoite and bradyzoite life stages

described for *T. gondii*. Moreover, our work has identified sensitivity to external stressors as a likely culprit contributing to the intriguing developmental and virulence differences between *T. gondii* and *H. hammondi,* a finding that we speculate may have a direct impact on the ability of *T. gondii* to cause disease in immunocompromised humans and may also underlie its extensive host and geographic range.

2.2 Results

2.2.1 *T. gondii* replicates 2-3X faster than *H. hammondi,* but both species have equal invasion rates

While *T. gondii* oocysts and sporozoites have been studied extensively *in vitro* and in multiple hosts (*80*, *162*, *163*), *H. hammondi* and *T. gondii* have been directly compared in only a handful of studies (*42*). Therefore, we performed a head-to-head characterization of sporozoite derived infections from both species during *in vitro* infections. As expected from previous work, we found that HhCatEth1 replicated significantly slower than TgVEG in multiple replicate assays (Figure 2A,B; ** *P*= <0.01, **** *P*= <0.0001). Based on median vacuole size (Table 2, Figure 2A,B), TgVEG replicated ~2-3X faster than HhCatEth1, with a maximum division time of 9.6 hours compared to 18 hours for HhCathEth1 (Table 2). Despite these differences in replication, TgVEG and HhCatEth1 sporozoites had similar infectivity rates in human foreskin fibroblasts (HFFs), defined as the number of vacuoles counted as a fraction of the number of input sporozoites (HhCatEth1 0.12 +/- 0.02 N=2; TgVEG; 0.10 +/- 0.04 N=2 *P*=0.64; Figure 2C-D). These data highlight parasite replication as a potentially important component in determining differences in

virulence between these species, since pathogenesis *in vivo* is often (but not always) linked to parasite burden (*165*).

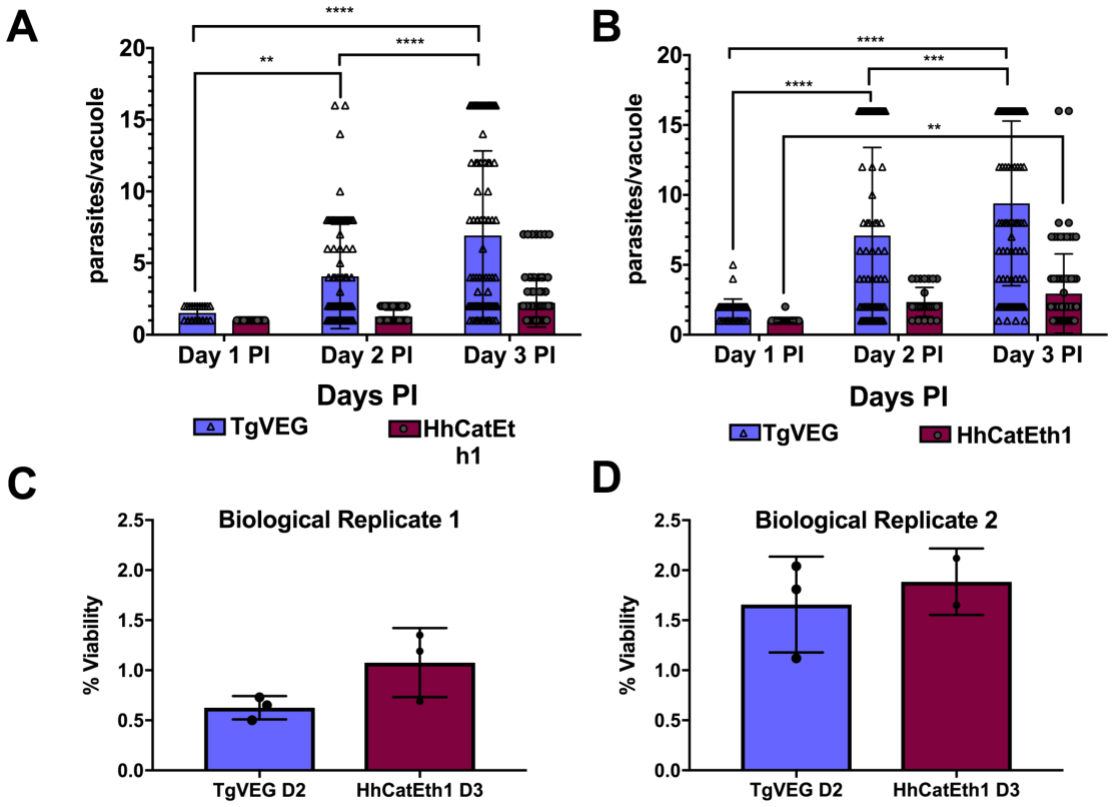

Figure 2. *T. gondii* and *H. hammondi* maintains similar infection rates, but *T. gondii* replicates at significantly higher rates.

A-B) Confluent monolayers of HFFs were infected with either HhCatEth1 or TgVEG sporozoites, obtained via *in vitro* excystation at an MOI of 0.5. Infected monolayers were fixed at 1, 2, and 3 DPI and assayed for the number of parasites observed in each vacuole for infection with *T. gondii and H. hammondi* for a total of 2 replicates, Replicate 1 (A) and Replicate 2 (B). Vacuoles containing more than 16 parasites were binned at 16 as it was defined as the limit of confident detection. Bars represent mean ± SD. For both Biological Replicate 1 & 2, there was a significant difference between the number of parasites per vacuole on Days 1, 2, &3 PI for TgVEG. For Biological replicate 1, there was no significant difference between the number of parasites per vacuole for HhCatEth1 on Days 1, 2 & 3 PI. For Biological Replicate 2, there was a significant difference in the number of parasites per vacuole between 1 and 3 DPI for HhCatEth1. Statistical significance was determined with a 2-Way ANOVA and Tukey's multiple comparison

test. C-D) There is no significant difference in sporozoite infectivity between HhEthCat1 and TgVEG. Graphs demonstrate the *in vitro* percent viability of excysted HhCatEth1 and TgVEG sporozoites 2 and 3 days, respectively, post excystation. Bars show the mean ± SD of three technical replicates. The viability assay was repeated with two biological replicates and there was no significance in viability between species within experiments, determined via unpaired t-test with Welch's correction.

Table 2. Median and maximum parasites per vacuoles during 1, 2, and 3 DPI for TgVEG and HHCatEth1

	Day 1	**Day 2**	**Day 3**
	Median, Maximum	**Median, Maximum**	**Median, Maximum**
HhCatEth1 Replicate 1	1, 1	1, 2	2, 4
HhCatEth1 Replicate 2	1, 2	2, 4	2, 16
TgVEG Replicate 1	2, 2	2, 16	4, 16+
TgVEG Replicate 2	2, 4	4, 16+	8, 16+

2.2.2 Both *T. gondii* and *H. hammondi* spontaneously form tissue cysts, but do so with different dynamics and efficiency

All *T. gondii* strains studied to date can be cultured indefinitely by serial passage in rodent intermediate hosts or in tissue/cell culture (*166*). In contrast, when grown in tissue culture *H. hammondi* ultimately differentiates into a cyst form that is only orally infectious to the definitive feline host (*42*). Interestingly, some strains of *T. gondii* (e.g., strains VEG and EGS (*80*, *162*, *167*)) are known to spontaneously form cysts in tissue culture. To elucidate the temporal dynamics of differentiation and tissue cyst formation in *H. hammondi* and compare them to *T. gondii*, we infected HFFs with TgVEG or HhCatEth1 sporozoites and stained them with *Dolichos biflorus* Agglutinin (DBA) at 4 and 15 days post-infection (DPI) to identify tissue cysts (Figure 3A). While all TgVEG and HhCatEth1 vacuoles were DBA-negative at 4 DPI, at 15 DPI ~80% (152/182) of *H. hammondi* vacuoles were DBA-positive, compared to 15% (34/355) of TgVEG vacuoles ($P<0.0001$; Figure 3B). To more precisely determine the temporal dynamics of tissue cyst formation, we quantified spontaneous cyst formation with TgVEG (Figure 3C) or HhCatAmer (Figure 3D) over the course of 23 days. Both TgVEG and HhCatAmer spontaneously formed DBA-positive tissue cysts as early as 8 and 12 DPI, respectively. By 23 DPI 100% of all HhCatAmer vacuoles were DBA-positive, while the percentage of DBA-positive TgVEG vacuoles never exceeded 20% (Figure 3C, D). TgVEG cultures had to be passed 3 times over the course of the experiment to prevent complete lysis of the host cell monolayers, which is consistent with their propagation as a mixed population of tachyzoites and bradyzoites. These data demonstrate that *H. hammondi* undergoes a much more rigid developmental program during *in vitro* cultivation compared to *T. gondii*, resulting in 100% tissue cyst conversion and what is likely a near complete arrest in growth.

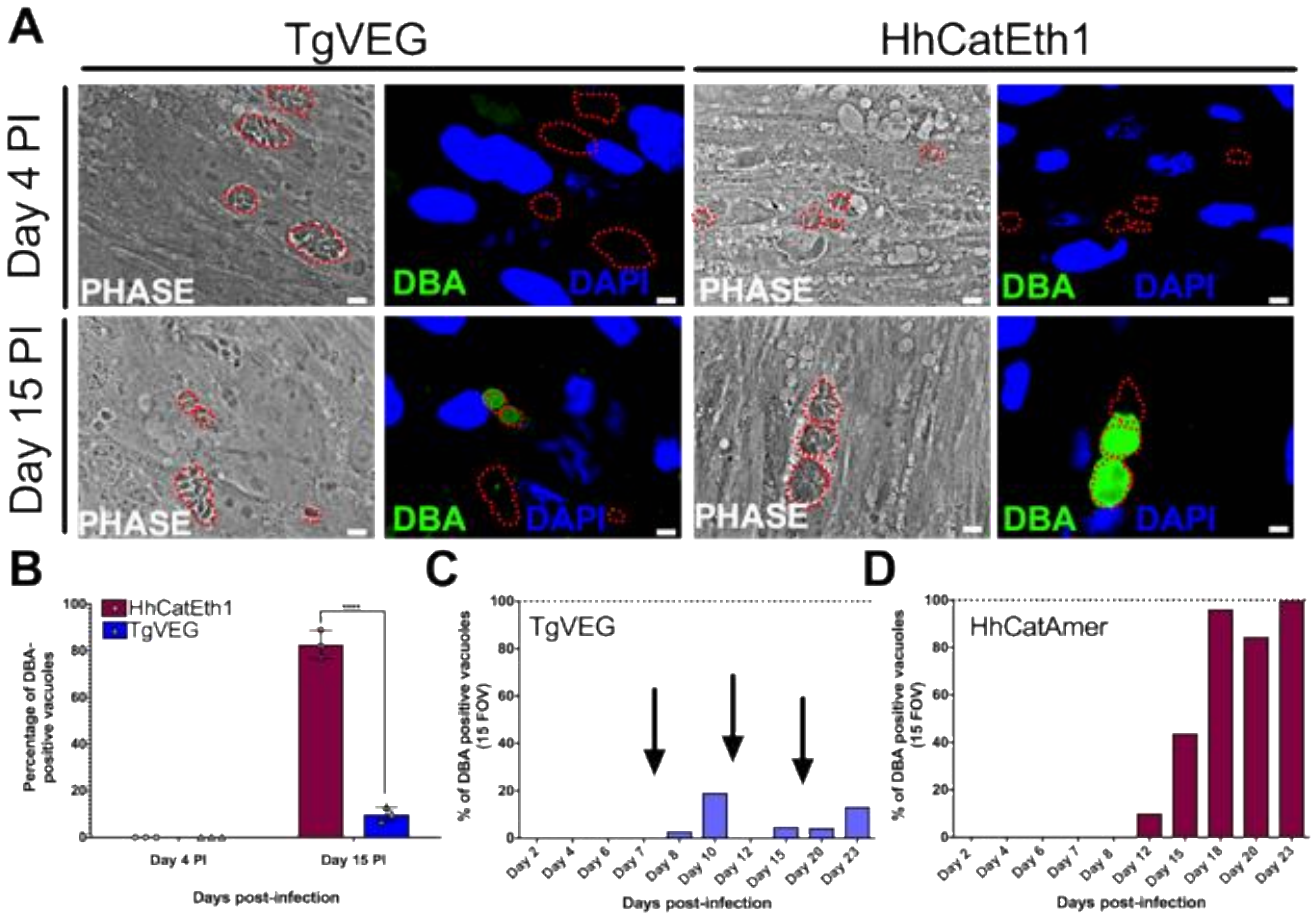

Figure 3. *T. gondii* and *H. hammondi* spontaneously form tissue cysts *in vitro*, but do so with different dymanics.

A) Representative images of cells infected with *T. gondii* (TgVEG) and *H. hammondi* (HhCatEth1) sporozoites that were fixed and stained with DBA after 4 and 15 DPI. Scale bar represents 5µm. B) Quantification of *T. gondii* and *H. hammondi* infection described in A demonstrating that after 4 days, neither *H. hammondi* or *T. gondii* spontaneously form tissue cysts, but both parasite species form tissue cysts after 15 DPI. However, the percentage of *H. hammondi* tissue cysts is significantly increased after 15 DPI when compared to *T. gondii.* Numbers above bars indicate number of DBA-positive vacuoles out of total vacuoles quantified. Statistical significance was determined using a 2-way ANOVA with Sidak's multiple comparison test. (****=P<0.0001). C and D) Average percentage of DBA-positive vacuoles in 15 FOV over a course of a 23 day infection with *T. gondii* (TgVEG) & *H. hammondi* (HhCatAmer). Arrows in (C) indicate when *T. gondii* was passed onto new host cells to prevent complete lysis. D) *H. hammondi* form tissue cysts after 12 DPI. The percentage of DBA-positive vacuoles increases until all vacuoles are DBA-positive

at 23 DPI. C) *T. gondii* forms tissue cysts at 8 DPI, however, the percentage of DBA-positive vacuoles does not reach 100% during the 23 day infection.

2.2.3 The spontaneous differentiation process in *H. hammondi* is characterized by the increased abundance of hundreds of known bradyzoite-specific genes

Our previous work showed that the *H. hammondi* oocyst transcriptome (consisting of sporulated and unsporulated oocysts) was significantly more "bradyzoite-like" than *T. gondii* sporozoites (*72*), and we reasoned that this was consistent with the propensity of this species to spontaneously form cysts during *in vitro* cultivation. However, these transcriptome studies were from the quiescent oocyst life stage and provided no insight into the developmental dynamics of the *H. hammondi* transcriptome compared to *T. gondii*. To compare the dynamics of the replicating *H. hammondi* and *T. gondii* transcriptomes during *in vitro* development, we used RNAseq on day 4 (D4) and day 15 (D15) *in vitro* cultured *H. hammondi* and *T. gondii*. Using existing genome annotations (*43*), we identified 7372 putatively orthologous genes between *T. gondii* and *H. hammondi* (ToxoDB.org; likely a conservative estimate of shared gene content between these species). As expected based on their *in vitro* growth rates (Figure 2), the number of reads mapping to the *H. hammondi* transcriptome was lower overall compared to those mapping to *T. gondii* (Figure 4A), and this was particularly pronounced at 15 DPI. To mitigate the effect this could have on falsely categorizing transcripts as being of higher abundance in *T. gondii* compared to *H. hammondi*, we included a given gene in downstream analyses only if one *H. hammondi* D4 and one *H. hammondi* D15 sample had at least 5 reads. This reduced the overall size of the queried gene set to 4146, and all analyses were performed with this subset.

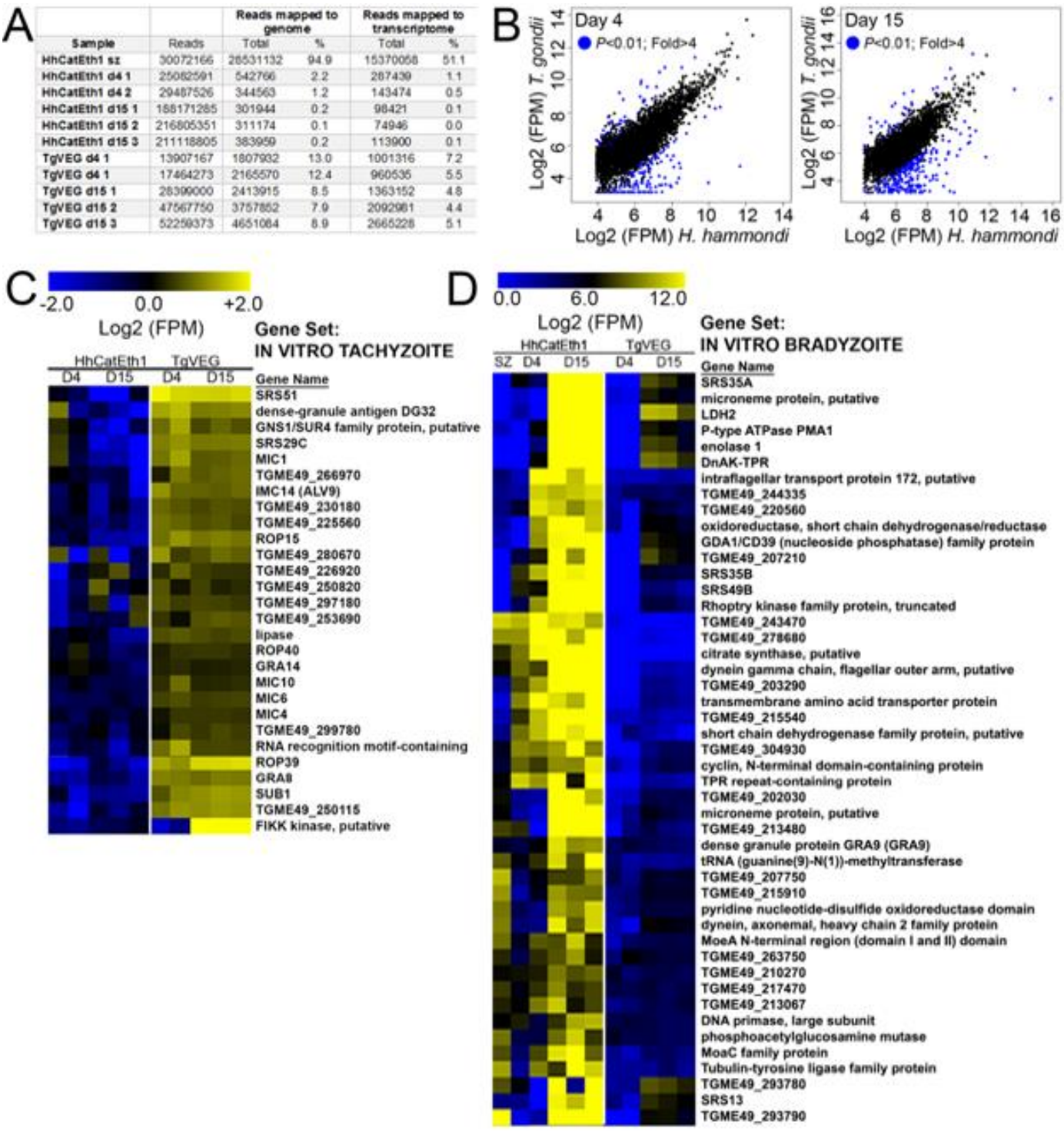

Figure 4. Transcriptional profiling and Gene Set Enrichment Analysis of *T. gondii* and *H. hammondi*

A) Summary of reads obtained for each parasite species and life stage, and the percentage of reads from each that mapped to the respective parasite genomes or transcriptomes. B) Log_2-transformed and normalized Fragments Per Million (FPM) data for the 4276 shared genes between *T. gondii* and *H. hammondi* that passed thresholds for detection

in both species. Genes of significantly different abundance (based on criteria as listed in inset) are blue. C) Hierarchical cluster (Euclidean distance, complete) of all detectable genes belonging to the *IN VITRO* TACHYZOITE gene set. Raw Log_2 transformed FPM values (taken from DESeq2 following normalization and transformation using "rlog") are shown. D) Hierarchical cluster (Euclidean distance, complete) of all detectable genes belonging to the *IN VITRO* BRADYZOITE gene set. Raw Log_2 transformed FPM values (taken from DESeq2 following normalization and transformation using "rlog") are shown. Gene sets are described in Table 3.

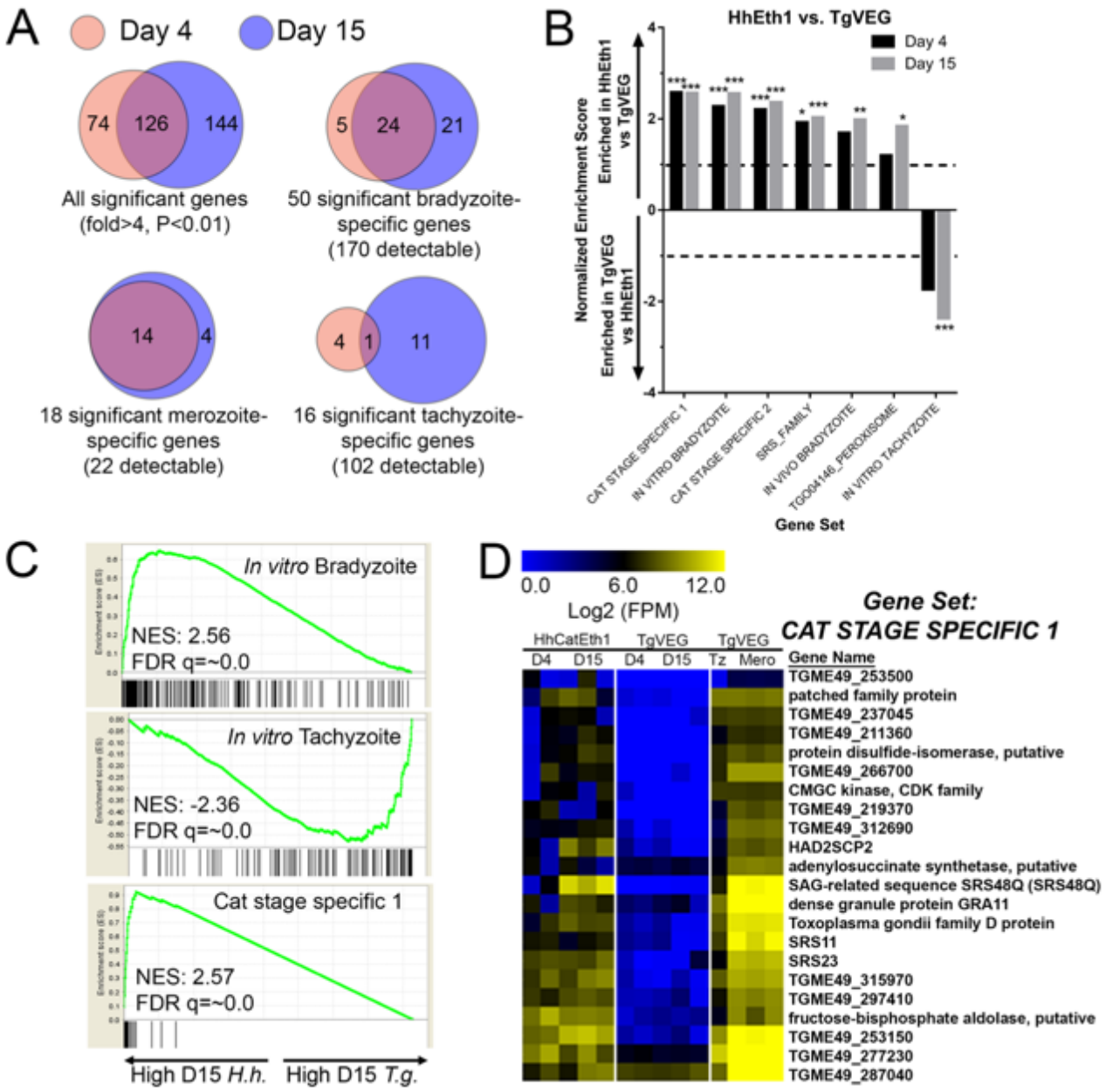

Figure 5. mRNAseq comparisons between *T. gondii* and *H. hammondi* indentify unique aspects of the *H. hammondi* transcriptome.

A) Venn diagrams indicating the degree of overlap in genes of significantly different transcript abundance between *T. gondii* and *H. hammondi* at D4 and D15 post-infection. B) Gene Sets found to be significantly (FDR q-value < 0.05) enriched in *H. hammondi* high-abundance transcripts (top) or *T. gondii* high-abundance transcripts (bottom) at either 4 or 15 days in culture. Gene Set Details can be found in Table 2. *: P<0.05; **: P<0.01; ***: P<0.001. C) GSEA plots of the *in vitro* bradyzoite, *in vitro* tachyzoite, and Cat stage specific 1 gene sets, showing enrichment profiles

between *H. hammondi* and *T. gondii* at 15 DPI. NES; Normalized enrichment score. FDR q: False discovery rate q-value. D) Hierarchically clustered expression data for detectable genes in the CAT STAGE SPECIFIC 1 gene set in *H. hammondi* or *T. gondii* grown for 4 or 15 days *in vitro*, or for *T. gondii* grown as tachyzoites or merozoites (in cat enteroepithelial cells).

When $\log_2$ transformed and DESeq2-normalized RPM (mapping Reads Per Million) values were plotted for D4 and D15 between species we observed a high correlation in transcript levels at both time points (Figure 4B). While the majority of genes were expressed at similar levels between *T. gondii* and *H. hammondi*, we identified multiple transcripts of significantly different abundance (Figure 5A and blue data points in Figure 4B).

We used Gene Set Enrichment Analysis (GSEA(*168*)) with previously published(*169*) and our own curated gene sets (Table 3) to identify gene classes with species-specific enrichment on D4 and D15 (see Methods and Table 2 for Gene Sets). We identified 7 gene sets that showed significant species-specific enrichment (FDR q-value<0.01; NES scores shown in Figure 3B). *H. hammondi* profiles showed significant enrichment for *in vitro* (D4, D15) and *in vivo* (D15) bradyzoite gene sets (Figure 5B,C; heat maps shown in Figure 4D), showing that replicating *H. hammondi* zoites maintain the "bradyzoite-like" transcriptional profile previously observed in sporozoites after at least 15 days in culture (25). Moreover, *T. gondii* showed significant enrichment compared to *H. hammondi* for *in vitro* tachyzoite genes at 15 DPI (Figure 5B; heatmap shown in Figure 4C), a time point at which VEG is <10% DBA-positive while *H. hammondi* is between 40-80% DBA-positive (Figure 3B,C). Overall, these data are consistent with our general understanding of transcript abundance changes that occur during the tachyzoite to bradyzoite transition (albeit entirely from studies using *T. gondii*).

Table 3. Additional gene sets used in Gene Set Enrichment analyses

Gene Set Name	Search Strategy on ToxoDB	Size
SRS_Family	Text search for "SAG-related sequence SRS"	111
AP2_family	Text search for "AP2 domain transcription factor"	66
CAT STAGE SPECIFIC 1	Cat enteroepithelial stages at least 40-fold higher than Tachyzoite at D3, D5 or D7	293
CAT STAGE SPECIFIC 2	Cat enteroepithelial stages >90th percentile in any of D3, D5 or D7; Tachyzoite expression between 0 and 50th percentile	81

A more unexpected finding was that at both D4 and D15, *H. hammondi* had a transcriptional profile that was significantly enriched for genes of high transcript abundance in *T. gondii* merozoites replicating in cat enteroepithelial cells but poorly expressed in other life stages(*169*, *170*) (CAT STAGE SPECIFIC 1, 2; Figure 5C,D). Specifically, out of the 21 detectable members of the "CAT STAGE SPECIFIC 1" gene set, 18 were ranked in the top 308/4146 (7.4%) and 174/4146 (4.2%) of genes of greater abundance in *H. hammondi* D4 and D15 zoites, respectively (Figure 5C). To validate this finding we performed RNAseq on *T. gondii* and *H. hammondi*-infected THP-1 cells 24 hours post-infection and found a consistent and highly significant enrichment for these same gene sets (Figure 6A-C), and in this case a similar number of reads from *H. hammondi* and *T. gondii* mapped to their respective parasite transcriptomes (Figure 6D). These data suggest that *H. hammondi* has aspects of its transcriptional profile that are independent of its spontaneous conversion to bradyzoites and that a subset of genes that are

uniquely expressed in *T. gondii* merozoites and sporozoites may not share these same profiles in *H. hammondi*.

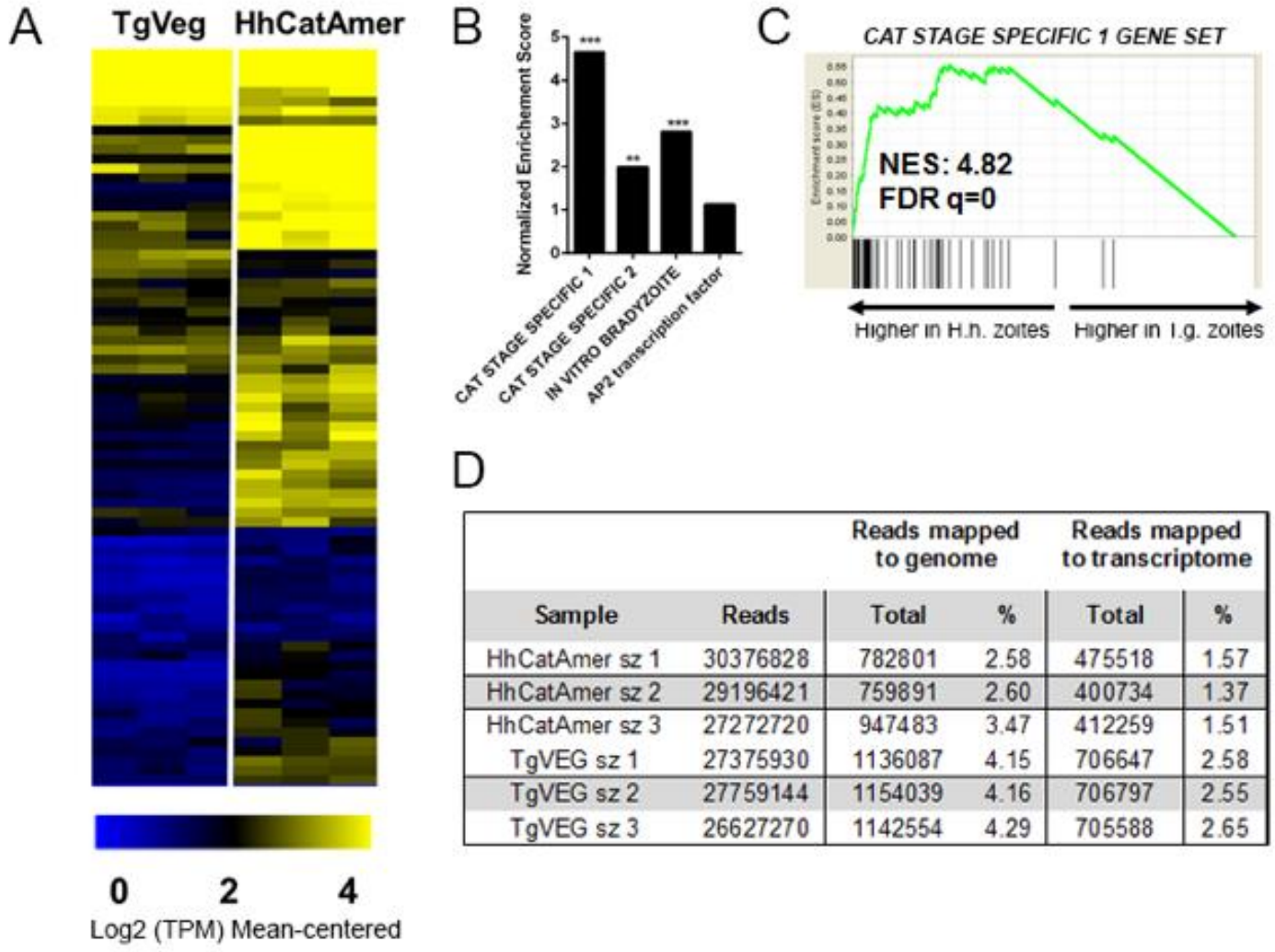

D

		Reads mapped to genome		Reads mapped to transcriptome	
Sample	Reads	Total	%	Total	%
HhCatAmer sz 1	30376828	782801	2.58	475518	1.57
HhCatAmer sz 2	29196421	759891	2.60	400734	1.37
HhCatAmer sz 3	27272720	947483	3.47	412259	1.51
TgVEG sz 1	27375930	1136087	4.15	706647	2.58
TgVEG sz 2	27759144	1154039	4.16	706797	2.55
TgVEG sz 3	26627270	1142554	4.29	705588	2.65

Figure 6. mRNA-seq comparisons between TgVEG and HhCatAmer sporozoites identify unique *H. hammondi* transcriptome profiles

A) A heat map illustrates differential expression profiles of cat stage specific genes enriched for TgVEG and HhCatAmer. The relative levels of gene expression (mean-centered log_2-fold change) are depicted using a color scale where blue indicates the lowest level of expression and yellow indicates the highest level of expression. B) Gene sets found to be enriched in *H. hammondi* high-abundance transcripts at 1 day post-excystation. Gene set details can be found in Table 2. (***: FDR q<0.001; **: FDR q<0.01). The AP2 transcription factor gene set is provided as a negative

control. C) GSEA plot of cat stage specific 1 gene set, showing enrichment profiles between *H. hammondi* and *T. gondii* at 1 day post-excystation. NES: Normalized enrichment score. FDR q: False discovery rate q-value. D) A summary of reads obtained for each parasite species, and the percentage of reads from each that mapped to the respective parasite genomes or transcriptomes. A total of 8912 genes that had at least 1 read in both TgVEG and HhCatAmer samples were selected for analysis.

We also validated a subset of transcripts that were of greater abundance in D4 and D15 cultivated *H. hammondi* parasites using qPCR (heatmap of selected genes in Figure 7A). We used *ROP18* as a control for a gene that was of significantly higher abundance in *H. hammondi* compared to *T. gondii* (TgVEG and other Type III strains express very little *ROP18* transcript due to a promoter indel (*68, 72, 171*) and *CDPK1* and *AMA1* as control genes of similar abundance between the two species. *GRA1* transcript levels were used as loading controls. We used validated primer sets for 8 genes (which had to be made separately for each species) to quantify 8 transcripts (plus *ROP18*) using qPCR on RNA freshly isolated from D4 and D15 HhCatEth1 and TgVEG cultures. As expected *ROP18* transcript was found to be >1000-fold greater in abundance in HhCatEth1 compared to TgVEG, while *CDPK1* and *AMA1* transcript levels were not significantly different between species (Figure 7B). The remaining 9 queried transcripts showed significantly higher abundance in *H. hammondi* compared to *T. gondii* (Figure 7B) confirming the validity of our approach to analyze, normalize and filter cross-species RNAseq data with significant differences in read counts.

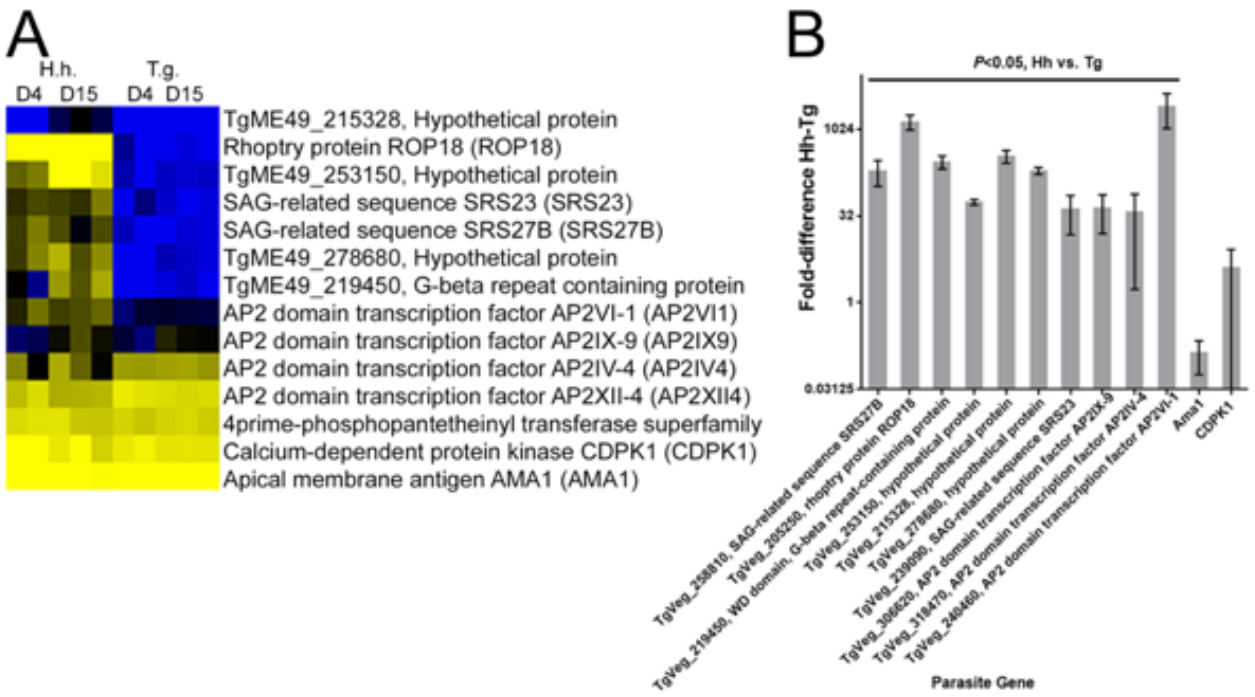

Figure 7. qPCR validation for nine transcripts that were found to be of higher abundance in D4 or D15 *H. hammondi* compared to *T. gondii.*

A) Clustered Log2(TPM) value taken from RNAseq expression profiles of HhCatEth1 and TgVEG at 4 and 15 DPI. Gene models are from TgME49 since that is the most well-annotated *T. gondii* genome and upon which our synteny maps were based. B) qPCR for 9 transcripts show significantly higher transcript level in HhCatEth1 compared to TgVEG at D4 pi. Fold difference of HhCatEth1 genes relative to TgVEG is shown; bars represent mean and SD from three biological replicates. Significance was determined from ΔCt values using multiple t-tests and the Holm-Sidak method, with alpha=5.0%. *Apical membrane antigen 1* (*AMA1*) and *calcium dependent protein kinase 1* (*CDPK1*) genes served as examples of transcripts found to not differ between species and transcript abundance values were normalized using parasite GAPDH genes. All genes were queried using species-specific primers.

2.2.4 *H. hammondi* can be subcultured successfully *in vitro*

From a phylogenetic standpoint, *H. hammondi* is a good model to understand the genetic basis for traits that are unique to *T. gondii*. However, unlike all *T. gondii* strains studied to date,

sporozoite-initiated cultures of *H. hammondi* in host cells from multiple organisms including humans, cattle, and non-human primates lose their ability to be subcultured *in vitro* (*55, 65*). In order to precisely define when *H. hammondi* sporozoites lose the ability to infect new cells, we attempted to subculture *H. hammondi* zoites after defined periods of cultivation (Figure 8A-B). We found that *H. hammondi* zoites were capable of infecting and replicating within new host cells for up to 8 days post-excystation (Figure 8C-F), while we did not observe any evidence of growth when subcultures were initiated on days 11 and 15 post-excystation (Figure 8G-H). In agreement with previous studies (*42, 55, 65*), we also observed that the number of visible *H. hammondi* vacuoles disappear over time (Figure 8C-E). We did not identify any vacuoles derived from lysing and re-invading parasites (which would have comparatively smaller sizes) after 10 DPI as we only observed a general increase in vacuole size prior to their disappearance from culture (Figure 9). Together, our data support previous work showing that *H. hammondi* cannot be subcultured with high efficiency after approximately one week or longer in culture (*55, 65*), but importantly we identified a previously unknown window prior to spontaneous tissue cyst formation where this parasite can be effectively subcultured.

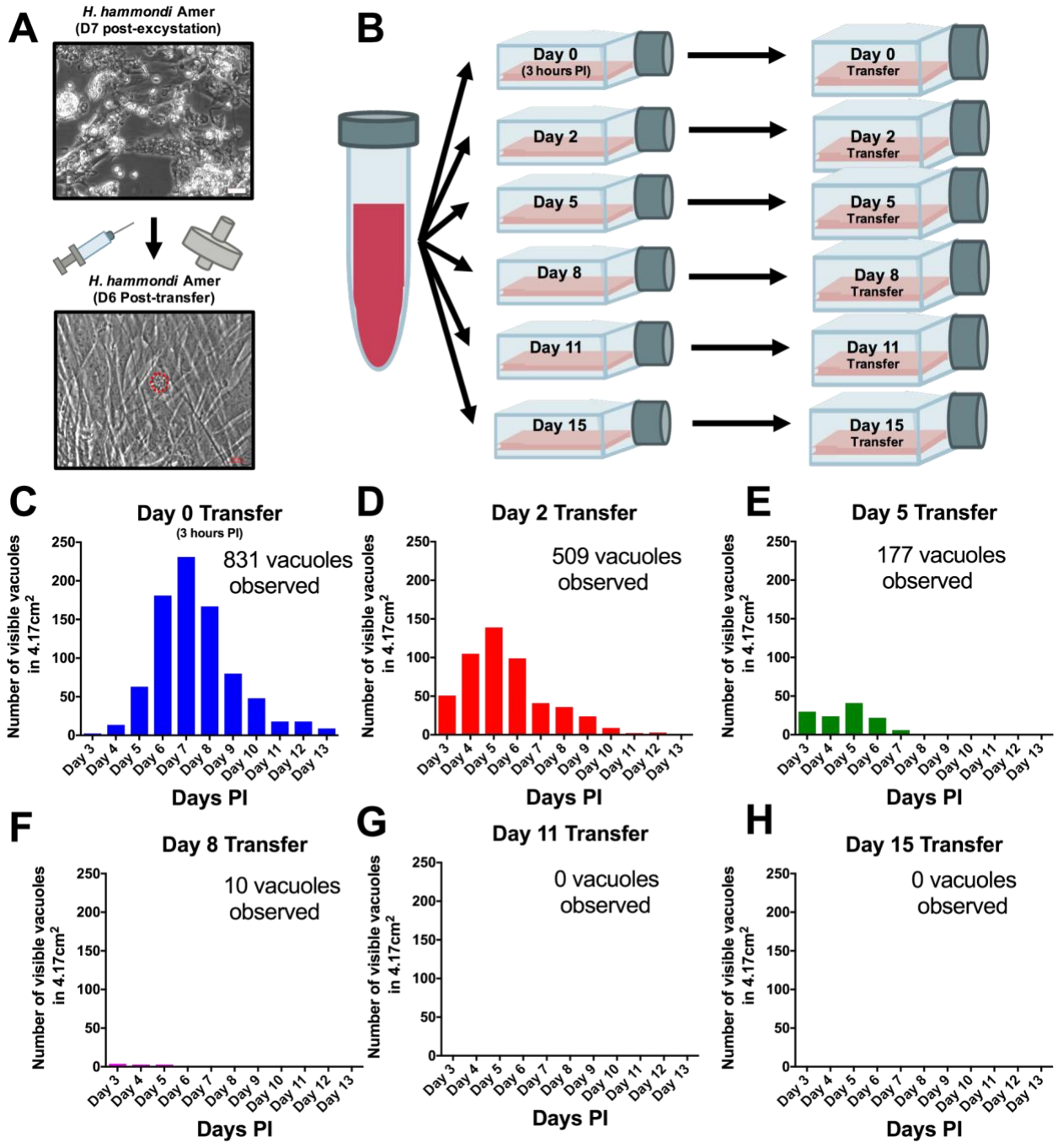

Figure 8. *H. hammondi* can be successfully subcultured *in vitro* for a limited period of time.

A) Monolayers containing HhCatAmer with oocyst debris were needle passaged, filtered, and used to infect a confluent monolayer of HFFs seven days post-excystation. Vacuoles were observed in subcultured monolayers after 6 DPI. B-H) Confluent monolayers of HFFs were infected with HhCatAmer sporozoites at an MOI of ~2. (2,812,500 sporozoites). After a three-hour incubation at 37° C, the Day 0 transfer flask was scraped, needle passaged, filtered,

and transferred to a new host cells. This process was repeated after 2, 5, 8, and 15 days of growth. Each flask was monitored daily for the number (C-H) for 13 DPI, or until visible vacuoles were no longer detected. The number of visible vacuoles increased in number for the first week post-excystation then began to decrease. Replicative capacity was greatest for sporozoites transferred to new host cells at Day 0 (C) and decreased during each subsequent passage. (D-H).

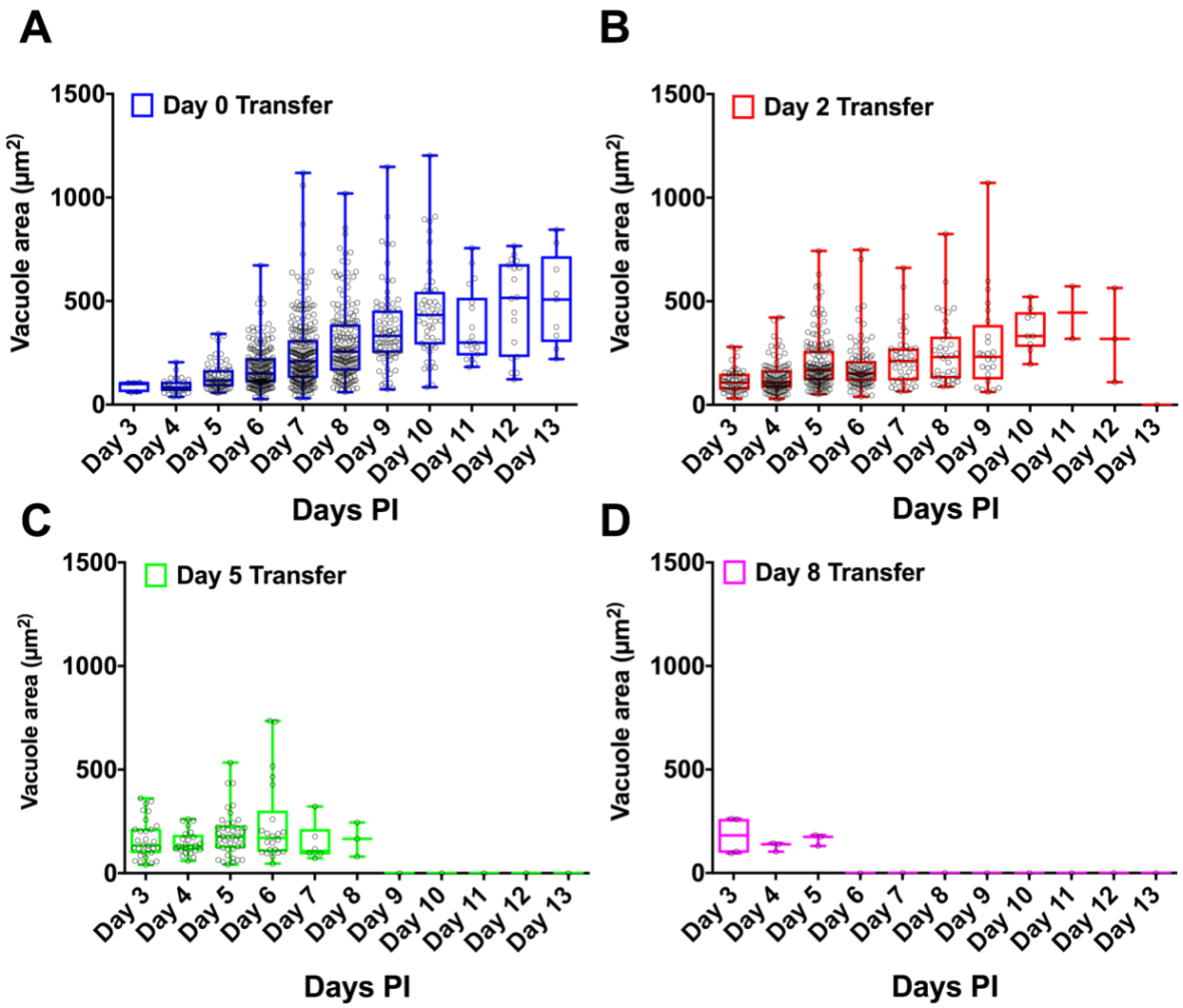

Figure 9. *H. hammondi* vacuole sizes following subculture.

A-D) Visible vacuoles sizes were measured using ImageJ (NIH) for each day of attempted subculture. Vacuole size progressively increases over the course of *in vitro* cultivation, after which the size plateaus.

When we performed similar experiments *in vivo*, we observed that the ability to be subcultured *in vitro* and infectivity in a mouse model of infection were temporally correlated. We cultivated *H. hammondi* sporozoites in HFFs for 5 days and used them to infect mice intraperitoneally (50,000 zoites). As early as 2 DPI, we measured interferon-gamma (IFNγ) production indicative of an active infection (Figure 10A). We used PCR to detect *H. hammondi* DNA in spleens and resident peritoneal cells in these same mice 3 weeks post-infection (PI) (Figure 10B). Histological examination of muscle from infected mice using anti-*Toxoplasma* antibodies that cross-react with *H. hammondi* showed the presence of the parasites in the muscle tissue of the mouse infected with *in vitro*-passed *H. hammondi* (right panel, Figure 10C) which were similar to those observed after oral inoculation with *H. hammondi* sporulated oocysts (middle panel; Figure 10C). Overall, these data show that *H. hammondi* parasites grown *in vitro* are capable of a) inducing an immune response in mice during the acute phase of infection, and b) disseminating to multiple mouse tissues and establishing a chronic infection that resembles an infection resulting from oral gavage with sporulated oocysts. To determine how long mouse infectivity was retained in *in vitro* cultivated *H. hammondi*, mice were injected intraperitoneally with 50,000 zoites grown *in vitro* for 6, 8, 10, 13, and 15 days, and monitored for signs of infection by measuring serum IFNγ levels. The ability to be subcultured *in vitro* correlated perfectly with the ability to initiate infections in mice *in vivo*. Specifically, we observed an increase in IFNγ levels in mice infected with 6 DPI or 8 DPI *in vitro* zoites (Figure 10D), while we did not see an increase in IFNγ levels in those infected with parasites cultured for 10, 13, and 15 days (Figure 10D). To our knowledge this is the first time that sporozoite-derived growth stages of *H. hammondi* have been used to initiate infections in an intermediate host, since all previous studies focused on parasite that had already terminally differentiated.

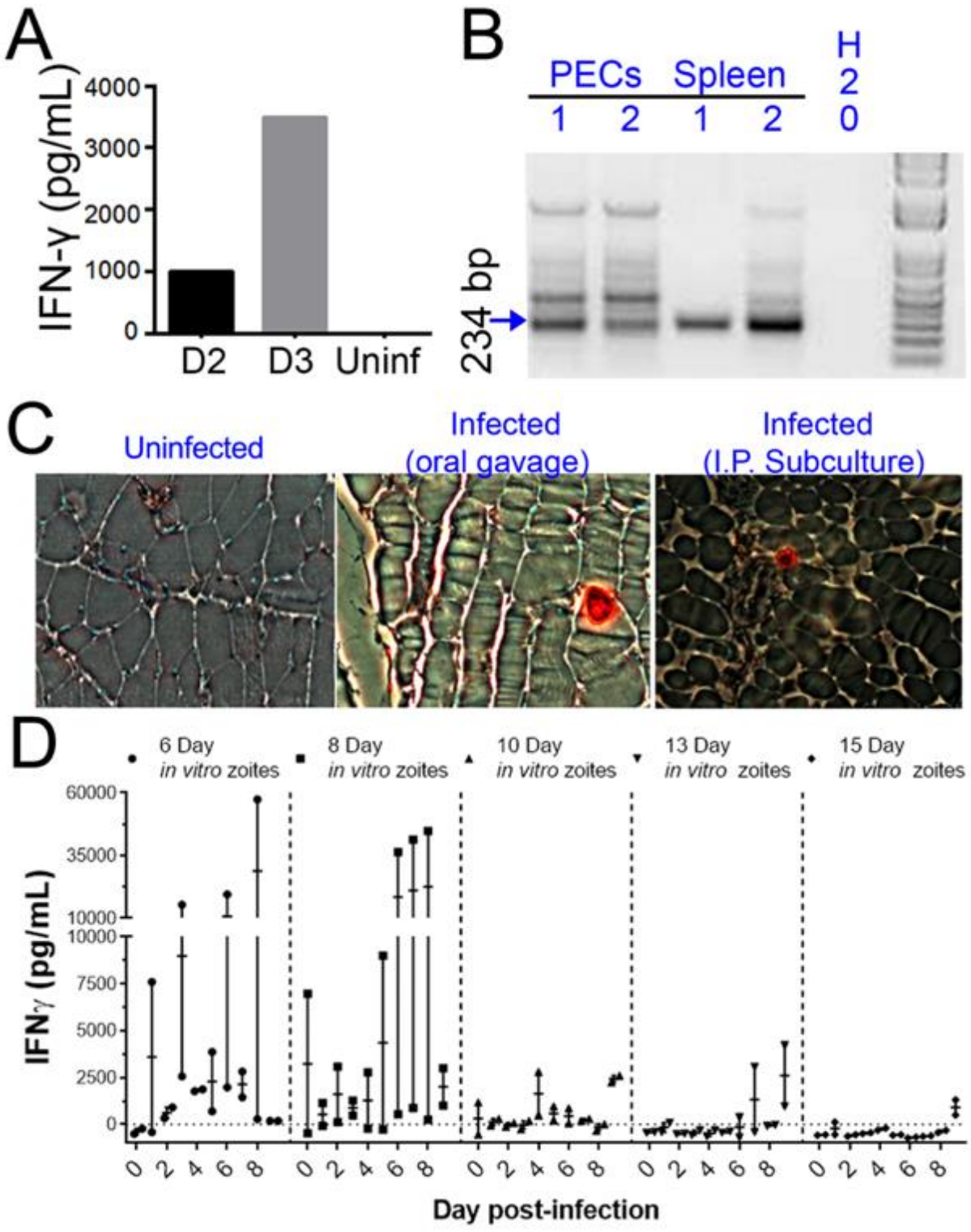

Figure 10. *H. hammondi* parasites can be grown *in vitro* and then used to successfully infect mice.

A-C) Two Balb/C mice were infected with ~50,000 *H. hammondi* zoites grown *in vitro* for 5 days. A) Serum was collected on days 2 and 3 and assayed for interferon-γ. B) Three weeks post-infection, DNA was harvested from

peritoneal lavage cells and spleen and assayed for *H. hammondi* DNA using *H. hammondi*-specific primers. Arrow indicates primary band for *H. hammondi*-specific PCR, although we also routinely see larger bands after PCR amplification. Samples were only considered positive if the 234 bp band was present (arrowhead). C) Leg muscles from infected mice were sectioned and stained with *H. hammondi*-reactive anti *Toxoplasma* antibodies and compared to uninfected mice and mice infected with *H. hammondi* by oral gavage with 50,000 sporulated oocysts. D) *In vitro* cultivation leads to a dramatic and predictable loss in the ability to infect mice. Two BALB/C mice were infected with 50,000 *H. hammondi* American parasites after 6, 8, 10, 13, and 15 days of *in vitro* growth. The mass of the mice was monitored and a serum sample was obtained daily for 9 days post-infection. Analysis of IFN-γ production was analyzed in serum samples using an ELISA. Mice infected with parasites grown *in vitro* for 6 days (1 of 2) showed spikes in IFN-γ levels. This IFN-γ spike was also observed in mice infected with parasites grown *in vitro* for 8 days (2 of 2), while no IFN-γ was observed in mice infected with parasite grown *in vitro* for 10, 13, or 15 days.

2.2.5 Generation of transgeneic *Hammondia hammondi*

Genetic manipulation of *H. hammondi* has not been reported in the literature. Given the genetic similarity between *T. gondii* and *H. hammondi* (*43*, *68*) and the apparent interchangeability of promoter sequences between them (*68, 72*), we transfected ~4 million HhCatAmer sporozoites with a UPRT-targeting CRISPR/CAS9-GFP plasmid (*172*) along with a PCR2.1 Topo-cloned *dsRED* cassette with 20 bp sequences flanking the CAS9 nuclease cut site within the *H. hammondi UPRT* gene. We used the *Toxoplasma*-specific plasmid to target *H. hammondi UPRT* as the gRNA sequence is identical between *T. gondii* and *H. hammondi*. Both plasmids were taken up and expressed by *H. hammondi*, as evidenced by GFP-fluorescence in the parasite nuclei and red fluorescence in the cytoplasm (Figure 11A). Importantly, transgenic parasites replicated *in vitro* as evidenced by the presence of multicellular vacuoles in the infected monolayer (Figure 11A). Transfection efficiency of viable parasites (as evidenced by those replicating *in vitro* with CAS9-GFP and/or dsRED staining) was ~4% (15 out of 350 vacuoles at 48 h post-transfection, data not

shown), which is consistent with typical transfection efficiencies observed with most strains of *T. gondii* (*173*).

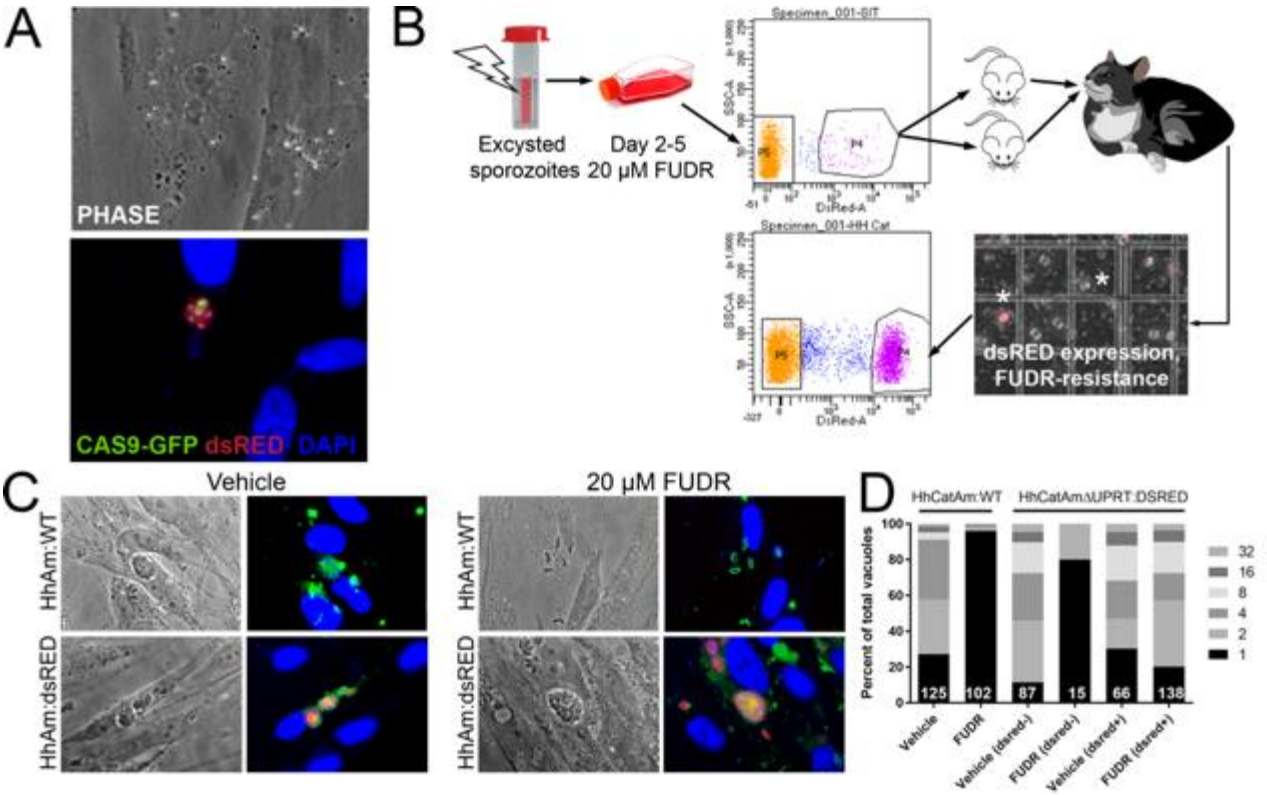

Figure 11. Generation of stable transgenic *Hammondia hammondi*.

A) *H. hammondi* zoites co-transfected with CRISPR/CAS9-GFP and a plasmid harboring a *T. gondii* dsRED expression cassette. We identified multiple parasites with both GFP-tagged nuclei (due to CAS9-GFP expression) and dsRED-tagged cytoplasm, indicating uptake of both plasmids within the same parasites. B) Protocol for generating stably transgenic *H. hammondi* using flow cytometry and drug selection to enrich for transgenic parasites prior to cat infections. C,D) Testing FUDR resistance in transgenic *H. hammondi* parasites. WT and transgenic *H. hammondi* sporozoites were incubated in the presence or absence of 20 µM FUDR, and vacuole size and presence/absence of dsRED was quantified in at least 100 vacuoles per treatment condition. While WT and non-dsRED-expressing *H. hammondi* from the transgenic population were highly susceptible to FUDR treatment (as evidenced by the fact that the majority of vacuoles contained only 1 parasite), dsRED expressing transgenic parasites were resistant to FUDR treatment, confirming that the parasites harbored two genetic markers.

To make a stable transgenic parasite line, we transfected ~4 million parasites with the Hh*UPRT*:dsRED repair cassette and the Hh*UPRT*gRNA:CAS9:GFP plasmid and cultured them in 10 µM FUDR for 5 days. After FACS sorting ~12,000 dsRED-expressing zoites (~3% of the total parasite population; Figure 11B), we injected two female Balb/c mice intraperitoneally with ~6000 dsRED-expressing zoites each. For the first week of the infection, mice were injected 1X daily with 200 µL of 1 mM FUDR, and mice were euthanized and fed to a cat 4 weeks PI. Fecal floats showed the presence of dsRED-expressing sporozoites within some of the oocysts (Figure 11B), and ~32% of isolated sporozoites expressed dsRED based on FACS analysis (Figure 11B, bottom FACS plot). PCR screening (Figure 12) and the inability to grow parasites long term *in vitro* confirmed the identity of the fluorescent parasites as *H. hammondi*.

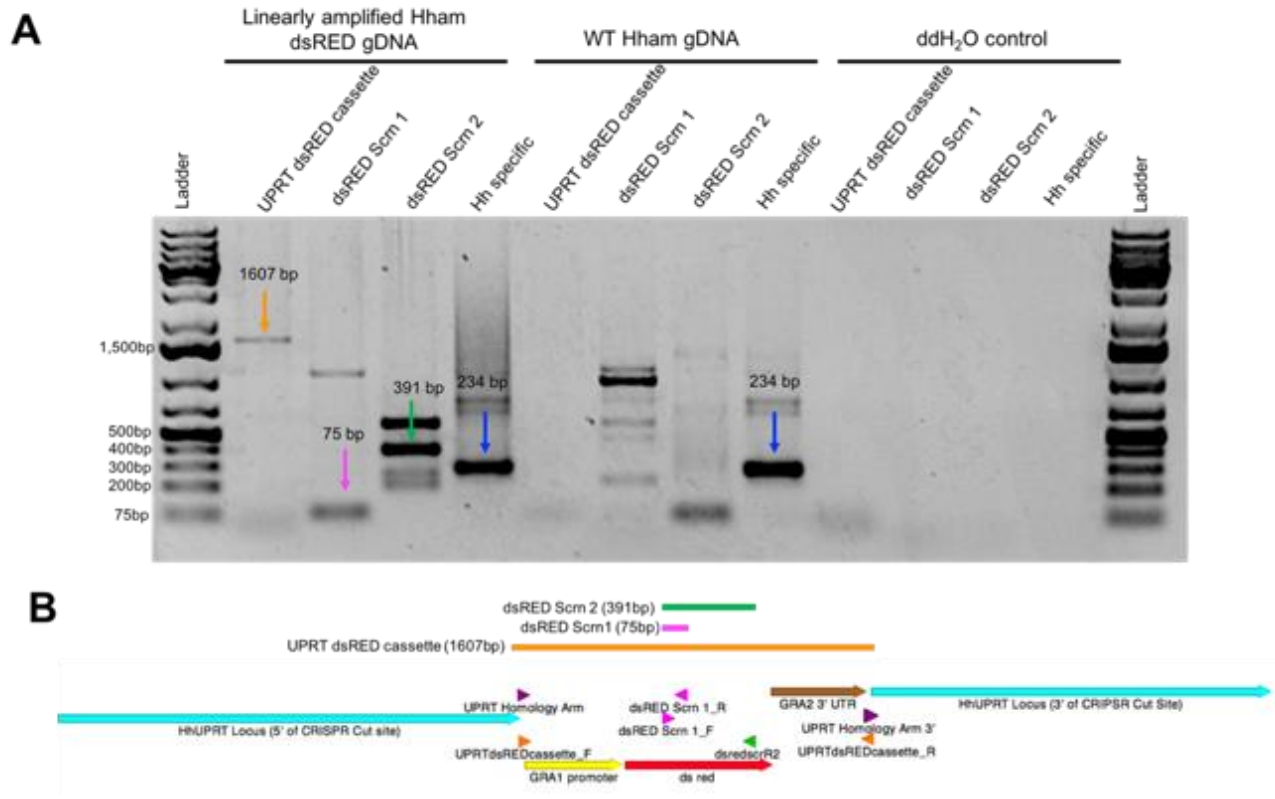

Figure 12. Validation of transgeneic *H. hammondi.*

A) PCR validation of *H. hammondi* dsRED-expressing parasites using primers targeting the UPRTdsREDcassette (1607bp product), dsRED (75 and 391bp products, respectively), and an *H. hammondi* specific sequence (234bp product). PCR reactions were conducted with 45ng of template DNA from linearly amplified Hham dsRED genomic DNA, WT Hham genomic DNA, of ddH_2O control. B) Schematic of UPRT dsRED cassette (generated using APE). Arrows indicate sequence features, arrowheads indicate location of primers. Colored lines indicate expected product.

To determine if our transgenic approach to disrupt the *UPRT* gene and insert a dsRED expression cassette was successful, we quantified the growth of $dsRED^{+}$ and $dsRED^{(-)}$ parasites in the presence of FUDR and compared it to wild type HhCatAmer. Fixed and permeabilized parasites were stained with cross-reactive anti-*Toxoplasma* antibodies to identify all vacuoles. After 4 DPI, we quantified vacuole size and dsRED-expression status in >100 vacuoles for each strain (WT and dsRED) and condition (Vehicle or 20 µM FUDR). As expected, HhCatAmer:WT grew poorly in FUDR (Figure 11C), while HhCatAmer:dsRED parasites grew similarly to untreated parasites (Figure 11C). When we separated parasite growth in FUDR based on dsRED expression, we found that $dsRED^{(-)}$ parasites in the *H. hammondi* population were just as susceptible to FUDR as were HhCatAmer:WT parasites (Figure 11D, first 4 bars), while $dsRED^{+}$ parasites grew equally well in FUDR compared to Vehicle (Figure 11D, right 2 bars). These data suggest that most, if not all, of the dsRED-expressing parasites are also null for the *UPRT* gene, either by direct replacement of the *UPRT* gene with the dsRED cassette or by incorrect non-homologous end joining and insertion of the dsRED cassette at another genomic location. This represents the first stably transgenic *H. hammondi* line. Furthermore, PCR analysis of linearly amplified genomic DNA from the HhCatAmer population expressing dsRED demonstrated that the Hh*UPRT*:dsRED repair cassette was incorporated into the genomic DNA of parasite within this population (Figure 12).

2.2.6 *H. hammondi* is completely resistant to pH-induced cysts formation

While *T. gondii* can spontaneously form tissue cysts following an *in vitro* sporozoite infection, it can also be chemically induced to form bradyzoites using a variety of treatments (*80*). Given the dramatic developmental differences between *T. gondii* and *H. hammondi in vitro* and *in vivo*, we reasoned that these parasite species may respond differently to external stressors that induced cyst formation. We therefore exposed *T. gondii* and *H. hammondi* zoites to alkaline pH bradyzoite induction media and identified cysts using DBA staining as above. As expected we found that TgVEG vacuoles grown in bradyzoite induction media were ~55% DBA-positive after 2 days of exposure and ~90% positive after 4 days of alkaline pH treatment (Figure 13A-B). However, we did not find a single DBA-positive *H. hammondi* vacuole at any time point (out of 297 total vacuoles; Figure 13A-B). Given the importance of parasite replication events and bradyzoite conversion (*174*), it is possible that the lack of cyst conversion in *H. hammondi* over a 4 day treatment was due to fewer replication cycles. While vacuole sizes for *T. gondii* and *H. hammondi* differed significantly after 2 days of growth in standard and bradyzoite induction media (Figure 13 C), pH treatment had no significant effect on vacuole size in either species (Figure 13C; P=0.63, 1.0, respectively). This result suggests that bradyzoite conversion occurs independently of changes or differences in replication rate and provides strong support for the fact that *H. hammondi* are immune to cellular stresses induced by bradyzoite induction conditions.

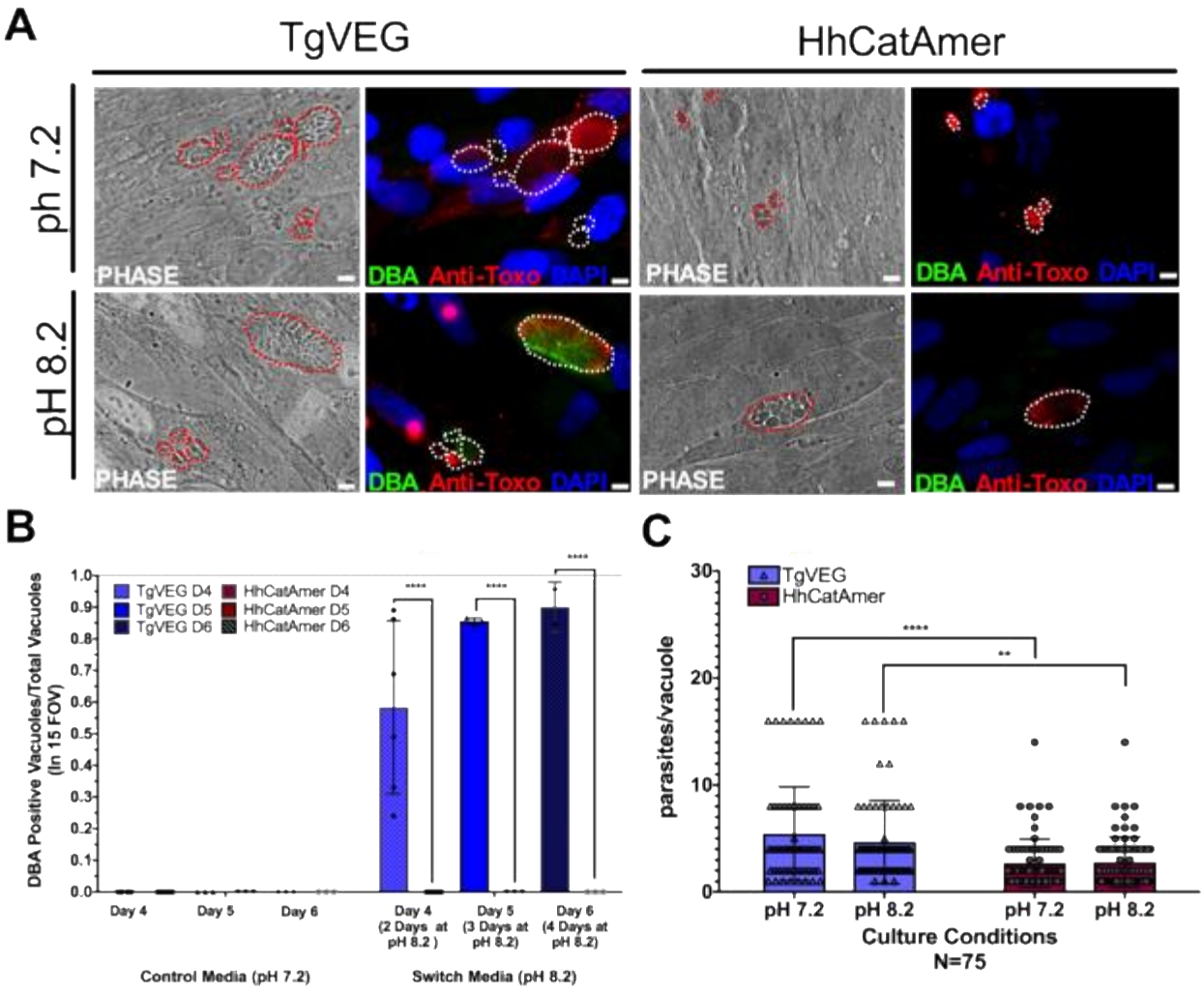

Figure 13. Conditions that induced *T. gondii* tissue cyst formation *in vitro* did not induce tissue cyst formation in *H. hammondi.*

A) Representative images of cells infected with *T. gondii* (TgVEG) and *H. hammondi* (HhCatAmer) sporozoites that were grown for 2 days in pH 7.2 media and switched to pH 8.2 media (bradyzoite induction conditions) for 2 days, fixed and stained with an Anti-*Toxoplasma gondii*/*Hammondia hammondi* antibody and DBA. Scale bar represents 5µm. B) Quantification of *T. gondii* and *H. hammondi* tissue cyst formation described in A demonstrating that *H. hammondi* does not form tissue cysts when exposed to conditions that promote tissue cyst formation in *T. gondii.* Number above bars indicated number of vacuoles quantified for each condition. Statistical significance was determined using a 2-way ANOVA with Tukey's multiple comparison test. (****=P<0.0001). C) Number of parasites per vacuole for both *T. gondii* & *H. hammondi* grown at pH 7.2 and pH 8.2. *T. gondii* has significantly more parasites

per vacuole than *H. hammondi* at both pH 7.2 and pH 8.2. There is no statistically significant difference between either *T. gondii* or *H. hammondi* between pH 7.2 and pH 8.2. Statistical significance was determined using a 2-way ANOVA with Sidak's multiple comparison test. (**=P<0.01 & ****=P<0.0001).

2.2.7 The *H. hammondi* transcriptome is mostly non-responsive to high pH exposure

Given the well-established impact of alkaline pH media on *T. gondii* cyst formation *in vitro* and the propensity of *H. hammondi* to spontaneously form cysts *in vitro*, we found it remarkable that we did not identify a single DBA-positive *H. hammondi* cyst after even 4 days of alkaline pH exposure. An intriguing hypothesis emerging from this result is that *T. gondii* is more adept than *H. hammondi* at responding to stress signals in its environment. To test this hypothesis with respect to pH exposure, we treated *T. gondii* and *H. hammondi* sporozoites with bradyzoite induction media for 2 days and performed RNAseq analysis to identify changes in their respective transcriptomes (Figure 14A). For *T. gondii* treated with alkaline pH, we observed significant enrichment in the *IN VITRO* BRADYZOITE and *IN VIVO* BRADYZOITE(*169*) gene sets (NES = -2.4902, -1.800, respectively; FDR q = ~0.00 for both) for TgVEG treated with alkaline pH (Figure 15 A-B), and the *IN VITRO* TACHYZOITE and *IN VIVO* TACHYZOITE gene sets under control conditions (NES = 1.94, FDR q = 0.001; NES = 1.87, FDR q=0.002, respectively; Figure 15A). This was in stark contrast to HhCatAmer in which members of the *IN VITRO* BRADYZOITE gene set showed no enrichment after alkaline pH exposure (NES = -1.1681, FDR q = 0.2078; Figure 15A-B). For the *H. hammondi* transcriptome, the *IN VITRO* BRADYZOITE gene set seemed to consist of two classes of genes: a) those that were not induced upon pH exposure in *H. hammondi* but were in *T. gondii* (top half of heatmap in Figure 15C) and b) those that were of high abundance in *H. hammondi prior* to exposure to high pH (lower half of heatmap

in Figure 15C). While we identified 90 transcripts that significantly differed in TgVEG following pH exposure (fold change value ≥ 2 and P_{adj} value < 0.01), we only identified 24 *H. hammondi* transcripts with pH-altered abundance (these are shown in Figure 15D). Importantly while the majority of pH-altered transcripts were of higher abundance in *T. gondii*, 21 out of 24 pH-altered transcripts in *H. hammondi* were of lower abundance, indicating that *H. hammondi* and *T. gondii* have distinct responses to high pH bradyzoite induction (Figure 15C,D; See supplementary file 2 for normalized RNAseq data). Since transcripts for the canonical bradyzoite genes *BAG1*, *LDH2*, and *ENO1* (*26*, *175*) were below the levels of detection defined for *H. hammondi* samples in our RNAseq analysis (see section 2.4.19), we conducted qPCR analysis of these genes in TgVEG and HhCatAmer treated with alkaline pH for 2 (TgVEG only) and 3 days. We found a significant increase in transcript abundance for all three genes in TgVEG exposed to pH 8.2 for 2 days (*BAG1* P=0.0023, *ENO1* P=0.0047, *LDH2* P=0.0079). In HhCatAmer, we did observe a significant pH-dependent increase in transcript abundance for *BAG1* (2 Days P=0.0261 and 3 Days P=0.0276), while *ENO1* and *LDH2* transcript levels remained statistically unchanged (Figure 14B). Taken together, our DBA staining, RNAseq and qPCR data strongly support the hypothesis that *H. hammondi* is refractory to alkaline pH induced stress at the transcriptional level, and this is correlates well with the complete lack of high pH-induced cyst wall formation in this species.

A

		Reads mapped to genome		Reads mapped to transcriptome	
Sample	Reads	Total	%	Total	%
HhCatAmer Ctl 1	30,324,186	182,616	0.6%	81,204	0.3%
HhCatAmer Ctl 2	22,020,030	124,909	0.6%	60,059	0.3%
HhCatAmer Ctl 3	22,075,263	119,538	0.5%	46,027	0.2%
TgVEG Ctl 1	23,596,271	261,388	1.1%	236,494	1.0%
TgVEG Ctl 2	25,284,503	285,275	1.1%	235,585	0.9%
TgVEG Ctl 3	22,946,736	239,225	1.0%	224,299	1.0%
HhCatAmer pH 1	14,723,763	104,528	0.7%	82,463	0.6%
HhCatAmer pH 2	23,582,901	182,488	0.8%	145,315	0.6%
HhCatAmer pH 3	18,232,707	352,144	1.9%	338,876	1.9%
TgVEG pH 1	20,234,844	1,042,196	5.2%	339,844	1.7%
TgVEG pH 2	23,767,394	1,278,155	5.4%	406,954	1.7%
TgVEG pH 3	20,708,401	920,135	4.4%	440,407	2.1%

B

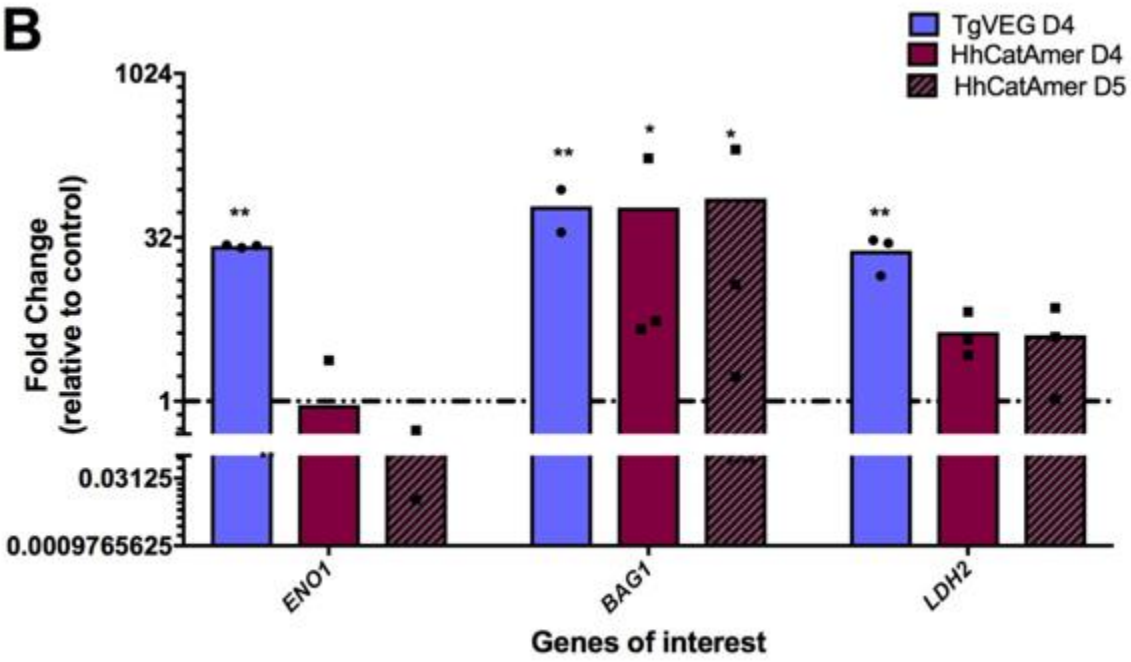

Figure 14. Transcriptional profiling and qPCR of pH vs control RNAseq data.

A) Summary of reads mapping from each sample for *T. gondii* and *H. hammondi* zoites treated with control or bradyzoite-induction media. B) Fold change in transcript abundance relative to control of canonical bradyzoite genes *ENO1, BAG1,* and *LDH2* determined by qPCR for TgVEG and HhCatAmer exposed to pH 8.2. * = P <0.05 and **= P <0.01

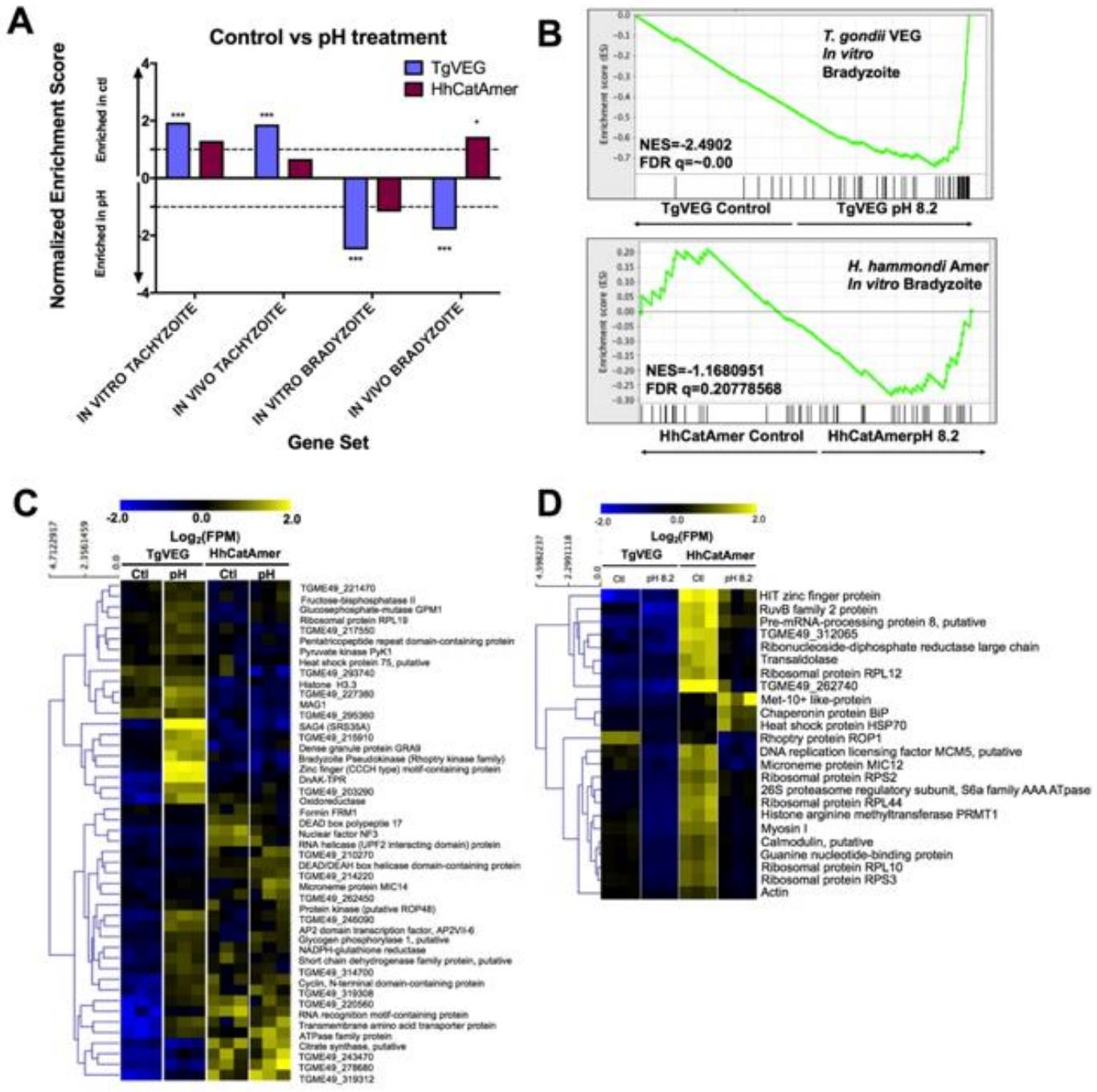

Figure 15. The *H. hammondi* transcriptome is refractory to pH-indued stress.

A) GSEA analysis comparing TgVEG (blue) and HhCatAmer (red) treated with control media to TgVEG and HhCatAmer treated with pH 8.2 media. Not all gene sets are significantly enriched. NES: Normalized enrichment score FDR q: False discovery rate q-value. See table supplement for FDR q-values for all analyses. Nominal p-value is indicated by * <0.05, ** <0.01, and ***<0.001. B) GSEA plots of the *IN VITRO* BRADYZOITE gene set comparing

control versus pH 8.2 treated TgVEG and HhCatAmer. C) Heat map showing mean centered $\log_2$(FPM) values for all detectable genes from the *IN VITRO* BRADYZOITE gene set. D) Mean centered, hierarchically clustered heatmap of $\log_2$(FPM) values of the 24 genes that significantly differed in transcript abundance (fold-change $\geq$ 1; $P_{adj}<0.01$) between control and pH 8.2 treated *H. hammondi*. As shown only 3 transcripts were found to be of higher abundance in pH-treated *H. hammondi*, while the remaining genes were of significantly lower abundance after pH exposure.

2.3 Discussion and conclusions

Parasites with multi-host life cycles undergo stereotyped patterns of development and growth in a given host, reaching a unique and often terminal developmental state that is then transmissible to the next host. With few exceptions, parasites with heteroxenous life cycles are obligately so; life stages that are infectious to one host (e.g., the definitive host) are not infectious to another host (e.g., an intermediate host). Among the Sarcocystidae (including such parasites as *Sarcocystis spp.*, *Besnoitia spp.*, *Neospora spp.*), all have exogenous life cycles for which they are obligately heteroxenous with the exception of *T. gondii*. Only in *T. gondii* oocysts and tissue cysts (i.e., bradyzoites) can infect, and ultimately be transmitted by, both intermediate and definitive hosts.

Given that the molecular determinants of life cycle dynamics such as those listed above are poorly understood in most parasite species, we have used the *T. gondii*/*H. hammondi* system as a means to better understand the genetic underpinnings of complex life cycles in Apicomplexa. In the present study, we conducted comparisons between one strain of *T. gondii* (VEG strain) and 2 strains of *H. hammondi* (HhCatEth1 and HhCatAmer), quantifying differences in *in vitro* and *in vivo* infectivity, replication rate, and in stage conversion. We identified dramatic differences in

parasite biology between these two species that likely contribute to their significant life cycle differences.

2.3.1 Stress-induced cyst formation is a unique trait in *T. gondii* compared to *H. hammondi*

While spontaneous cyst formation during growth *in vitro* has been reported for a handful of *T. gondii* strains (*80, 167*), *T. gondii* of most genetic backgrounds can be induced to form tissue cysts *in vitro* through the application of a variety of chemical modifications (e.g., alkaline pH, nitric oxide donors, serum starvation (*80, 110, 145*)) and these cysts are infectious to both the definitive and intermediate host (*11*). *H. hammondi* was resistant to high pH exposure at the transcriptome level, and 100% resistant with respect to tissue cyst formation. This highlights a key distinction between *T. gondii* and *H. hammondi* biology: the dynamic nature of the *T. gondii* tachyzoite permits movement in both directions along the tachyzoite-bradyzoite continuum which is at least partly driven by sensing changes in the external environment. The ability to dynamically alter (and even delay) stage conversion may be made possible by the existence of *T. gondii* effectors that block responses to host immune effectors like IFN-γ (e.g., *Toxoplasma* inhibitor of STAT1-dependent transcription (TgIST) (*176*)) or otherwise manipulate the host response. If the progression from replicating *H. hammondi* zoite to tissue cyst is as predictable *in vivo* as it is *in vitro* (which is unknown but likely given that even IFN-γ knockout mice survive infection with *H. hammondi* (*42*)), and *H. hammondi* has non- or less-functional orthologs of genes like *TgIST* (*177–179*), this may prevent the fixation of any polymorphisms in the population that might result in the suppression of spontaneous bradyzoite conversion. Given that bradyzoites induce less inflammation (*180*) and are protected from immune assaults by the tissue cyst wall (*181, 182*), the timing of these events may be under very strong selective pressure in *H. hammondi*. It will be

interesting to see how the developmental dynamics of *H. hammondi in vivo* are timed with that of the intermediate host immune response, particularly in rodents (*5*, *45*, *55*), since this may have directly impacted the timing of cyst formation during the evolution of this parasite. It is likely that *H. hammondi* is capable of sensing the stresses that are induced upon high pH exposure of the host cell (as evidenced by significantly reduced transcript abundance for 24 *H. hammondi* genes), but if so it is clear that this species responds quite differently than *T. gondii*.

The link between stage conversion and parasite replication (*174*) makes it possible that the lack of cyst wall formation after pH stress in *H. hammondi* is because the parasite is arrested in a phase of the cell cycle that prevents conversion. However, in the present study there were no significant differences in vacuole and/or tissue cyst size between *T. gondii* and *H. hammondi* after pH exposure, indicating that parasite replication continued in both species at a similar (albeit slightly slower) rate. Moreover, in *T. gondii* stress-induced (*100*) or spontaneous (*80*) cyst formation, slowed replication is a requirement for expression of bradyzoite antigens and ultimately stage conversion.

2.3.2 *H. hammondi* possesses unique life stages

When taken together with the dynamics of spontaneous differentiation in *H. hammondi*, these data further demonstrate that *H. hammondi* terminally differentiates into a unique life stage that is no longer infectious to anything but the definitive host. While we did not conduct any formal analyses of the cell cycle stage(s) found within replicating and tissue cyst-like forms of *H. hammondi*, we would predict that spontaneous *H. hammondi in vitro*-derived tissue cysts form after a set number of division and would be homogenous in terms of cell cycle stage (likely G_0 and 1N) given their terminal differentiation phenotype. It is also not known if terminally differentiated

parasites are capable of reinvading neighboring cells after egress, nor if they could be coaxed to infect cat gut epithelial cells *in vitro*, although the existence of cat intestinal organoids (*183*) might allow for this to be tested directly in an accessible *in vitro* system.

Some insight into the *H. hammondi* developmental processes underlying these unique life stages can be gleaned from the D4 and D15 transcriptional profiling data. *H. hammondi* consistently had higher transcript levels for genes previously defined as being uniquely expressed in *T. gondii* bradyzoites (whether *in vivo* or *in vitro*) as early as 4 DPI, indicating that there is a high degree of similarity between the spontaneous differentiation process that occurs in *H. hammondi* and the stress-induced process observed in *T. gondii* (*26*, *80*, *166*, *169*, *175*, *184*). Importantly, this enrichment for bradyzoite genes became more robust by 15 DPI compared to 4 DPI, indicating that the parasites are changing their transcriptional profiles throughout *in vitro* development (rather than becoming less viable or dying). Less expected, however, was the higher expression of genes in *H. hammondi* (observed in 24 hours PI, 4 DPI, and 15 DPI zoites) that have been found previously to be expressed more abundantly in *T. gondii* cat enteroepithelial stages and sporozoites (*170*, *185*). While the exact role of these gene products in determining life cycle and growth differences between *T. gondii* and *H. hammondi* are unknown, this provides strong evidence that sporozoite-derived life stages of *T. gondii* and *H. hammondi* are distinct, at least when grown *in vitro*. Importantly, this enrichment becomes more apparent at 15 DPI, indicating that this is not entirely due to residual transcript from the sporozoite stage. Assuming that the majority of these transcript expression differences are manifested at the protein level (which is expected based on multiple studies in *T. gondii* (*186*, *187*), it is exciting to consider what impact these distinct expression profiles might have on parasite development and even the host response. Expression of these *T. gondii* merozoite-specific genes in *H. hammondi* zoites may reflect its

terminally differentiated state, being infectious only the felid host (*42*). At a minimum our data may implicate only a subset of so-called "merozoite-specific" genes (*170, 185*) as being truly key distinguishing features of the *T. gondii* merozoite, since a number of them are highly expressed in *H. hammondi* zoites growing in HFFs.

2.3.3 Developmental predictability allows for genetic manipulation in *H. hammondi*

In contrast to previously published work, we identified a short but very predictable replicative window during which *H. hammondi* could be used to infect new host cells and identified the precise timing of what appears to be an inevitable developmental program towards cyst formation. This finding is in contrast to previous studies where subculture was unsuccessful (*55, 65*), although in these studies subculture was attempted after 1, 2, 4, and 6 weeks of growth and therefore most were outside of the window of infectivity we identified for *H. hammondi*. We exploited this window to genetically manipulate *H. hammondi* using transfection and gene editing strategies developed for *T. gondii* (*172*). Our transgenic *H. hammondi* parasite line expresses dsRED (30-40% after the first round of selection) and is >99% resistant to FUDR. This represents a new tool in the arsenal to track *H. hammondi* biology *in vitro* and *in vivo*, and opens up the door for the development of genetic screens to potentially disrupt spontaneous differentiation in *H. hammondi* to generate a mutant that can be cultured indefinitely, as well as utilized in gene-by-gene phenotypic screens.

2.3.4 Replication rate and tissue cyst formation may contribute to limited virulence and dissemination of *H. hammondi*

The nearly 3-fold difference in replication rate is likely a major determinant of reduced *H. hammondi* virulence (Table 2, Figure 2D-E), assuming this phenotype is recapitulated *in vivo*. Besides the impact that a slower replication rate would have on acute virulence, it may also impact infection outcome in the chronic phase. While *H. hammondi* parasites can at times be detected in the brains of mice after infection with oocysts (*42*), central nervous system (CNS) infection which is a hallmark of *T. gondii* infection (*42*, *173*) is much less common after exposure to *H. hammondi* (although *H. hammondi* parasites have been detected in mouse brains) (*42*). A simple explanation for reduced CNS infection in *H. hammondi* is that it never reaches a high enough burden to infect the CNS at any significant level. It is also possible that *H. hammondi* has additional deficiencies that underlie differences in tropism (such as poor trafficking by innate immune cells and/or inability to cross the blood-brain barrier (*188–190*)), although these have yet to be thoroughly explored. In contrast to differences in replication rate, we observed no substantial differences in the ability of *T. gondii* and *H. hammondi* to invade and form vacuoles within HFFs, suggesting that their invasion machinery is mostly conserved and intact. This idea finds some support in our transcriptome data, where we detected no enrichment for gene sets consisting of microneme, rhoptry or dense granule genes, and detected similar amounts of crucial invasion genes like AMA1, SpAMA1, as well as multiple rhoptry neck proteins. Moreover, all genes known to be a part of the cellular invasion machinery appear to be well-conserved in both sequence and expression between these species (*43*).

2.3.5 Potential for human exposure to and infection by *H. hammondi*

T. gondii and *H. hammondi* oocysts co-occur in the natural environment. A study conducted in Germany and surrounding countries found that the number feline fecal samples that contained either *T. gondii* or *H. hammondi* oocysts was strikingly similar (*52*), meaning that humans would be just as likely to encounter *H. hammondi* oocysts as those of *T. gondii*. While more studies are needed to determine if co-occurrence is a widespread phenomenon, it raises important questions about the likelihood that *H. hammondi* is capable of infecting humans. Importantly, at present all serological tests would be expected to misdiagnose a *H. hammondi* infection as a *T. gondii* infection due to antibody cross-reactivity (*42*). While this is a very poorly explored line of research, based on our data we would predict that an infection with *H. hammondi* should be less lethal than one with *T. gondii* since we would not expect a significant amount of recrudescence to occur. To further address the question of human infection and associated disease, mouse reactivation models and the development of differential diagnostic serological tests will be required in order to further determine human and animal infection rate differences between *H. hammondi* and *T. gondii* in the field.

2.4 Materials and methods

2.4.1 Parasite strains and oocyst isolation

Oocysts of *Hammondia hammondi* strain HhCatEth1(*164*), HhCatAmer (*5*), and *Toxoplasma gondii* strain VEG (*162*) were isolated from experimentally infected cats as described

previously. Ideally, one *H. hammondi* strain would be used for all experiments, but two strains of *H. hammondi* were utilized due to oocyst availability at the time of experimentation. Briefly, wild type (for *T. gondii*) or interferon-γ (IFN-γ) knockout (for *H. hammondi*) mice were orally infected with 10^4 sporulated oocysts and sacrificed 4-6 weeks post-infection, and leg muscle (for *H. hammondi*) or brain (*T. gondii*) tissue were fed to 10-20 week old specific pathogen-free cats. Feces were collected during days 7-11 post-infection, and unsporulated oocysts were isolated via sucrose flotation. Oocysts were placed at 4°C in 2% H_2SO_4 to allow for sporulation to occur and for long-term storage.

Due to the limited availability and difficulty associated with the generation of oocysts, two strains (HhCatEth1 and HhCatAmer) of *H. hammondi* generated from multiple cat-derived oocysts preparations were used in experiments described below. Furthermore, various MOIs were utilized throughout the experiments described below to compensate for differences in replication between *T. gondii* and *H. hammondi.*

2.4.2 Excystation of *T. gondii* and *H. hammondi* oocysts

Sporulated oocysts were washed 3X in Hanks' balanced salt solution (HBSS; Life Technologies, 14175145) and treated with 10% bleach in PBS for 30 minutes while shaking at room temperature. Washed pellets were resuspended in 3 mL of HBSS in a 15-mL falcon tube, and 4g sterile glass beads (710-1,180 µM; Sigma-Aldrich, G1152) were added. Parasites were vortexed on high speed for 15 seconds on/15 seconds off, 4X. Supernatant was removed and pelleted by centrifugation. The pellet was resuspended and syringe-lysed using a 25 gauge needle in 5 mLs of pre-warmed (37°C) and freshly made, sterile-filtered excystation buffer (40 mL PBS, 0.1 g Porcine Trypsin (Sigma-Aldrich, T4799), 2 g Taurocholic Acid (Sigma-Aldrich, T4009), pH

7.5). After 45 minutes in a 37°C water bath, the suspension was syringe lysed again, and 7 mLs of cDMEM (100U/mL penicillin, 100µg/mL streptomycin, 2mM L-glutamine, 10% FBS, 3.7g NaH_2CO_3/L, pH 7.2) was added to quench the excystation media. The mixture was centrifuged, the pellet was resuspended in cDMEM, and used in downstream applications described in more detail below.

2.4.3 Fixing parasites for immunofluorescence assays

Parasites were washed twice with PBS, fixed with 4% paraformaldehyde in PBS (Affymetrix, 19943), washed twice with PBS, and blocked/permeabilized in blocking buffer (50mL PBS, 5% BSA, 0.1% Triton X-100).

2.4.4 Quantification of sporozoite viability and replication rate

After 10 minutes incubation on HFFs at 37°C in 5% CO_2, monolayers containing freshly excysted parasites were scraped, serially syringe lysed (25 and 27 gauge needles), and pelleted. The pelleted parasites were resuspended in cDMEM, filtered through a 5 µM syringe-driven filter (Fisher Scientific, SLSV025LS) and used to infect 4-chambered slides (Lab-Tek® II, 154526) containing a confluent monolayer of HFFs at an MOI of 0.5 for both *H. hammondi* CatEth1 and *T. gondii* VEG. After 1, 2, and 3 days of growth, cells and parasites were fixed as described above and stored in blocking buffer at 4°C until needed. Cells were immunostained with goat polyclonal *Toxoplasma gondii* Antibody (ThermoFisher Scientific, PA1-7256, RRID: AB_561769) at 1:500. The secondary antibody, Alexa Fluor® 594 Donkey anti-Goat IgG (H+L) (ThermoFisher

Scientific, A-11037, RRID: AB_2534105) was used at 1:1000. Coverslips were mounted to 4-chambered slides using VECTASHIELD Antifade Mounting Medium with or without DAPI, depending on the application (Vector labs, H-1000).

Vacuole formation was used as a proxy for sporozoite invasive capacity. To quantify this, the number of vacuoles with at least 1 parasite was determined in 100 random FOVs (1000x magnification) for 3 technical replicates for each parasite species at 1, 2, and 3 DPI. The entire experiment was repeated twice with different cat-derived oocyst preparations. For replication rate quantification, images of parasite-containing vacuoles were taken with an Axiovert 100 inverted fluorescent microscope with Zen lite 2012 software. The number of parasites per vacuole was determined for each image (biological replicates 1 & 2), and vacuole size (Biological replicate 1 only) was determined for each image using ImageJ software (NIH).

2.4.5 Quantification of spontaneous *Dolichos biflorus*-positive cyst formation *in vitro*

For *Dolichos Biflorus* Agglutinin (DBA) staining, monolayers containing freshly excysted parasites were scraped, syringe lysed, and pelleted 24 hours after growth. The pellet was resuspended in cDMEM, filtered through a 5 µM syringe-driven filter (Fisher Scientific, SLSV025LS), and passed at MOIs of 0.3 (HhCatEth1) and 0.001 for (TgVEG) onto coverslips containing a confluent monolayer of HFFs. Three coverslips were infected per strain for each time point analyzed. At 4 and 15 DPI, cells and parasites were fixed as described above and stored in blocking buffer at 4°C until immunostaining was conducted.

In addition to being stained with rabbit *Toxoplasma gondii* Polyclonal Antibody (Invitrogen, PA1-7252 RRID: AB_561769) at a dilution of 1:500 and a 1:1000 dilution of Alexa Fluor® 594 goat anti-rabbit IgG (H+L) (ThermoFisher Scientific, A-11037, RRID: AB_2534095),

coverslips were stained with Fluorescein labeled *Dolichos biflorus* Agglutinin (DBA; Vector Labs, FL-1031) at a dilution of 1:250. Coverslips were then mounted to microscope slides using ProLong® Diamond Antifade Mountant with DAPI (ThermoFisher Scientific, P36962).

The number of DBA-positive vacuoles and total vacuoles were quantified in 20 FOVs in 3 coverslips for each parasite at 4 and 15 DPI. Images were obtained with an Axiovert 100 inverted fluorescent microscope with Zen lite 2012 software and edited using ImageJ software (NIH).

For time course tissue cyst formation analysis, freshly excysted and filtered HhCatAmer and TgVEG sporozoites were used to infect confluent monolayers of HFFs grown on glass coverslips at an MOI of 0.5. After three days of growth, the media was changed every 2 to 3 days. At designated time points, coverslips were was twice with PBS, fixed with 4% formaldehyde in PBS, washed twice with PBS, and stored in blocking buffer 4°C until immunostaining was conducted using Rhodamine labeled DBA. The number of DBA-positive vacuoles and number of total vacuoles were quantified in 15 parasite-containing FOVs for each time point.

2.4.6 Induction of bradyzoite formation in *T. gondii* and *H. hammondi*

Monolayers containing freshly excysted parasites were scraped, syringe lysed, and filtered through a 5 µM syringe-driven filter (Fisher Scientific, SLSV025LS) after 24 hours of growth. Filtered parasites were pelleted and passed at MOIs of 0.5 (*H. hammondi*) and 0.1 for (*T. gondii*) onto coverslips containing a monolayer of HFFs. Three coverslips were infected per parasite per treatment group. After 2 days, media was changed to pH 8.2 bradyzoite switch media (DMEM with 100U/mL penicillin, 100µg/mL streptomycin, 2mM L-glutamine 10mM HEPES, 2g/L NaHCO3, and 1% FBS)(*145*) or cDMEM. Coverslips with pH 8.2 media were grown at 37°C in the absence of CO2. Media was changed again at 3 DPI. After 4 DPI, cells and parasites were fixed

as described above and stored in blocking buffer at 4°C until needed. DBA and counter-staining was conducted using Fluorescein or Rhodamine labeled DBA and rabbit Toxoplasma gondii Polyclonal Antibody as described above. The number of DBA-positive vacuoles was quantified in 15 FOVs in 3 coverslips for each strain grown at either pH 7.2 or pH 8.2 and the percentage of DBA-positive vacuoles was determined. Images were obtained and analyzed as described above.

2.4.7 Subculture of *H. hammondi*

Sporozoites were obtained using the excystation protocol described above with the exception of syringe lysis and previously described host cell incubation. Six confluent monolayers of HFFs grown in T-25's were infected with *H. hammondi* American (HhCatAmer) sporozoites at an MOI of ~2 (2.8 million sporozoites). After a three-hour incubation at 37°C, the Day 0 Transfer flask was scraped, syringed lysed 5X with 25 gauge needle, filtered through a 5 µM syringe-driven filter (Fisher Scientific, SLSV025LS), and passed to a new confluent monolayer of HFFs grown in a T-25. This process was repeated after 2, 5, 8, 11, and 15 days post-excystation. After 3 days of growth following passage, 4.17cm^2 of the T-25 was monitored daily. Images of vacuoles were obtained with an Axiovert 100 inverted fluorescent microscope with Zen lite 2012 software with a 40X objective, and vacuole sizes were quantified using ImageJ software (NIH). Similar methods were used to generate parasite samples for RNAseq analysis, except cells were processed for RNA harvest using methods described below.

2.4.8 Characterizing limits of *in vivo* infectivity of *H. hammondi* grown *in vitro*

Sporozoites were obtained using the excystation protocol described above. After 24 hours, HFF monolayers infected with excysted sporozoites were scraped, syringe lysed 5X with a 25-gauge needle, and pelleted. The pellet was resuspended in cDMEM, filtered through a 5µM syringe-driven filter (Fisher Scientific, SLSV025LS) and passed onto confluent monolayers of HFFs grown in T-25s. Infected host cells were incubated at 37 °C 5% CO_2 from 6, 8, 10, 13, and 15 days. The media was replenished after 5-7 days. At each time point, infected host cells were scraped, syringe lysed 3X with a 25-gauge needle and 3X with a 27 gauge needle, and pelleted. Parasites were counted and diluted in PBS, and a dose of 50,000 parasites was injected intraperitoneally in 2 BALB/C mice for each time point. Serum samples were obtained from infected mice daily for 9 days post-infection and the mass of the mice was also monitored daily. After 9 days of infection, the mice were sacrificed and dissected. Tissue samples were preserved in 10% neutral buffered formalin (Sigma HT501128) until immunohistochemistry analysis was performed.

2.4.9 Tissue sectioning and staining

Fixed tissue samples were embedded in paraffin, sectioned, and stained using rabbit anti-*Toxoplasma* antibody (ThermoScientific Cat# RB-9423-R7) by Research Histology Services at the University of Pittsburgh. For antigen retrieval, deparaffinized slides were steamed at pH=6.0 in 10 mM Citrate buffer. After exposure to 3% H_2O_2, slides were washed in Tris-buffered saline with 2.5% Tween-20 (TBST), and blocked for 20 min each with Avidin and Biotin blocking reagents (Vector labs; SP-2001) with TBST washes in between. Slides were blocked in 0.25%

casein:PBS for 15 min, and incubated overnight in primary antibody (1:100 dilution in 3% goat serum in PBS). Slides were washed in PBST and incubated for 30 minutes with biotinylated goat anti-rabbit (Vector laboratories; BA-1000; 1:200 dilution in 3% goat serum in PBS). Following 3 washes with PBST, slides were incubated for 30 minutes with streptavidin-HRP (Vector laboratories; PK-6100), washed 3X with PBST, and incubated with AEC substrate (Skytec; ACE-500/ACD-015) for 15 minutes. Following rinses in water, slides were counterstained with aqueous hematoxylin and blued using Scott's tapwater substitute. Slides were mounted in Crystal Mount.

2.4.10 Interferon-gamma (IFNγ) ELISA

Blood samples were obtained from mice daily via submandibular bleed, allowed to clot for 4-24h at 4°C, and centrifuged at 100xg. Serum was stored at -20°C until ELISAs were performed. IFN-γ levels were determined using the BD OptEIA™ Set Mouse IFN-γ kit (Cat.# 555138) according to manufacturer's instructions. Serum samples were diluted 1:20.

2.4.11 Transfection of *Hammondia* parasites and selection of recombinant parasites

Excysted sporozoites were prepared as described above and incubated overnight in a T-25 flask with confluent monolayer of HFFs. After 24 hours, the monolayer was scraped, syringe lysed 3X with a 25 gauge and 27 gauge needle and filtered using a 5 µM syringe-driven filter (Fisher Scientific, SLSV025LS). The filtered contents were pelleted by centrifugation at 800 x g for 10 min, and the pellet was resuspended in 450 µl of cytomix with 2 mM ATP and 5 mM glutathione. Resuspended parasites were transferred to a cuvette, electroporated at 1.6 KV and a capacitance of 25 µF and used to infect confluent HFF monolayers on coverslips. The coverslips were fixed 5

DPI as described above and mounted using ProLong® Diamond Antifade Mountant with DAPI (ThermoFisher Scientific, P36962).

To create stable transgenic *H. hammondi* parasite lines, the CRISPR/CAS9 plasmid expressing a gRNA sequence targeting the uracil phosphoribosyl transferase gene (*UPRT;*(*172*) kindly provided by David Sibley, Washington University) and a repair template consisting of 20 bp *UPRT*-targeting sequences flanking a PCR-amplified a dsRED expression cassette driven by the *T. gondii GRA1* promoter with a *GRA2* 3' UTR (amplified from the dsRED:LUC:BLEO plasmid(*191*, *192*) were used for transfection. Following centrifugation (800 x g, 10 min), 24 h *H. hammondi* zoites were resuspended in 450 µl of cytomix with ATP and glutathione containing 20 µg of the CRISPR/CAS9:*UPRT*:gRNA plasmid and 20 µg of PCR2.1 TOPO vector containing the dsRED repair template. The parasites were electroporated as above and each transfection contained at least 4 million parasites. Transfected parasites were then transferred to HFFs and grown for 2 days in cDMEM, then selected for 3 days by incubation in cDMEM containing 10 µM FUDR (Figure 11B). Parasites were again scraped, syringe lysed and filtered, and dsRED-expressing parasites were collected in PBS using flow cytometry. Sorted parasites were injected intraperitoneally into 2 BALB/c mice. After 3 weeks of infection, mice were euthanized, skinned, and the intestines were removed before feeding to specific pathogen-free cats. The oocysts were collected and purified as described above, and oocysts, sporozoites and replicating parasites were evaluated for dsRED fluorescence using microscopy, flow cytometry and FUDR resistance.

2.4.12 FUDR resistance of transgenic parasites

To test for deletion of the *UPRT* gene we quantified transgenic *H. hammondi* resistance to 5-fluoro-2'-deoxyuridine (FUDR). To do this, sporozoites of wild type and dsRED-expressing

parasites were incubated overnight in a T25 flask with confluent monolayer of HFFs. After 24 hours, parasites were isolated by needle passage and filtration as above. We infected coverslips containing confluent HFFs with 50,000 parasites, and parasites were exposed to media alone or media containing or 20 μM FUDR. The parasites were allowed to grow for 4 days and then fixed using 4%PFA for 20 minutes. After blocking overnight in PBS/BSA/triton, coverslips were stained with rabbit anti-*Toxoplasma* antibody at a 1:500 dilution for an hour and stained with Alexa-fluor 488-labeled goat anti Rabbit antibody (RRID: AB_143165). For each treatment/strain combination, we counted the number of parasites in at least 100 vacuoles, and for HhdsRED parasites we also quantified growth in both red and wild type vacuoles (since the HhdsRED parasites were from a mixed population).

2.4.13 Genomic DNA isolation

To isolate genomic DNA from *H. hammondi*, freshly excysted parasites were used to infect HFFs. Following 7 days of growth, infected host cells were scraped, syringe lysed, pelleted and resuspended in 200μL of PBS. Genomic DNA was isolated with the GeneJET genomic DNA Purification kit (ThermoFisher, K0721) according to the manufacture. Alternatively, identical procedures were used on freshly excysted and filtered sporozoites.

2.4.14 Linear amplification of HhamdsRED gDNA

We used the Genomiphi Linear DNA amplification kit to linearly amplify DNA taken from our population of dsRED-expressing H. hammondi American parasites. We used ~5 ng of input

DNA in a single reaction, and ethanol precipitated amplified DNA prior to quantification and use in PCR reactions.

2.4.15 PCR verification of dsRED cassette

To verify that the dsRED cassette incorporated into the HhCatAmer genome, linearly amplified pure parasite genomic DNA (HhamdsRED) was amplified using primer sets targeting the UPRT homology arms of the dsRED cassette, the dsRED transgene, and a sequence specifically found in *H. hammondi* (*63*). (See supplementary file 3 for primer sequences) Controls included wild type HhCatAmer genomic DNA, purified from infected HFFs, and a water control. PCR reactions were conducted using 12.5µL of 2X BioMix Red (Bioline, BIO-25006), 1nM of both forward and reverse primers, 45ng of template DNA, and water to 25µL. Cycling conditions began with 5 minutes of 95 °C denaturation, followed by 30 cycles of 95 °C for 30 seconds, 50 °C for 30 seconds, 72°C for 1 minute and 30 seconds, followed by 72 °C for 5 minutes and a 4°C hold. PCR products were visualized on a 1% agarose gel.

2.4.16 RNAseq data collection and enrichment analysis for D4 and D15 zoites

Sporozoites were isolated from HhCatEth1 and TgVEG sporulated oocysts as described above and used to directly infect confluent HFF monolayers in 96 well tissue culture plates with MOIs of 3, 1 or 0.5 purified sporozoites for each species. On day 4 post-infection, wells were observed and chosen for RNA analysis based on similar numbers of parasite-containing vacuoles lack of significant host cell lysis in both species. For the Day 4 samples, the MOI=3 infected wells were chosen for *H. hammondi*, while the MOI=0.5-infected wells were chosen for *T. gondii*. Wells

were washed 3X with ~200 μL cDMEM, and RNA was harvested using Trizol (Invitrogen). Remaining *H. hammondi* wells were washed with 3X with cDMEM on Day 4 and then again on Day 9 prior to harvest on Day 15 post-infection. For *T. gondii*, remaining MOI=3 and 1-infected wells were scraped and syringe lysed on Day 4 and Day 9 and used to infect new monolayers in 96 well plates at an MOI of either 0.5 (Day 4) or 0.3 (Day 9). On Day 15, wells for both *H. hammondi* (not subcultured) and *T. gondii* (subcultured 2x) were washed 1X with cDMEM and then harvested for RNAseq analysis. Two samples were harvested for each species on Day 4, and 3 samples were harvested from each species on Day 15. Total RNA samples were processed for Illumina next generation sequencing using the Mobioo strand-specific RNAseq library construction kit. Samples were analyzed on an Illumina Nextseq and demultiplexed using NextSeq System Suite software. Reads were aligned to their respective species genome assembly (*H. hammondi* v10 or *T. gondii* strain ME49 v10; toxodb.org) using the Subread package for Linux (v. 1.4.6) with subread-align using default parameters except for –u to keep only uniquely mapping reads. featureCounts from the subread package(*192*) was used to quantify the number of mapping reads per transcript, using default settings except for –s 2 (for stranded read mapping), –t CDS, –g Parent (for specific compatibility with the *T. gondii and H. hammondi* gff files), –Q 10 (minimum mapping quality required). The –t CDS option was chosen for both *T. gondii* and *H. hammondi* because to date no 5' or 3' UTR sequences have been predicted for *H. hammondi* (in contrast to *T. gondii*). Fastq files have been deposited in the NCBI short read archive (SRX3734444-SRX3734449).

2.4.17 RNA sequencing and differential expression analysis of 24h-infected THP-1 cells (a human monocyte cell line)

To validate genesets that were significantly enriched in D4 and D15 H. hammondi compared to *T. gondii*, we extracted sporozoites from oocysts and grew them overnight in HFFs as described above. Parasites were released by scraping and needle passage as above, and then passed through a 5μm syringe-driven filter (Fisher Scientific, SLSV025LS). Filtered parasites were used to infect monocytes (THP-1, RRID: CVCL_X588) at MOI of 4. At 24 hours post-infection, RNA was harvested using RNeasy Mini Kit (Qiagen; three samples for each species). Total RNA samples were processed for Illumina next generation strand-specific sequencing using the Illumina TruSeq stranded mRNA sequencing kit. Fastq files have been deposited in the NCBI short read archive (SRX3734421-SRX3734428). FASTQ reads were aligned to their respective species genome assembly (*H. hammondi* release 34 or *T. gondii strain* ME49 release 30; toxodb.org) with CLC Genomics Workbench v10.0.1 (http://www.qiagenbioinformatics.com/) using default parameters for reverse strand mapping. Raw count data (with at least 1 read in at all samples for HhCatAmer) generated by CLC Genomics Workbench were loaded into R statistical software and analyzed using the DESeq2 package.(*193*) Read count data of HhCatAmer were compared to TgVEG to identify genes of different abundance and genes were deemed differentially expressed according to the threshold of $\log_2$ (fold) > 1 and P_{adj}<0.01. Log_2 transformed data were used for enrichment analysis using Gene Set Enrichment Analysis (GSEA) (*168*). Data were compared to previously curated gene sets (434 total; as previously published (*170*) as well as in 7 additional gene sets that we curated ourselves (listed in Table 3). All enrichment profiles were deemed significant if the FDR q-value was ≤0.01. We also identified

1069 genes that were of different abundance between HhCatAmer and TgVEG at this 24 h time point in THP-1 cells.

2.4.18 RNAseq from pH-treated *T. gondii* and *H. hammondi* zoites

Sporozoites were isolated from HhCatAmer and TgVEG sporulated oocysts as described above and used to directly infect confluent HFF monolayers in 24 well tissue culture plates with MOI of 1.3 for HhCatAmer and 1 for TgVEG. Infected host cells were maintained as described the induction of bradyzoite section above. On day 4 post-infection, wells were washed twice with 1X PBS and RNA was harvested using the RNeasy Kit according to the manufacturer (Qiagen, 74104) using QiaShredder spin columns (Qiagen, 79654) to homogenize samples, and RNase-free DNase to degrade contaminating DNA (Qiagen, 79254). Total RNA samples were ethanol precipitated and processed for Illumina next generation strand specific sequencing as described for infected THP-1 RNAseq experiments. Library preparation and read alignment were performed as described in infected THP-1 RNAseq experiments.

2.4.19 Identification of differentially expressed genes using DESeq2 and gene set enrichment analysis

Raw count data per transcript (generated by featureCounts or CLC genomics) were loaded into R statistical software and analyzed using the DESeq2 package (*193*, *194*). Comparisons of D4 and D15 read count data were used to identify transcripts of different abundance at each time point, and differences were deemed significant at $P_{adj}<0.05$. Data were $\log_2$ transformed and normalized using the *rlog* (with the blind=TRUE option) function in DESeq2 for use in downstream analyses.

Log_2 transformed, normalized data from DESeq2 (hereafter referred to as Log_2 (FPM)) were analyzed for enrichment using Gene Set Enrichment Analysis (GSEA) (*168*). Since read count overall from the *T. gondii* libraries were much greater than those from the *H. hammondi* libraries, we took the 7372 genes matched based on the previously published gene-by-gene annotation (*43*) and selected only those that had at least 1 day 4 sample and 1 day 15 sample with >5 reads for the D4 and D15 data and samples that had reads for each replicate and a total read average of 5 reads per three replicates for pH 8.2 analysis. In total, 4146 genes for the D4 and D15 analysis and 907 genes for the pH 8.2 analysis passed these benchmarks and were used in subsequent analyses. We used this approach to identify gene sets that were significantly different between days 4 and day 15 in culture in both species and those that were different between species at both day 4 and day 15 and in pH 8.2 treated and control samples. We compared these data using previously curated gene sets (*169*) (434 total) as well as 7 additional gene sets that we curated ourselves. These are listed in Table 2. All enrichment profiles were deemed significant if the FDR q-value was ≤ 0.05.

2.4.20 cDNA synthesis and qPCR

For qPCR analysis, after 24 hours of growth, monolayers containing excysted sporozoites were scraped, syringe lysed, and pelleted. The pellet was resuspended in cDMEM, filtered through a 5 μM syringe-driven filter (Fisher Scientific, SLSV025LS) and passed at MOIs of 1 (*T. gondii*) and 7 (*H. hammondi*) into 96-well plates or 24-well plates containing HFF monolayers. Mock-infected controls consisted of filtering parasites through a 0.22 μM syringe-driven filter (Fisher Scientific, SLGL0250S). Three replicates were made for each sample per isolation time point. RNA for D4 and D15 RNAseq validation was collected at day 4 and day 15 post-infection, (equivalent to day 5 and day 16 post-excystation) from parasites and mock infections grown in 96-

well plates. RNA for pH induced bradyzoite transcript analysis was collected from day 4 and 5 post-infection samples grown in 24-well plates. RNA was collected using the RNeasy Kit according to the manufacturer (Qiagen, 74104) using QiaShredder spin columns (Qiagen, 79654) to homogenize samples, and RNase-free DNase to degrade contaminating DNA (Qiagen, 79254). Isolated RNA was ethanol precipitated, resuspended in RNase-free water, and these preparations were used to create cDNA using Superscript III Reverse Transcriptase Kit using Oligo(dT) primers according to the manufacturer (ThermoFisher Scientific, 18080051). All RNA samples were kept at -80°C, and all cDNA reactions were kept at -20°C. Prior to qPCR use, cDNA was diluted 1:10 (for RNAseq validation) or 1:5 (for bradyzoite transcript analysis) with H_20.

qPCR assays were performed on a QuantStudio 3 Real-Time PCR System in a 10 µl reaction volume containing 5 µl 2x SYBR Green Master Mix (VWR International, 95030-216), 3 µl of cDNA template, 1 µl H_20, and 1 µl 5 µM primer. Controls included a reverse transcription negative control and a water-template control. The thermal cycling protocol was 95°C, 10 min; 40 cycles of (95°C, 15s; 60°C, 1 min); 4°C hold. The melt curve protocol was 95°C, 15 s; 60°C 1 min, 95°C 15 s. The control gene was dense granule 1 (GRA1), and samples were tested in duplicate or triplicate. Melt curves were performed on each plate (with the exception of 2 plates). Data were analyzed using the $2^{-\Delta\Delta Ct}$ method(*195*), and statistical analyses were conducted on the ΔCt values.(*196*)

3.0 Cross-species comparisons between *Toxoplasma gondii* and *Hammondia hammondi* identify ROCY1 as a regulator of cystogenesis

3.1 Introduction

A fundamental characteristic of all organisms is that they must be able to respond to stimuli from their environment. This characteristic is especially true for parasitic organisms with multi-stage life cycles that occur in different environments or different hosts, such as in tissue cyst forming Apicomplexan parasites. *Toxoplasma gondii* and *Hammondia hammondi* are both coccidian Apicomplexans that exist as multiple life stages optimized for growth and survival in a variety of environments and hosts. *T. gondii* and *H. hammondi* are closely related, sharing over 7,000 orthologous genes (*43*) in near perfect genomic synteny (*68*). These two parasite species are morphologically and antigenically similar, share the same definitive host and organelles, and transition between similar life stages as they progress through their life cycle (*3*, *5*, *42*).

Even though these parasites have many similarities, *H. hammondi* follows a strictly obligate heteroxenous life cycle (*3*, *5*) while *T. gondii* has a facultative heteroxenous/homoxenous life cycle. This is driven by the unique ability of *T. gondii* bradyzoites, the slow-growing tissue cyst forming life stage of the parasite responsible for chronic infection, to convert back to tachyzoites, the rapidly replicating life stage that can lead to disease (*2*, *11*). This unique interconversion phenomenon is not shared with *H. hammondi*. Bradyzoite to tachyzoite interconversion allows for *T. gondii* to pass between intermediate hosts, thus expanding its transmission dynamics (*17*). Furthermore, this interconversion can be lethal or result in severe disease in immune compromised organ transplant patients, cancer patients, and individuals with

HIV/AIDS (*35*, *36*). Despite their importance for transmission and disease, the genetic components and regulatory network comprising the mechanisms used by *T. gondii* to transition to the bradyzoite life stage are only starting to be discovered.

The similarities between *T. gondii* and *H. hammondi* bradyzoites paired with the stark contrast in when and how bradyzoites form in each species makes interspecies comparison a promising strategy for uncovering critical components driving the bradyzoite developmental program. *H. hammondi's* strict obligate heteroxenous life cycle restricts its ability to initiate infection in organisms other than its definitive feline host after it transitions into its bradyzoite life form (*42*, *44*, *55*, *65*). Moreover, *H. hammondi* cannot be induced to form bradyzoites in its early life stages when treated with alkaline pH stress (*44*), a known and potent inducer of cystogenesis in *T. gondii* (*88*, *89*, *95*). Yet, *H. hammondi* predictably and reliably forms tissue cysts spontaneously which is also accompanied by robust transcriptional changes resembling those observed in *T. gondii* as they differentiate into bradyzoites (*42*, *44*).

Numerous studies designed to characterize the *T. gondii* bradyzoite have led to the identification of several bradyzoite specific proteins along with their function (*76*) and have characterized the major transcriptional differences that occur during bradyzoite development in *T. gondii (73, 114, 169, 197–199)*. However, until recently the mechanisms used by *T. gondii* to initiate bradyzoite development were elusive. The first major class of transcription factors identified in Apicomplexans were AP2 transcription factors (*124*), which begun to broaden our understanding of the regulation of bradyzoite development. These transcription factors play fundamental roles in regulating stage conversion associated gene expression in closely related *Plasmodium* species (*125*, *200*). In *T. gondii*, this family of proteins are important for cystogenesis and function as activators and repressors of stage conversion associated gene expression *(118,*

127–131). In addition to AP2 factors, another *T. gondii* transcription factor that regulates the tachyzoite to bradyzoite transition, Bradyzoite-Formation Deficient-1 (BFD1) was recently identified as a transcription factor that completely abolishes tissue cyst formation *in vitro* and *in vivo* when depleted (*132*). The identification of BFD1 as a regulator of differentiation was a fundamental finding and has greatly contributed to our understanding of the bradyzoite developmental pathway in *T. gondii*. However, our understanding of this process and all its major contributors remains unclear.

Primarily, the identification of factors controlling bradyzoite development occurred through identification of parasite factors with homology to other known transcriptional regulators (AP2 factors) (*124*) or from genome-wide Cas9-mediated knockout screens (BFD1) (*132*) in *T. gondii*. Here, we used a novel interspecies comparative approach that exploits our knowledge of the critical differences in tissue cyst formation between *T. gondii* and *H. hammondi* to identify factors that are important for driving cystogenesis. Using this system, we identified a *T. gondii* gene, Regulator of Cystogenesis 1 (ROCY1), as a gene that plays a critical role in tissue cyst formation both *in vitro* and *in vivo*, is an important factor for *T. gondii's* alkaline pH induced transcriptional response, and may be a downstream target of BFD1.

3.2 Results

3.2.1 Comparative transcriptomics between *T. gondii* and *H. hammondi* identifies candidate genes involved in tissue cyst development

To identify candidate *T. gondii* genes implicated in tissue cyst development, we leveraged species-specific differences in spontaneous and alkaline pH-induced tissue cyst formation that we previously identified in *T. gondii* and *H. hammondi* parasites (*44*). When *T. gondii* sporozoites (VEG) are exposed to alkaline pH-induced stress conditions at 3 days post excystation (DPE), they robustly form Dolichos biflorus agglutinin (DBA)-positive tissue cysts *in vitro*. However, *H. hammondi* fails to form DBA-positive tissue cysts under these conditions. But, *H. hammondi* spontaneously forms DBA-positive tissue cysts beginning at 12DPE and the percentage of tissue cysts increases to 100% over a 23-day time course, while only low levels (<20%) of tissue cyst formation is observed in *T. gondii* during this time (Summarized in Figure 16A) (*44*).

We hypothesized that some of the genes that change in transcript abundance during alkaline pH stress exposure in *T. gondii* and during spontaneous development in *H. hammondi* would have critical regulatory roles in tissue cyst development. To identify candidate genes that could be driving tissue cyst formation, we performed RNA sequencing experiments on *T. gondii* and *H. hammondi* sporozoite-derived infections exposed to alkaline pH, low serum, and CO_2 starvation for 48 hours beginning at 3DPE and on *T. gondii* and *H. hammondi* grown in control conditions. We then used this new transcriptional data in combination with our previously published data (*44*) to identify genes that had 1) significant changes in transcript abundance ($|Log_2FC| > 1$, $P_{adj} < 0.01$) in *T. gondii* in alkaline pH stress conditions compared to control condition in at least 1 of 2 experiments, 2) genes that did not have significant changes ($|Log_2FC| < 1$ and/or $P_{adj} > 0.01$) in *H.*

hammondi during stressed conditions relative to control conditions in at least one of 2 experiments as *H. hammondi* fails to form DBA-positive tissue cysts in response to this treatment, and 3) genes with significant changes in transcript abundance ($|Log_2FC| > 1$, $P_{adj} < 0.01$) during spontaneous tissue cyst development in *H. hammondi* (D4 vs D15). We identified 80 candidate genes fitting these criteria (Figure 16 A-B). To prioritize these 80 candidates for further investigation, we sought to identify potential transcription factors that could be responsible for driving the global transcriptional changes needed for the transition from tachyzoite to bradyzoite. To do this we first removed candidates with a predicted signal peptide or transmembrane domains, leaving 48 candidates. Next, we identified 22 genes containing predicted nuclear localization sequences using NLSmapper (*201*) and NLStradamus (*202*) using default settings. Finally, to further prioritize our candidate genes, we utilized data from a genome-wide CRISPR screen in *T. gondii* that predicts whether a gene contributes to tachyzoite fitness by calculating a CRISPR phenotype score from the ratio of the abundance of gRNAs present following *in vitro* growth in tachyzoite conditions to the abundance of gRNAs present in the initial library (*203*). We then selected bradyzoite induction factors (BIFs) if their transcript abundance increased during tissue cyst formation (stress-induced and spontaneous) in both species that also had a CRISPR phenotype score > -1, as we hypothesized that these factors would not be needed during tachyzoite growth. We also selected bradyzoite suppression factors (BSFs), genes whose transcript abundance decreased during tissue cyst formation, with low (< -1) CRISPR phenotype scores, as we predicted that these factors would be required for the maintenance of tachyzoite growth and therefore have poor fitness *in vitro*. After selecting candidates that fit these criteria, we had 17 final high priority candidates. (16 BIFs and 1 BSF) (Figure 16 C-D).

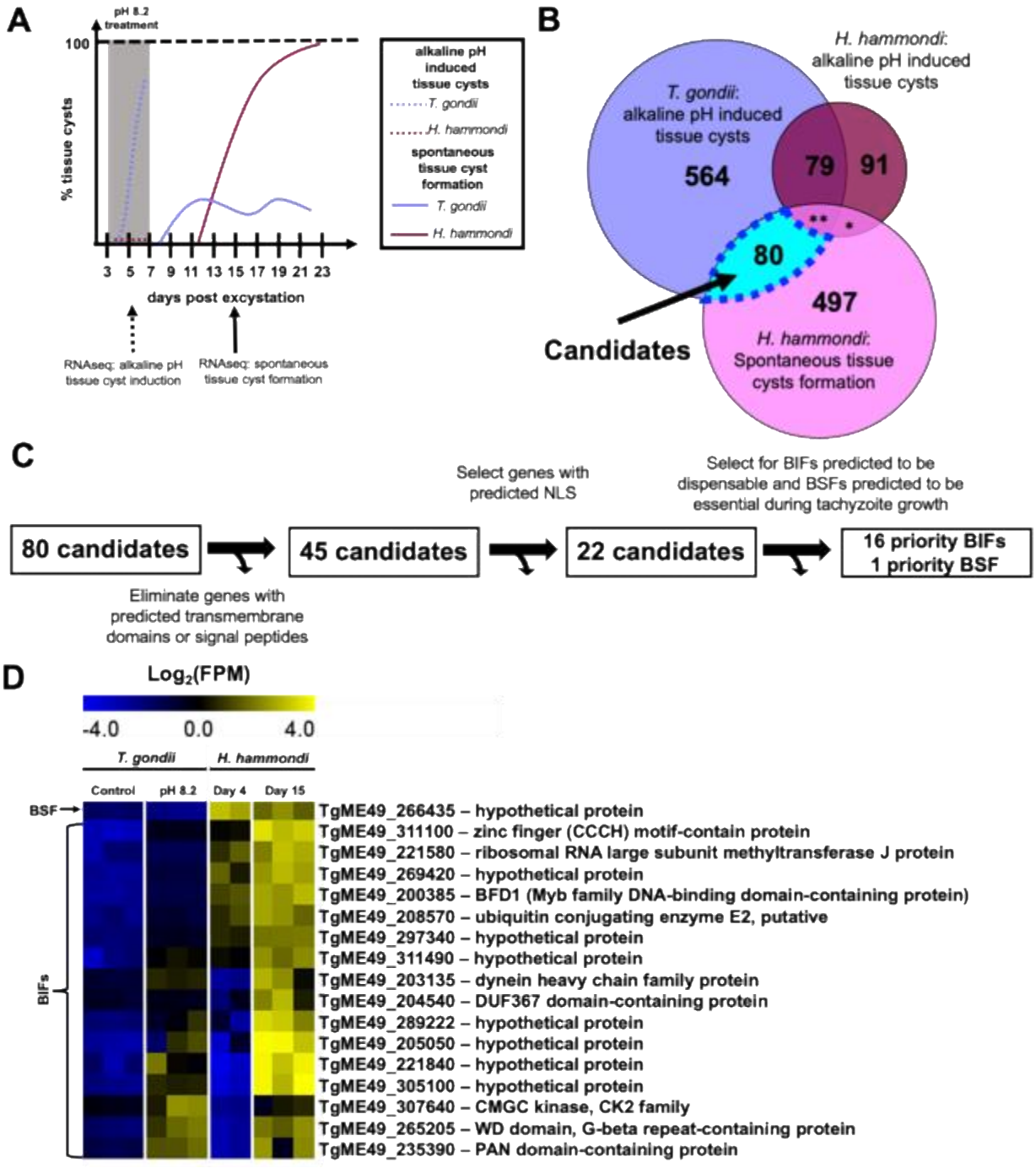

Figure 16. Comparative transcriptomics between *T. gondii* and *H. hammondi* identifies candidate genes involved in tissue cyst development.

Schematic depicting spontaneous and alkaline pH induced tissue cyst formation phenotype over a 23-day time course in *T. gondii* VEG and *H. hammondi* Amer (*44*). B) Venn diagram showing genes with significant (|Log_2 Fold Change|

≥ 1, $P_{adj} < 0.01$) differences in transcript abundance during alkaline pH induced stress in *H. hammondi* and *T. gondii* (at least 1 of 2 independent experiments) and during spontaneous development in *H. hammondi*. *=7, **=22 C) Schematic representing the prioritization strategy used to identify priority candidates predicted to be involved in tissue cyst formation. D) Mean centered heat map showing 16 priority candidate BIFs and 1 priority candidate BSF.

3.2.2 Disruption of candidate genes using CRISPR/Cas9 gene editing

To determine if our candidate genes were involved in tissue cyst formation, we sought to disrupt the locus of select genes using CRISPR/Cas9. We disrupted our candidate genes by transfecting parasites with a plasmid expressing Cas9-GFP under the control of the *T. gondii* SAG1 promoter as well as U6 gRNA expression cassette (*204*) that we modified to express a guide specific for our candidate gene or a non-targeting gRNA for control transfections. We co-transfected parasites with a linear repair cassette encoding either the HXGPRT selectable marker for use in CEPΔHXGRPT-GFP-LUC (TgCEP) parasites or the DHFR-TS selectable marker for use in oocyst derived TgVEG parasites. We isolated clonal parasite strains using limiting dilution and used a series of PCR reactions to verify the incorporation of the linear repair cassette in our candidate gene (knockout and repair strategy depicted in Figure 17A). We generated and validated successful disruptions for TgCEP_221840 (TgME49_221840) (Figure 17B), TgVEG_207210 (TgME49_207210) (Figure 17C), TgVEG_311100 (TgME49_311100) (Figure 17D), and TgVEG_200385 (TgME49_200385) (Figure 17D). Although TgVEG_207210 was not a final candidate in our screen, we were originally interested in this gene because of its transcriptional profile in *H. hammondi.* For the disruption of TgCEP_221840, we observed an insertion of the HXGPRT linear repair cassette in the TgCEPΔ221840 parasites as indicated by a ~3,000bp band in RXN1 that was not present in TgCEP WT parasites (RXN5), which amplified across the cut site

of the TgCEP_221840 locus, suggesting that a single copy of the repair cassette was inserted (Figure 17B). For TgVEG_207210 (Figure 2C), TgVEG_311100 (Figure 17D), and TgVEG_200385 (Figure 17D) we observed amplification of appropriately sized bands with a gene specific forward primer starting in the gene's coding sequence upstream of the cut site and a reverse primer (DHFR-TS_R or DHFT-TS_F as the linear repair cassette could incorporate in either orientation, see Figure 17A). These bands were also sequenced to verify that they contained the correct product. Moreover, these products were not present in the passaged-matched WT parasites. These data indicate that the DHFR-TS repair cassette inserted into the locus of each gene candidate. Furthermore, we were no longer able to amplify across the cut site with only gene specific primers for the parasite clones that indicated locus disruption via amplification with a gene specific primer and a DHFR primer, suggesting that a large insertion of potentially multiple repair cassettes occurred at a given locus.

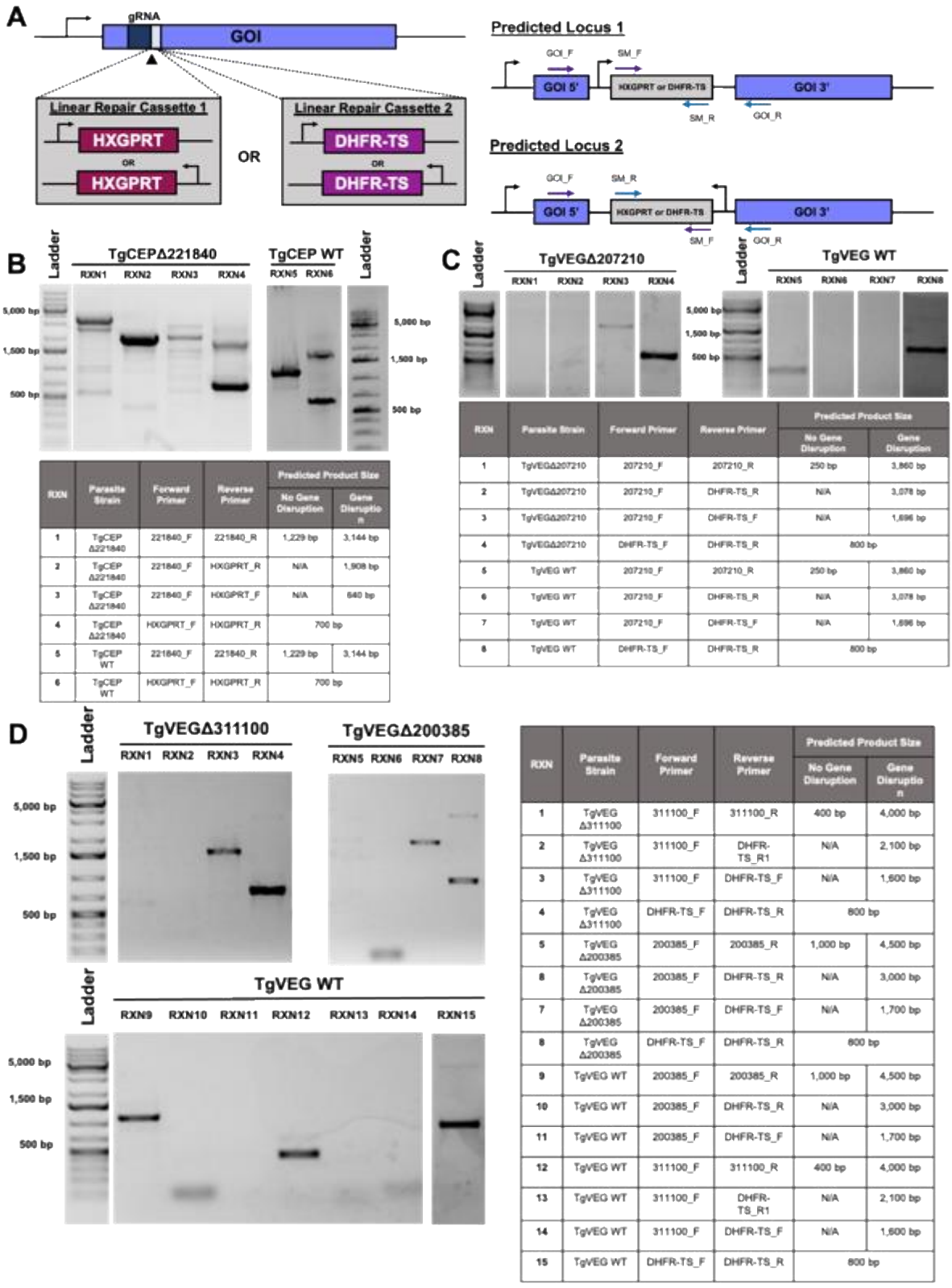

RXN	Parasite Strain	Forward Primer	Reverse Primer	Predicted Product Size	
				No Gene Disruption	Gene Disruption
1	TgCEP Δ221840	221840_F	221840_R	1,229 bp	3,144 bp
2	TgCEP Δ221840	221840_F	HXGPRT_R	N/A	1,908 bp
3	TgCEP Δ221840	221840_F	HXGPRT_F	N/A	640 bp
4	TgCEP Δ221840	HXGPRT_F	HXGPRT_R	700 bp	
5	TgCEP WT	221840_F	221840_R	1,229 bp	3,144 bp
6	TgCEP WT	HXGPRT_F	HXGPRT_R	700 bp	

RXN	Parasite Strain	Forward Primer	Reverse Primer	Predicted Product Size	
				No Gene Disruption	Gene Disruption
1	TgVEGΔ207210	207210_F	207210_R	250 bp	3,860 bp
2	TgVEGΔ207210	207210_F	DHFR-TS_R	N/A	3,078 bp
3	TgVEGΔ207210	207210_F	DHFR-TS_F	N/A	1,696 bp
4	TgVEGΔ207210	DHFR-TS_F	DHFR-TS_R	800 bp	
5	TgVEG WT	207210_F	207210_R	250 bp	3,860 bp
6	TgVEG WT	207210_F	DHFR-TS_R	N/A	3,078 bp
7	TgVEG WT	207210_F	DHFR-TS_F	N/A	1,696 bp
8	TgVEG WT	DHFR-TS_F	DHFR-TS_R	800 bp	

RXN	Parasite Strain	Forward Primer	Reverse Primer	Predicted Product Size	
				No Gene Disruption	Gene Disruption
1	TgVEG Δ311100	311100_F	311100_R	400 bp	4,000 bp
2	TgVEG Δ311100	311100_F	DHFR-TS_R1	N/A	2,100 bp
3	TgVEG Δ311100	311100_F	DHFR-TS_F	N/A	1,600 bp
4	TgVEG Δ311100	DHFR-TS_F	DHFR-TS_R	800 bp	
5	TgVEG Δ200385	200385_F	200385_R	1,000 bp	4,500 bp
6	TgVEG Δ200385	200385_F	DHFR-TS_R	N/A	3,000 bp
7	TgVEG Δ200385	200385_F	DHFR-TS_F	N/A	1,700 bp
8	TgVEG Δ200385	DHFR-TS_F	DHFR-TS_R	800 bp	
9	TgVEG WT	200385_F	200385_R	1,000 bp	4,500 bp
10	TgVEG WT	200385_F	DHFR-TS_R	N/A	3,000 bp
11	TgVEG WT	200385_F	DHFR-TS_F	N/A	1,700 bp
12	TgVEG WT	311100_F	311100_R	400 bp	4,000 bp
13	TgVEG WT	311100_F	DHFR-TS_R1	N/A	2,100 bp
14	TgVEG WT	311100_F	DHFR-TS_F	N/A	1,600 bp
15	TgVEG WT	DHFR-TS_F	DHFR-TS_R	800 bp	

Figure 17. Generation of knockout of high priority candidate genes using CRISPR/Cas9.

Schematic of CRISPR/Cas9 knockout and repair strategy and diagram of predicted loci of gene of interest (GOI) after incorporation of linear repair cassettes of selectable markers (SM) HXGPRT or DHFR-TS. Arrows indicate general location of primers. B) Gel image and PCR reactions used to identify disruption of the TgCEP_221840 locus along with passaged-matched control. C) Gel image and PCR reactions used to identify disruption of the TgVEG_207210 locus along with passage-matched control. E) Gel image and PCR reactions used to identify disruption of the TgVEG_311100 (*ROCY1*) locus and TgVEG_200385 (B*FD1*) and passaged matched controls.

3.2.3 Disruption of the *ROCY1* locus impairs *in vitro* tissue cyst formation

After validating locus disruption of our candidate genes (Figure 17), we determined the impact of each gene disruption on alkaline-pH-stress-induced tissue cyst formation. After 48 hours of stress, we identified no significant differences in the number of DBA-positive tissue cysts between the TgCEPΔ221840 (Figure 18A) and TgVEGΔ207210 (Figure 18B) knockouts relative to their passage-matched control. However, we did observe a significant decrease (P=0.0011) in the number of DBA-positive vacuoles for the TgVEGΔ311100 parasites (~25%) as compared to their WT controls (~65%) (Figure 18C). These data suggest that TgVEG_311100 is an important factor for the stress-induction of cystogenesis. We named this factor Regulator of Cystogenesis 1 (ROCY1). Previous work has identified another transcription factor, Bradyzoite-formation Deficient 1 (BFD1), that drives cystogenesis in *T. gondii* and results in a complete loss of tissue cyst formation in response to alkaline pH stress (*132*). Due to the importance of BFD1 in differentiation, we wanted to determine how disruption of ROCY1 compared to disruption of BFD1. Therefore, we generated TgVEG strains with a disruption in the BFD1 locus (Figure 17D) with the same passage history as our TgVEGΔ*ROCY1* parasite strain to eliminate any impact of passage history on tissue cyst formation. We then performed a head-to-head comparison of tissue cyst formation in response to alkaline pH stress and found that the TgVEGΔ*BFD1* parasites failed

to form DBA-positive tissue cysts (Figure 18D), consistent with previously published results in type II strains of *T. gondii (132)*. While a larger number of TgVEGΔ*ROCY1* parasites were capable of forming DBA-positive vacuoles in response to pH compared to TgVEGΔ*BFD1* parasites, they again formed significantly fewer tissue cysts compared to the WT control (P=0.026). Furthermore, when quantifying tissue cyst formation, we observed that for those TgVEGΔ*ROCY1* parasites that were DBA-positive the observed staining was less robust than the staining in WT parasites (Figure 18F). Therefore, we quantified the DBA fluorescence intensity of all parasites and found a significant decrease in fluorescence intensity between TgVEGΔ*ROCY1* and WT parasites (P<0.001), between TgVEGΔ*BFD1* and WT parasites (P<0.001), and between TgVEGΔ*ROCY1* and TgVEGΔ*BFD1* parasites (P=0.006) (Figures 18E-F). Together, this data suggests that ROCY1 plays an important role in the development of tissue cysts *in vitro*. Furthermore, the partial/impaired tissue cyst formation phenotype in the TgVEGΔ*ROCY1* parasites, as opposed to the near complete loss of DBA staining in the TgVEGΔ*BFD1* parasites, led us to hypothesize that ROCY1 may function downstream of BFD1.

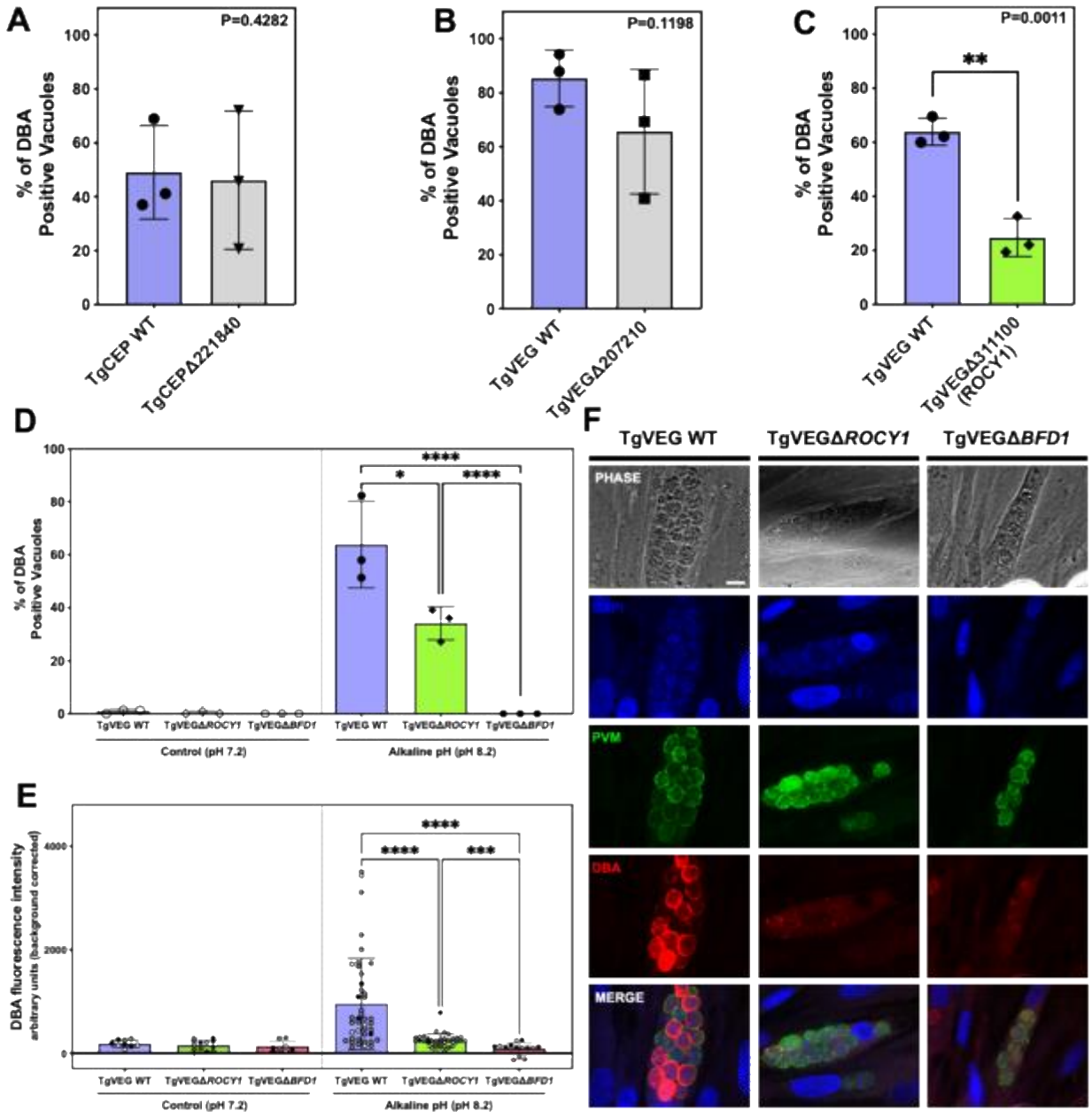

Figure 18. Disruption of the *ROCY1* locus impairs *in vitro* tissue cyst formation.

A-C) Quantification of tissue cyst formation in knockout parasites A) TgCEPΔ221840 B) TgVEGΔ207210 C) TgVEGΔ311100 (*ROCY1*) and passaged matched WT strains after 48 hours of alkaline pH induced stress. The mean and standard deviation (N=3 biological replicates) of the percentage of DBA-positive vacuoles observed in 15 parasite containing fields of view is plotted. Statistical significance was determined using a Student's one-tailed t-test on arcsine transformed percentage data. D) Quantification of tissue cyst formation in TgVEGΔ*ROCY1*, TgVEGΔ*BFD1*, and passaged matched TgVEG WT strains after growth in control conditions or after 48 hours of alkaline pH induced

stress (pH 8.2). The mean and standard deviation (N=3 biological replicates) of the percentage of DBA-positive vacuoles observed in 15 parasite containing fields of view is plotted. Statistical significance was determined for the alkaline pH condition using a One-Way ANOVA with Tukey's multiple comparisons tests on arcsine transformed percentage data. *P=0.0255, ****P <0.0001 E) Quantification of fluorescence intensity TgVEGΔ*ROCY1* and TgVEGΔ*BFD1* from E. The mean and standard deviation of the fluorescence intensity (background corrected) is plotted. Each point represents a single vacuole. Black, gray, and white symbols indicate from which replicate (N=3) the intensity measurement was derived. Statistical significance was determined for alkaline pH conditions using a Brown-Forsythe and Welch ANOVA test with Dunn's T3 multiple comparisons. ***P=0.0006 ****P <0.0001 G) Representative images of vacuoles exposed to alkaline pH stress for 48 hours. DNA was stained with DAPI (blue), the parasitophorous vacuole membrane (PVM) was stain with an anti-MAF1-b mouse polyclonal antibody (green), and tissue cysts were stained with rhodamine-labeled *Dohlichos biflorus* Agglutinin (DBA) (red). Scale bar represents 10 µm.

3.2.4 Disruption of the *ROCY1* locus dramatically alters the alkaline pH-stress-induced transcriptional response

To better understand how ROCY1 alters tissue cyst formation and compares with BFD1, we performed RNAseq on human foreskin fibroblasts (HFFs) infected with TgVEGΔ*ROCY1*, TgVEGΔ*BFD1*, and TgVEG WT parasites exposed to either control growth conditions (pH 7.2) alkaline pH stress conditions (pH 8.2) for 48 hours. Using principal component analysis (PCA) to take a broad look at the transcriptional responses of these parasites (Figure 19A), we found that separation along PC1 (62%) mostly represented the effect of pH and nutrient stress. All parasites grown in control conditions (WT, TgVEGΔ*ROCY1*, TgVEGΔ*BFD1*) clustered together along PC1 with minor separation in TgVEGΔ*ROCY1* and TgVEGΔ*BFD1* parasites from our TgVEG WT parasites along PCA2. Interestingly, we also saw a clear separation between TgVEG WT,

TgVEGΔ*ROCY1*, and TgVEGΔ*BFD1* exposed to stressed conditions on both PC1(62% of variance) and PC2 (9% of variance). Stressed TgVEG WT parasites were the most separated on PC1 compared to the control grouping but the least separated on PC2, while TgVEGΔ*BFD1* stressed parasites separated the least on PC1 but were the most separated on PC2 (Figure 19A). TgVEGΔ*ROCY1* parasites fell in the middle between the TgVEG WT and TgVEGΔ*BFD1* parasites exposed to stressed conditions. This transcriptional data is consistent with the intermediate DBA-staining phenotype that we observed in our immunofluorescence assays (Figure 18D-E).

We next compared changes in transcript abundance by conducting differential expression analysis using differential expression analysis with DESeq2. We found that both TgVEGΔ*ROCY1* parasites and TgVEGΔ*BFD1* parasites exposed to control conditions had similar transcriptional profiles to TgVEG WT parasites exposed to control conditions as we did not identify any genes with significant changes in transcriptional abundance in either TgVEGΔ*ROCY1* parasites or TgVEGΔ*BFD1* parasites in comparison to WT parasites ($|Log_2FC| > 1$, $P_{adj} < 0.01$) (Figure 19C-D). These data suggest that disruption of ROCY1 or BFD1 does not play a significant role during tachyzoite growth. We next looked at the transcriptional changes that occur in TgVEGΔ*ROCY1*, TgVEGΔ*BFD1*, and WT parasites in alkaline pH stress conditions (pH 8.2) relative to control conditions (pH 7.2). For WT parasites, as expected, we identified hundreds (265) genes with significant differences in transcriptional abundance in response to treatment with alkaline stress as compared to control conditions ($|Log_2FC| > 1$, $P_{adj} < 0.01$) (Figure 19B and E). However, the alkaline-stress-induced transcriptional response was dramatically impaired for both the TgVEGΔ*ROCY1* parasites (54 genes with significant changes in abundance in stress conditions as compared to control conditions; Figure 19B and F) and TgVEGΔ*BFD1* parasites (43 genes with

significant changes in abundance in stress conditions as compared to control conditions; Figure 19B and G). Overall, we found that 82% of the transcripts that change significantly in response to alkaline stress in WT parasites failed to change significantly when the *ROCY1* locus was disrupted and 87% of those genes failed to change significantly when the *BFD1* locus was disrupted (Figure 19H). These findings suggest that ROCY1 is another critical regulatory factor involved in initiating and/or mediating the early alkaline pH stress response in *T. gondii*. Strikingly, we also found that 74% of the transcripts that change in WT parasites no longer change significantly when either the *ROCY1* locus or the *BFD1* locus is disrupted (Figure 19H), suggesting that BFD1 and ROCY1 regulate transcriptional abundance of the same set of genes or that BFD1 activates the expression of ROCY1 very early in the bradyzoite developmental pathway. This finding, along with the intermediate phenotype observed from *in vitro* tissue cyst formation and PCA analysis, led us to hypothesize that ROCY1 may be regulated by BFD1 and function immediately (or nearly immediately) downstream to alter the transcriptional response to alkaline stress. To begin to address this hypothesis, we took a closer look at ROCY1 and found that it is predicted to encode a 920-amino acid protein (*126*) that contains a predicted nuclear localization signal (diagramed in blue in Figure 19J) and 3 CCCH type Zinc finger domains (SMART accession SM000356; diagramed in yellow in Figure 19J, the second CCCH motif is split between exons 2 and 3). When we examined the upstream region predicted to include the promoter and transcriptional start site (2,300bp directly before the start codon) of ROCY1 (identified using our transcriptional data and BFD1 Cleavage Under Targets and Release Using Nuclease CUT&RUN data (*132*)) we found 3 occurrences of a predicted BFD1 binding motif (CACTGG) within the previously identified CUT&RUN peaks (*132*), two of which were found downstream of the predicted transcriptional start site (TSS) and another found upstream of the TSS (diagramed in pink in Figure 19J). The

presence of BFD1 binding motifs, along with our transcriptional data, suggest that *ROCY1* transcription could be directly regulated by BFD1. To further investigate the hypothesis that BFD1 is responsible for the regulation of ROCY1, we used DESeq2 to compare TgVEGΔ*ROCY1* parasites and TgVEGΔ*BFD1* parasites grown in alkaline pH stress conditions to TgVEG WT parasites grown in alkaline stress conditions to identify dysregulated genes. We found that in stress conditions, TgROCY1 transcript abundance is significantly decreased ($Log_2FC = -1.46$, $P_{adj} < 0.001$) in TgVEGΔ*BFD1* parasites relative to WT parasites but TgBFD1 transcript did not change significantly in TgVEGΔ*ROCY1* parasites relative to WT parasites ($Log_2FC = -0.58$, $P_{adj} = 0.04$) (Table 4). Furthermore, we found that the majority of the dysregulated genes (23 of 26) in TgVEGΔ*ROCY1* parasites were also dysregulated in TgVEGΔ*BFD1* (Figure 19I). Most of the dysregulated genes were down regulated (18 of 26 in TgVEGΔ*ROCY1* and 53 of 74 in TgVEGΔ*BFD1*) and many of those genes are known bradyzoite genes such as CST1, BPK1, and MCP4 that are components of the cyst wall (*91*, *199*, *205*) (Table 4). Taken together these data suggest that ROCY1 functions as a positive regulator of bradyzoite transcription and is a likely downstream target of BFD1, and the significant overlap between BFD1- and ROCY1-dependent stress-induced transcripts suggests that these two factors are likely very proximal in the bradyzoite development pathway.

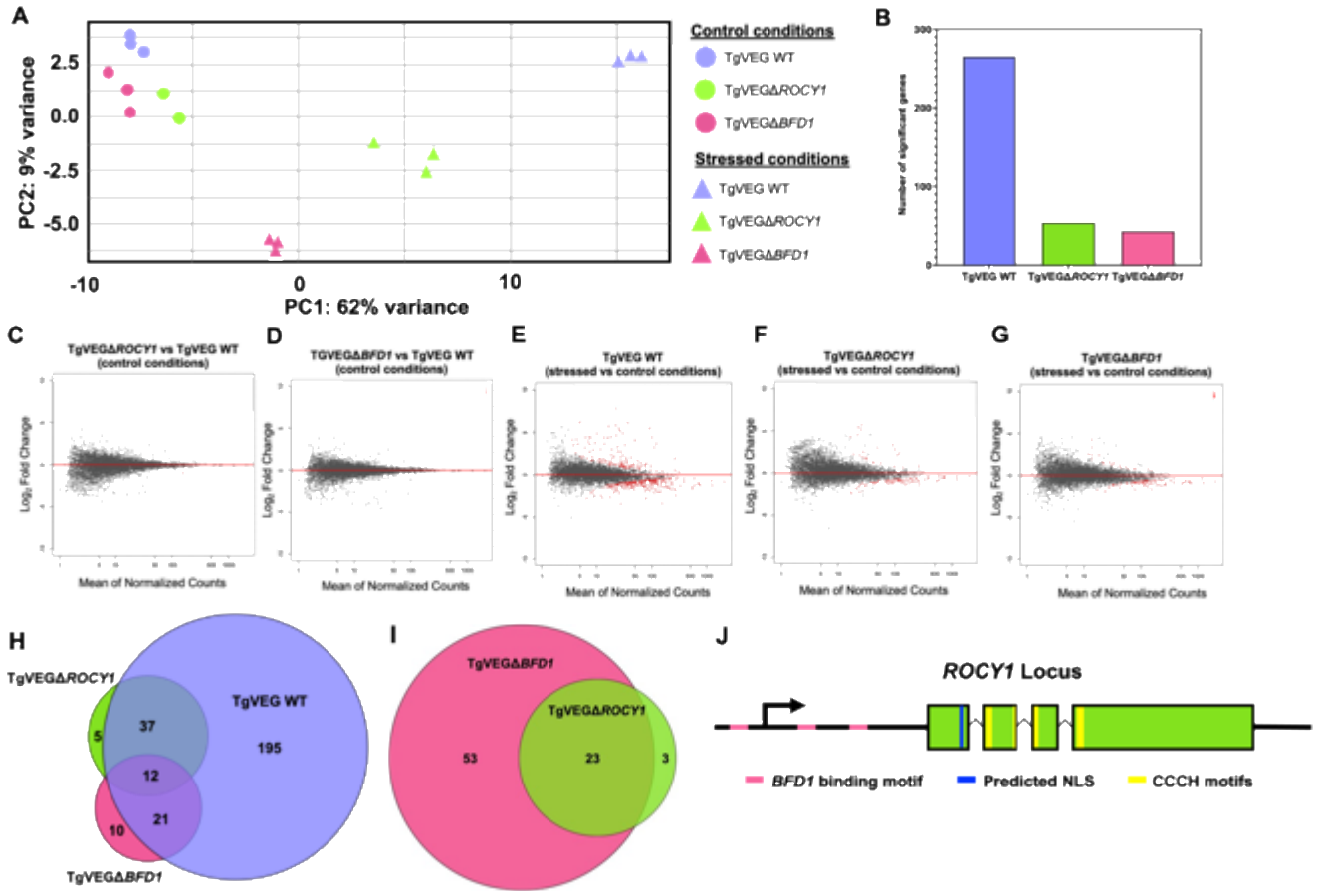

Figure 19. Disruption of the ROCY1 locus dramatically alters the alkaline pH-stress-induced transcriptional response.

A) Principal components (PC) 1 and 2 of cells infected with TgVEG WT, TgVEGΔ*ROCY1*, and TgVEGΔ*BFD1* expose to either control (●) or alkaline pH stress (▲) conditions for 48 hours. (B) Number of significantly different transcript observed for infection with TgVEG WT, TgVEGΔ*ROCY1*, and TgVEGΔ*BFD1* ($|\text{Log}_2 \text{ Fold Change}| \geq 1$, $P_{adj} < 0.01$). C-D) MA-plots representing changes in transcript abundance in TgVEGΔ*ROCY1* (C) or TgVEGΔ*BFD1* (D) infection compared to TgVEG WT infection in control conditions. Red dots (●) genes with a P_{adj} value < 0.01. E-G) MA-plots representing changes in transcript abundance in TgVEG WT (E), TgVEGΔ*ROCY1* (F), or TgVEGΔ*BFD1* (G) infections in alkaline stress conditions compared to control conditions. Red dots (●) genes with a P_{adj} value < 0.01. H) Venn diagram of genes with significant differences in transcript abundance in alkaline stress conditions compared to control conditions ($|\text{Log}_2 \text{ Fold Change}| \geq 1$, $P_{adj} < 0.01$). I) Venn diagram of genes with significant differences in transcript abundance in TgVEGΔ*BFD1* (pink) and TgVEGΔ*ROCY1* (green) parasites compared to TgVEG WT parasites in alkaline stress conditions ($|\text{Log}_2 \text{ Fold Change}| \geq 1$, $P_{adj} < 0.01$). (J) Diagram of

ROCY1 locus showing predicted BFD1 binding sites both upstream and downstream of the predicted transcriptional start site, a predicted NLS, and 3 zinc finger CCCH motifs (second motif is split between exon 2 and 3).

Table 4. Significantly dysregulated genes in TgVEGΔ*ROCY1* and/or in TgVEGΔ*BFD1* parasites compared to TgVEG WT parasites in alkaine stress conditions

Gene ID	Annotation	TgVEGΔ*ROCY1*		TgVEGΔ*BFD1*	
		Log_2 FC	P_{adj}	Log_2 FC	P_{adj}
TGME49_209755	hypothetical protein	-4.14	4.31E-35	-9.30	1.04E-12
TGME49_202020	DnAK-TPR	-3.21	2.06E-20	-3.94	4.22E-16
TGME49_280570	SRS35A	-3.02	1.39E-34	-5.09	1.56E-26
TGME49_311100	zinc finger (CCCH type) motif-containing protein (ROCY1)	-2.99*	3.75E-26*	-1.46	4.69E-08
TGME49_207160	SRS49D	-2.91	2.99E-16	-8.83	3.57E-11
TGME49_207210	hypothetical protein	-2.84	4.27E-21	-6.60	3.60E-12
TGME49_216140	tetratricopeptide repeat-containing protein	-2.22	6.45E-12	-3.96	6.88E-13
TGME49_290970	8-amino-7-oxononanoate synthase	-1.70	1.61E-09	-8.77	3.50E-11
TGME49_264660	SRS44 (CST1)	-1.69	1.53E-31	-4.34	7.75E-64
TGME49_263270	glycerophosphodiester phosphodiesterase family protein	-1.54	1.06E-08	-3.20	1.59E-14

TGME49_253330	Bradyzoite Pseudokinase1 (BPK1)	-1.52	6.67E-32	-3.91	3.17E-67
TGME49_208730	MCP4	-1.51	2.15E-22	-6.90	5.87E-32
TGME49_293780	hypothetical protein	-1.46	2.56E-08	-2.64	6.23E-12
TGME49_203290	hypothetical protein	-1.22	8.89E-08	-3.45	8.24E-19
TGME49_266120	thioredoxin-dependent peroxidase TPX1/2	-1.19	6.79E-04	---	---
TGME49_262710	Ctr copper transporter family protein	-1.17	6.60E-06	---	---
TGME49_275320	penicillin amidase	-1.15	3.88E-07	---	---
TGME49_237170	hypothetical protein	-1.11	2.68E-04	-1.62	1.23E-04
TGME49_204050	subtilisin SUB1	1.01	8.55E-08	1.55	5.11E-14
TGME49_260600	Pumilio-family RNA binding repeat-containing protein	1.12	8.80E-06	1.33	1.02E-05
TGME49_315320	SRS52A	1.18	6.97E-09	1.12	9.32E-06
TGME49_249300	hypothetical protein	1.21	5.80E-04	1.34	4.61E-03
TGME49_276930	hypothetical protein	1.32	3.66E-04	1.38	5.89E-03
TGME49_244280	hypothetical protein	1.39	1.05E-09	1.16	8.70E-05
TGME49_250955	KRUF family protein	1.60	4.29E-05	2.08	5.43E-06
TGME49_294990	hypothetical protein	1.96	5.81E-05	2.33	7.47E-05
TGME49_253790	zinc finger (CCCH type) motif-containing protein	---	---	-7.77	9.28E-09

TGME49_259020	bradyzoite antigen 1 (BAG1)	---	---	-7.61	5.23E-08
TGME49_291040	lactate dehydrogenase 2 (LDH2)	---	---	-7.40	5.47E-08
TGME49_293790	hypothetical protein	---	---	-7.34	1.17E-07
TGME49_312330	hypothetical protein	---	---	-4.48	1.14E-27
TGME49_295960	hypothetical protein	---	---	-4.02	8.18E-12
TGME49_208740	MCP3	---	---	-3.80	1.02E-62
TGME49_295950	KRUF family protein	---	---	-3.42	1.45E-09
TGME49_261650	hypothetical protein	---	---	-2.75	1.10E-10
TGME49_270240	MAG1	---	---	-2.28	4.62E-79
TGME49_305460	methionine aminopeptidase 2, putative	---	---	-2.11	1.08E-08
TGME49_315270	hypothetical protein	---	---	-2.08	2.63E-13
TGME49_225540	hypothetical protein	---	---	-2.02	5.43E-10
TGME49_249770	Nmda1 protein	---	---	-1.82	5.83E-03
TGME49_268790	hypothetical protein	---	---	-1.77	3.11E-13
TGME49_269660	TFIIH basal transcription factor complex helicase XPB subunit	---	---	-1.70	2.47E-03
TGME49_213445	hypothetical protein	---	---	-1.68	2.73E-06
TGME49_260520	hypothetical protein	---	---	-1.62	2.40E-04
TGME49_290300	hypothetical protein	---	---	-1.58	1.44E-04

TGME49_201840	aspartyl protease ASP1	---	---	-1.56	6.02E-06
TGME49_297710	hypothetical protein	---	---	-1.53	9.00E-03
TGME49_226420	peptidase family M3 protein	---	---	-1.42	6.65E-05
TGME49_248990	hypothetical protein	---	---	-1.36	1.04E-06
TGME49_261970	hypothetical protein	---	---	-1.36	1.44E-04
TGME49_236010	prenylcysteine oxidase	---	---	-1.31	5.07E-07
TGME49_299030	RNA recognition motif 2 protein	---	---	-1.27	1.55E-03
TGME49_269690	hypothetical protein	---	---	-1.27	2.62E-04
TGME49_297340	hypothetical protein	---	---	-1.24	1.04E-07
TGME49_200385	Myb family DNA-binding domain-containing protein (BFD1)	---	---	-1.22*	1.39E-05*
TGME49_262970	hypothetical protein	---	---	-1.15	2.26E-03
TGME49_269420	hypothetical protein	---	---	-1.14	2.05E-03
TGME49_296121	hypothetical protein	---	---	-1.13	9.04E-05
TGME49_245530	hypothetical protein	---	---	-1.11	5.83E-03
TGME49_247440	hypothetical protein	---	---	-1.10	2.23E-07
TGME49_262560	hypothetical protein	---	---	-1.06	4.27E-04
TGME49_215910	hypothetical protein	---	---	-1.03	3.98E-05
TGME49_273320	hypothetical protein	---	---	-1.02	8.46E-03
TGME49_214320	facilitative glucose transporter GT1	---	---	-1.02	2.82E-05

TGME49_203630	ribosomal protein RPL44	---	---	1.01	6.70E-04
TGME49_250115	hypothetical protein	---	---	1.06	1.20E-03
TGME49_241300	hypothetical protein	---	---	1.06	8.92E-03
TGME49_234550	ribosomal protein RPL29	---	---	1.08	8.17E-10
TGME49_211720	AP2 domain transcription factor AP2IV-5	---	---	1.09	1.23E-04
TGME49_308090	rhoptry protein ROP5	---	---	1.15	2.59E-14
TGME49_299780	hypothetical protein	---	---	1.17	6.65E-05
TGME49_291890	microneme protein MIC1	---	---	1.24	4.85E-19
TGME49_241240	hypothetical protein	---	---	1.40	3.74E-25
TGME49_239010	hypothetical protein	---	---	1.41	4.83E-04
TGME49_252065	KRUF family protein	---	---	1.92	3.47E-06
TGME49_233450	SRS29A (SUS1,SRS1)	---	---	2.09	7.43E-05
TGME49_250950	KRUF family protein	---	---	2.12	5.44E-03

*Transcriptional difference due to disruption of the TgVEGΔ*ROCY1* and TgVEGΔ*BFD1* loci.

3.2.5 Engineering TgVEG WT, TgVEGΔ*ROCY1*, and TgVEGΔ*BFD1* parasites to express GFP and luciferase

To facilitate future experiments comparing TgVEG WT, TgVEGΔ*ROCY1*, and TgVEGΔ*BFD1* parasites, we inserted GFP under the control of the SAG1 promoter and Click Beetle Luciferase under the control of the DHFR promoter from the pClickLUC-GFP-SNR1HA plasmid via co-transfection with the pCRISPR-SNR1 plasmid (see materials and methods and

Figure 20A), to disrupt the SNR1 gene which is a negative selectable marker that confers resistance to sinefungin, an known inhibitor of parasite growth (*206*). We then generated clonal parasites for each sinefungin resistant strain using limiting dilution and validated that these parasite strains expressed both luciferase (LUC) (Figure 20B) and GFP (Figure 20C). Because the SNR1 gene is a putative amino acid transporter and nutrient stress can impact differentiation (*206*), we verified that the tissue cyst formation phenotype in response to alkaline pH induced stress was the same as the non-GFP-LUC strains with an intact SNR1 gene by exposing these parasites to alkaline stress (pH 8.2) for 48 hours and quantifying tissue cyst formation as indicated by DBA (Figure 20D) staining and DBA fluorescence intensity (Figure 20E and 20F). We observed the same tissue cyst formation phenotype as we did for our non-GFP-LUC strains (Figure 20D-F), which demonstrates that the addition of GFP and luciferase to these parasite strains did not impact their ability to form tissue cysts in response to alkaline pH derived stress.

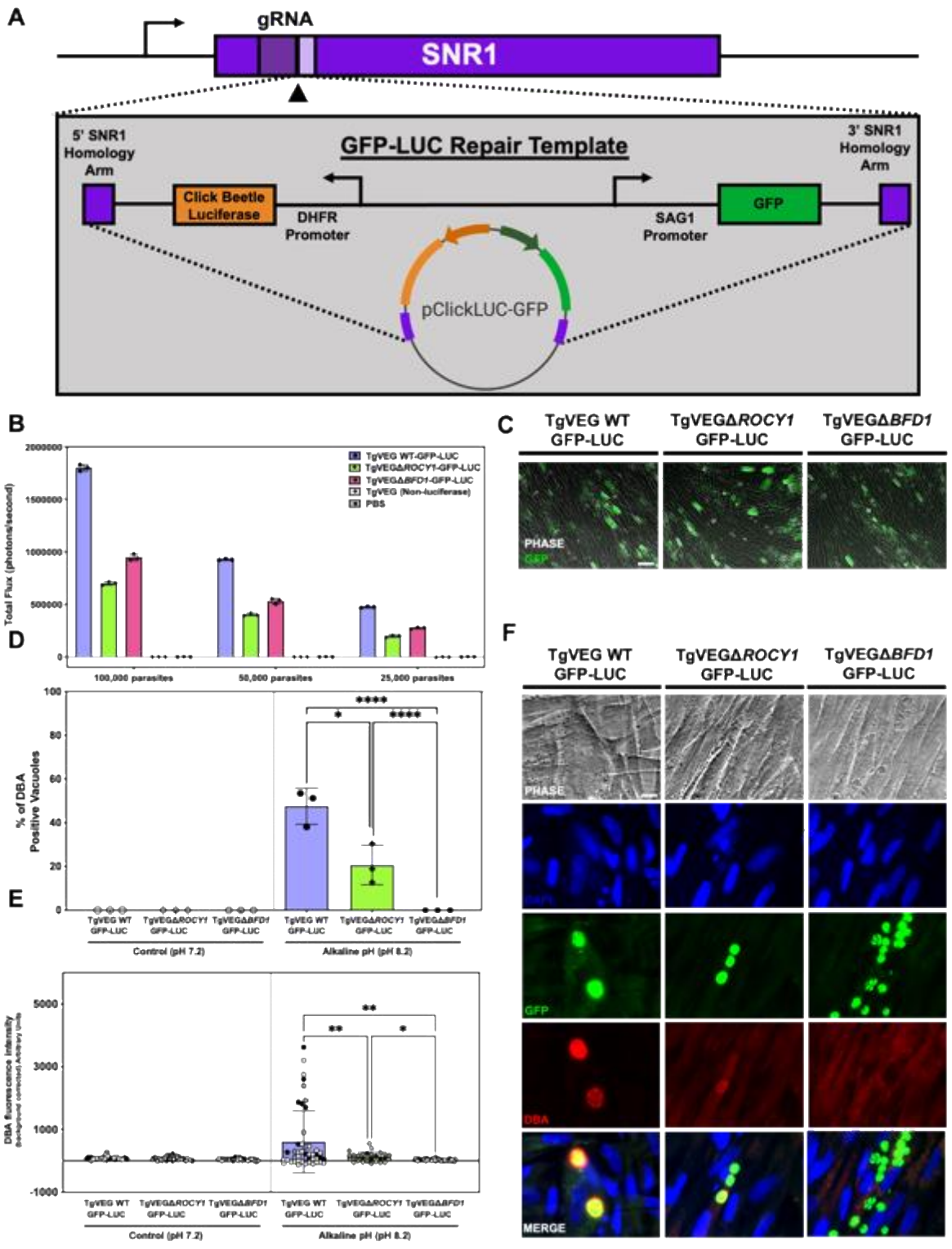

Figure 20. Engineering TgVEG WT, TgVEGΔ*ROCY1*, and TgVEGΔ*BFD1* parasites to express GFP and luciferase.

A) Schematic representing the strategy used to insert GFP and luciferase into the SNR1 gene (TgVEG_ 290860). B) Quantification of luciferase signal (photons/sec) after incubating 100,000, 50,000, and 25,000 parasites (TgVEG WT-GFP-LUC, TgVEGΔ*ROCY1*-GFP-LUC, TgVEGΔ*BFD1*-GFP-LUC, and TgVEG; PBS was used as a control) with d-Luciferin for 10 minutes. C) Representative images showing GFP expressing parasites. Scale bar represents 100µm. D) Quantification of tissue cyst formation in TgVEGΔ*ROCY1*-GFP-LUC, TgVEGΔ*BFD1*-GFP-LUC, and passaged matched TgVEG WT-GFP-LUC strains after growth in control conditions or after 48 hours of alkaline pH induced stress (pH 8.2). The mean and standard deviation (N=3 biological replicates) of the percentage of DBA-positive vacuoles observed in 15 parasite containing fields of view is plotted. Statistical significance was determined for the alkaline pH condition using a One-Way ANOVA with Tukey's multiple comparisons tests on arcsine transformed percentage data. *P=0.0118, ****P <0.0001 E) Quantification of fluorescence intensity TgVEG WT-GFP-LUC, TgVEGΔ*ROCY1*-GFP-LUC, and TgVEGΔ*BFD1*-GFP-LUC from E. The mean and standard deviation of the fluorescence intensity (background corrected) is plotted. Each point represents a single vacuole. Black, gray, and white symbols indicate from which replicate (N=3) the intensity measurement was derived. Statistical significance was determined for alkaline pH conditions using a Brown-Forsythe and Welch ANOVA test with Dunn's T3 multiple comparisons. *P=0.0112, **P =0.0076 (WT vs Δ*ROCY1*), and **P=0.0010 (WT vs Δ*BFD1)* G) Representative images of vacuoles exposed to alkaline pH stress for 48 hours. DNA was stained with DAPI (blue), parasites expressed GFP, and tissue cysts were stained with rhodamine labeled *Dohlichos Biflorus* Agglutinin (DBA) (red). Scale bar represents 10 µm.

3.2.6 ROCY1 is necessary for brain tissue cyst formation during murine infections

Our *in vitro* data as well our transcriptional data suggest that ROCY1 is an important regulator of cystogenesis and is likely induced early in the BFD1-driven cyst formation process. To determine if ROCY1 is also important for cyst formation in animals, we infected CBA/J mice with TgVEG WT-GFP-LUC, TgVEGΔ*ROCY1*-GFP-LUC, and TgVEGΔ*BFD1*-GFP-LUC parasites and monitored pathogenesis, morbidity and mortality using multiple approaches including weight loss and *in vivo* bioluminescence imaging. Mice were first imaged at 3 h post-

infection and we observed no significant differences in luciferase signal at this time point (P= 0.089 TgVEG WT-GFP-LUC vs TgVEGΔ*ROCY1*-GFP-LUC, P=0.36 TgVEG WT-GFP-LUC vs TgVEGΔ*BFD1*-GFP-LUC, and P=0.71 TgVEGΔ*ROCY1*-GFP-LUC vs TgVEGΔ*BFD1*-GFP-LUC). Parasite proliferation for all 3 strains were similar during the first 5 days of infection. At days 7 and 8 post infection, we observed a significant decrease in luciferase signal in the TgVEGΔ*ROCY1*-GFP-LUC parasites as compared to the TgVEG WT-GFP-LUC parasites (P=0.0350 at day 7 and P=0.0203 at day 8) (Figure 21A). All mice survived for the entire 21-day infection, demonstrating that there are no substantial differences in mortality between these parasite strains (Figure 21E-G). Interestingly, we observed a significant difference in the mass of the TgVEGΔ*BFD1*-GFP-LUC infected mice as compared to the TgVEG WT-GFP-LUC infected mice at days 16 and 18 post-infection (P=0.0033 at day 16 post infection and P=0.032 at day 18 post infection) (Figure21D). These data suggest that BFD1 knockout parasites may cause more severe disease at this late time point.

After 3 weeks, we euthanized the infected mice and quantified the number of parasites per brain using quantitative PCR and the number of tissue cysts per brain using fluorescence microscopy. Mice infected with TgVEGΔ*ROCY1*-GFP-LUC parasites had significantly fewer parasites per brain as compared to both TgVEG WT-GFP-LUC and TgVEGΔ*BFD1*-GFP-LUC infected mice (P=0.0001 for TgVEGΔ*ROCY1*-GFP-LUC vs TgVEG WT-GFP-LUC and P=0.0085 for TgVEGΔ*ROCY1*-GFP-LUC vs TgVEGΔ*BFD1*-GFP-LUC) (Figure 21B). These data suggest that ROCY1 is important for either 1) survival of the parasites during chronic infection or 2) for the parasites ability to colonize the brain. Despite being able to isolate and quantify tissue cysts from the brains of mice infected with TgVEG WT-GFP-LUC we failed to isolate tissue cyst from the brains of mice infected with either TgVEGΔ*ROCY1*-GFP-LUC and TgVEGΔ*BFD1*-GFP-LUC

(limit of detection = 40) (Figure 21C). This result demonstrates that, like BFD1, ROCY1 is necessary for tissue cyst formation in murine brains. These data suggest that ROCY1 is also a critical parasite factor needed for the establishment of a chronic infection *in vivo*, and again emphasizes that its position in the bradyzoite development pathway may be very proximal to BFD1 as suggested by our transcriptional analyses.

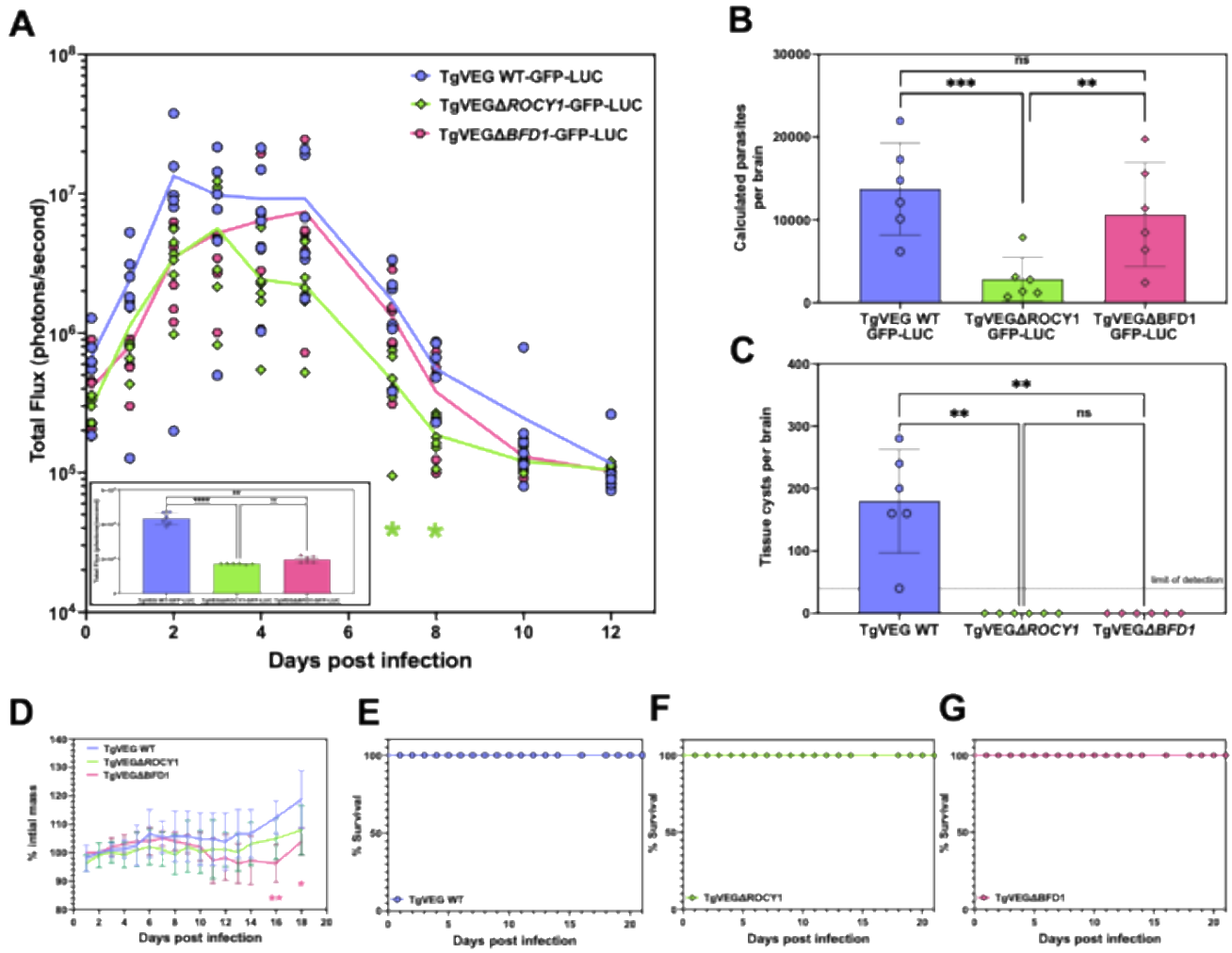

Figure 21. ROCY1 is necessary for tissue cyst formation and the establishment of chronic infection in mice.

A) Quantification of bioluminescent imaging of mice infected with TgVEG WT-GFP-LUC, TgVEGΔ*ROCY1*-GFP-LUC, and TgVEGΔ*BFD1*-GFP-LUC parasite (N=6). Each point represents an individual mouse and the line represents the mean. Statistical significance was determine using a repeated-measures two-way ANOVA with Geisser-Greenhouse correction and Tukey's multiple comparisons test on log transformed total flux data. *P=0.0350 (D7)

*P=0.0203 (D8). A-Inset) Luciferase signal from 250,000 extracellular parasites immediately after infection. Statistical significance was determined using a Brown-Forsythe and Welch ANOVA with Dunn's T3 multiple comparisons test. ****P <0.0001 B) Quantification of parasite genomes per brain in infected mice at 3 weeks post infection. Mean and standard deviation are plotted. Each point represents and individual mouse. Statistical significance was determined using a one-way ANOVA with Tukey's multiple comparison test on ΔC_t values. **P_{adj}=0.0085 ***P_{adj}=0.0001 C) Brain tissue cysts burden observed in infected mice at 3 weeks post infection. Mean and standard deviation are plotted. Each point represents and individual mouse. Limit of detection = 40. Statistical significance was determined using a Kruskal-Wallis test with Dunn's multiple comparisons. **P=0.0015 D) Average mass of infected mice normalized to initial mass during the 3-week infection. Mean (line) and standard deviation are plotted. Statistical significance was determined using using a repeated-measures two-way ANOVA with Geisser-Greenhouse correction and Tukey's multiple comparisons test. *P=0.0324 **P=0.0033 E-G) Survival curves for mice infected with E) TgVEG WT-GFP-LUC, F) TgVEGΔ*ROCY1*-GFP-LUC, and G) TgVEGΔ*BFD1*-GFP-LUC.

3.2.7 Reactivation in Δ*ROCY1* parasites is delayed compared to wild type and Δ*BFD1* parasites

Even though we failed to observe tissue cysts in the brains of either the TgVEGΔ*ROCY1*-GFP-LUC and TgVEGΔ*BFD1*-GFP-LUC parasites, we wanted to determine if these parasite strains were able to establish a chronic infection that could reactivate and lead to morbidity and mortality in mice. To determine if reactivation was possible, we infected mice with TgVEG WT-GFP-LUC, TgVEGΔ*ROCY1*-GFP-LUC, and TgVEGΔ*BFD1*-GFP-LUC parasites and assigned them to either the control group (N=6) or the reactivation group (N=6). On day 30 post infection, mice in the reactivation group were given dexamethasone in their drinking water to induce reactivation and subsequent reactivation was monitored using bioluminescence imaging *(165, 207)*. We monitored reactivation by imaging the infected mice on days 4, 6, 7, 8, 10, 12, and 14

after dexamethasone treatment (Figure 22A-B). On day 4 post-dexamethasone treatment, one mouse in the TgVEGΔ*ROCY1*-GFP-LUC infection/dexamethasone treatment group died likely due to handling or because of an adverse reaction to anesthesia (Figure 22B, indicated by ✝). We removed this mouse from future analyses quantifying parasite burden using luminescence. We observed a significant increase in luciferase signal measured as total flux in dexamethasone-treated mice infected with TgVEG WT-GFP-LUC parasites as compared to control mice at day 4 post-dexamethasone treatment (P_{adj}=0.038) and at day 8 post dexamethasone treatment (P_{adj}=0.0466) (Table 4), indicative of reactivation. We observed similar results for the dexamethasone-treated mice infected with TgVEGΔ*BFD1*-GFP-LUC parasites, where we found a significant increase in luciferase signal on days 6, 7, 8, 10, and 14 post-dexamethasone treatment in dexamethasone-treated mice compared to controls (Figure 22B, Table 5). However, for dexamethasone-treated mice infected with TgVEGΔ*ROCY1*-GFP-LUC parasites, reactivation was delayed in comparison to mice infected with TgVEG WT-GFP-LUC and TgVEGΔ*BFD1*-GFP-LUC, as we only found a significant difference in luciferase signal between control and dexamethasone-treated mice infected with TgVEGΔ*ROCY1*-GFP-LUC on day 8 post dexamethasone treatment, 4 days later than initially observed for TgVEG WT-GFP-LUC infection and 2 days later than initially observed for TgVEGΔ*BFD1*-GFP-LUC infection, and this increase in average luciferase signal for TgVEGΔ*ROCY1*-GFP-LUC parasites continued to be observed on days 10 and 12 post-dexamethasone treatment (Figure 22B). We also observed a significant increase in luciferase signal in dexamethasone-treated mice infected with TgVEGΔ*BFD1*-GFP-LUC as compared to dexamethasone treated mice infected with TgVEGΔ*ROCY1*-GFP-LUC on days 7, 8, 10, and 14 following dexamethasone treatment (Table 5). Overall, these data indicate that Δ*ROCY1* parasites are significantly impaired in their brain colonization during the acute phase of infection and/or in

their ability to persist in the brain (Figure 21B), and that this results in a delayed reactivation phenotype compared to WT and Δ*BFD1* parasites.

Table 5. P_{adj} values from analysis of reactivation bioluminescence imaging.

Day post DEX	P_{adj}					
	WT (CTL vs DEX)	**Δ*ROCY1* (CTL vs DEX)**	**ΔBFD*1* (CTL vs DEX)**	**DEX (WT vs Δ*BFD1*)**	**DEX (WT vs Δ*ROCY1*)**	**DEX (Δ*ROCY1* vs Δ*BFD1*)**
0	0.3239	0.0677	0.9865	0.599	0.1604	0.832
4	**0.038**	0.1201	0.1762	0.7631	0.8724	0.9986
6	0.2192	0.2778	**0.0157**	0.5238	0.9569	0.0858
7	0.0712	0.0731	**0.0033**	0.7577	0.4502	**0.0225**
8	**0.0446**	**0.0306**	**<0.0001**	0.9977	0.7285	**0.0702**
10	0.0578	0.091	**0.0062**	0.8985	0.2222	**0.0275**
12	0.0816	0.0816	0.0922	0.8056	0.5897	0.069
14	0.0732	0.0666	**0.0016**	0.652	0.796	**0.0217**

Repeated measures two-way ANOVA with Geisser-Greenhouse correction and Sidak's multiple comparisons performed on log transformed total flux data from reactivation infection.

We also looked at the difference in the survival of mice infected with TgVEG WT-GFP-LUC, TgVEGΔ*ROCY1*-GFP-LUC, and TgVEGΔ*BFD1*-GFP-LUC and treated with dexamethasone. We found that dexamethasone treated mice infected with TgVEGΔ*BFD1*-GFP-LUC died significantly sooner than dexamethasone treated mice infected with TgVEG WT-GFP-LUC (Log-rank (Mantel-Cox) test, Bonferroni-corrected threshold for multiple comparisons = 0.017, P=0.0020) and dexamethasone-treated mice infected with TgVEGΔ*ROCY1*-GFP-LUC

(P=0.0136) (Figure 22C). We observed no difference in survival for dexamethasone-treated mice infected with TgVEG WT-GFP-LUC and TgVEGΔ*ROCY1*-GFP-LUC. Taken together, our data suggest that despite having a delayed reactivation phenotype, infection with parasites lacking ROCY1 does not seem to have a significant impact on survival.

In addition to monitoring reactivation, we also quantified the number of parasites in the brain as well as the number of brain cysts from the mice in our control (normal drinking water) group at 9 weeks post infection. We found significantly fewer TgVEGΔ*ROCY1*-GFP-LUC and TgVEGΔ*BFD1*-GFP-LUC parasites in the brain as compared to TgVEG WT-GFP-LUC (Figure 22E). This result differed from our quantification of parasites in the brain at 3 weeks post infection, where we only found fewer TgVEGΔ*ROCY1*-GFP-LUC parasites compared to TgVEG WT-GFP-LUC (while TgVEGΔ*BFD1*-GFP-LUC parasite numbers were similar to TgVEG WT-GFP-LUC parasite numbers) (Figure 21B). While these results are not directly comparable, as they are from two different experiments, they suggest that parasites lacking BFD1 are eliminated from the brain as infection progresses while those lacking ROCY1 may be primarily impaired in brain colonization. Similar to our experiment performed at 3 weeks post-infection, we again were unable to identify any tissue cysts in the brains of mice infected with either TgVEGΔ*ROCY1*-GFP-LUC and TgVEGΔ*BFD1*-GFP-LUC parasites (limit of detection = 7) at 9 weeks post infection (Figure 22F). This result further demonstrates that ROCY1, like BFD1, is necessary for tissue cyst formation in the mouse brain.

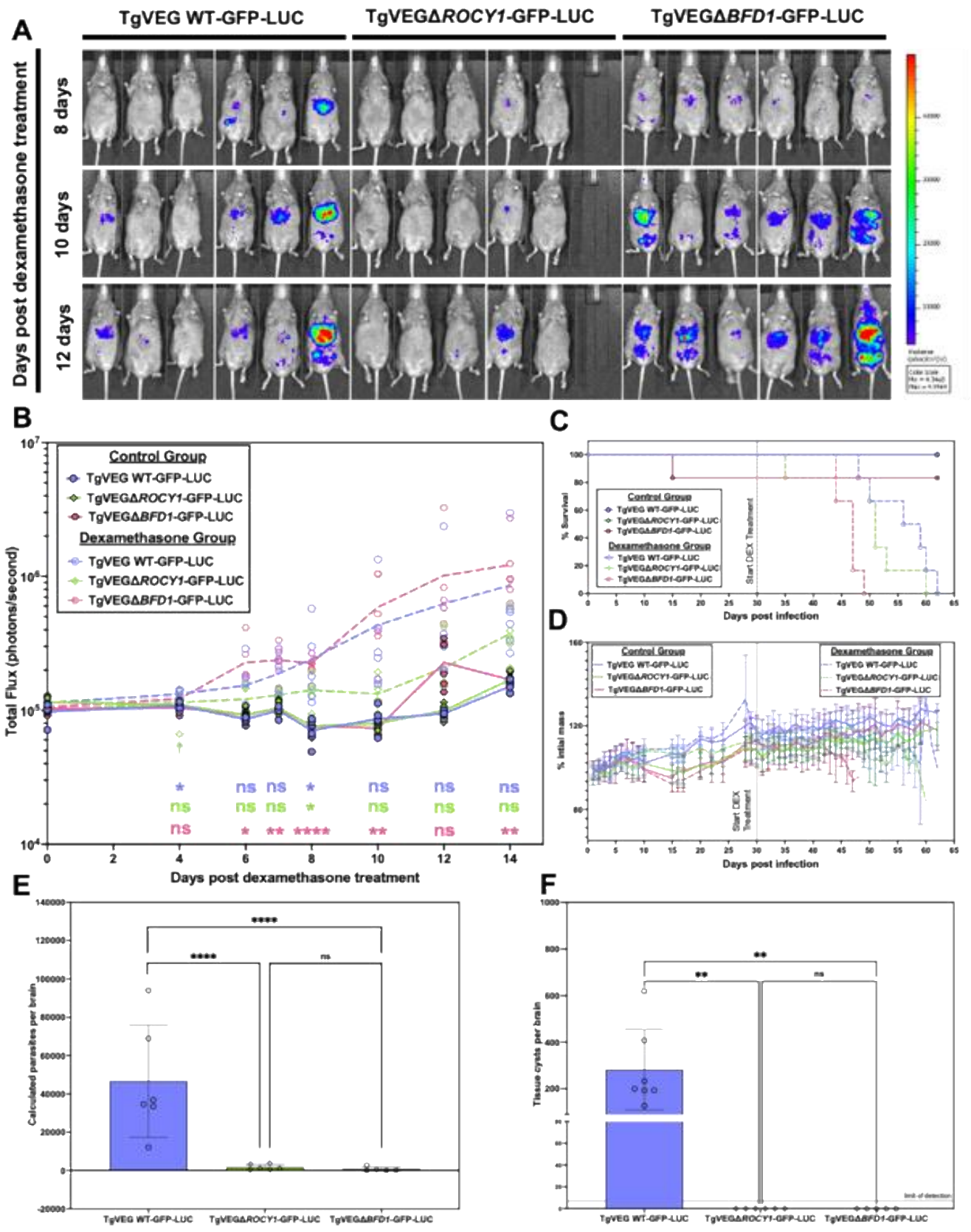
A
TgVEG WT-GFP-LUC
TgVEGΔROCY1-GFP-LUC
TgVEGΔBFD1-GFP-LUC
Days post dexamethasone treatment
8 days
10 days
12 days
B
Control Group
TgVEG WT-GFP-LUC
TgVEGΔROCY1-GFP-LUC
TgVEGΔBFD1-GFP-LUC
Dexamethasone Group
TgVEG WT-GFP-LUC
TgVEGΔROCY1-GFP-LUC
TgVEGΔBFD1-GFP-LUC
Total Flux (photons/second)
Days post dexamethasone treatment
C
% Survival
Start DEX Treatment
Days post infection
D
% Initial mass
Start DEX Treatment
Days post infection
E
Calculated parasites per brain
TgVEG WT-GFP-LUC
TgVEGΔROCY1-GFP-LUC
TgVEGΔBFD1-GFP-LUC
F
Tissue cysts per brain
TgVEG WT-GFP-LUC
TgVEGΔROCY1-GFP-LUC
TgVEGΔBFD1-GFP-LUC

Figure 22. TgVEGΔ*ROCY1* parasites display a delayed reactivation phenotype

A) Select bioluminescent images showing parasites-derived luciferase signal in CBA/J mice infected with TgVEG WT-GFP-LUC, TgVEGΔ*ROCY1*-GFP-LUC, and TgVEGΔ*BFD1*-GFP-LUC parasites and treated with dexamethasone (20mg/L) provided in their drinking water. B) Quantification of bioluminescent imaging of mice infected with TgVEG WT-GFP-LUC, TgVEGΔ*ROCY1*-GFP-LUC, and TgVEGΔ*BFD1*-GFP-LUC parasite belonging to either the control group (N=6 per parasite strain) or the dexamethasone treatment group (N=6 per parasite strain). Each point represents an individual mouse, and the line represents the mean. The double cross symbol (†) represents death due to handling/anesthesia. Statistical significance was determined using a repeated measures two-way ANOVA with Geisser-Greenhouse correction and Tukey's multiple comparisons performed on log transformed total flux data. Annotations represent dexamethasone group compared to control group for each parasites strain. Blue annotations represent TgVEG WT-GFP-LUC, green annotations represent TgVEGΔ*ROCY1*-GFP-LUC, and pink annotations represent TgVEGΔ*BFD1*-GFP-LUC. C) Survival of mice in the infection described in A and B. D) Average mass of infected mice normalized to initial mass during the infection. Mean and standard deviation are plotted. E) Quantification of parasite genomes per brain in infected mice from the control group at 9 weeks post infection. Mean and standard deviation are plotted. Each point represents and individual mouse. Statistical significance was determined using a one-way ANOVA with Tukey's multiple comparison test on ΔC_t values. ****P_{adj}<0.001 F) Brain tissue cysts burden observed in infected mice from the control group at 9 weeks post infection. Mean and standard deviation are plotted. Each point represents and individual mouse. Limit of detection =7. Statistical significance was determined using a Kruskal-Wallis test with Dunn's multiple comparisons. **P_{adj}=0.0017 for TgVEG WT-GFP-LUC vs TgVEGΔ*ROCY1*-GFP-LUC, **P_{adj}=0.0032 for TgVEG WT-GFP-LUC vs TgVEGΔ*BFD1*-GFP-LUC.

3.3 Discussion and conclusions

The formation of bradyzoites and tissue cysts are fundamental for the success of *T. gondii* as these life stages play a critical role in transmission, reproduction, and disease progression. The

formation of bradyzoites is necessary for the establishment of chronic infection which is fundamentally important for persistence of the parasite within its host and transmission to the next host (*11*, *12*, *76*, *151*). Despite the importance of bradyzoites, our understanding of the developmental pathways and the regulatory networks used by *T. gondii* to differentiate into these life stages is only starting to be elucidated. By using cross-species comparisons with *H. hammondi* at critical developmental time points, we have identified a previously uncharacterized parasite gene, *ROCY1*, that is important for tissue cyst formation *in vitro* and *in vivo*.

Our *in vitro* cyst induction assays along with our transcriptional analysis suggest that ROCY1 is critical for bradyzoite development. Our transcriptional data suggests that ROCY1 has a role in increasing the transcriptional abundance of key bradyzoites transcripts, such as DnAK-TPR, CST1, BPK1, and MCP4. Some of these bradyzoite specific transcripts have also been shown to be regulated by other known transcription factors such as the bradyzoite transcriptional repressors AP2IX-4 (*130*) AP2IV-4 (*129*), AP2IX-9 (*127*), and bradyzoite transcriptional activators AP2XI-4 (*131*) and AP2IV-3 (*128*). We identified extensive overlap in the dysregulated genes in TgVEGΔ*ROCY1* parasites as compared to TgVEGΔ*BFD1* parasites (Figure 19 H and L), implying that ROCY1 functions downstream of BFD1. Moreover, our data suggests that ROCY1 is partially regulated by BFD1. This regulation is further supported by the presence of multiple BFD1 binding motifs in the promoter of ROCY1 (*132*). These findings demonstrate that ROCY1 is proximal to BFD1 in the bradyzoite developmental pathway and plays a critical role in regulating the formation of tissue cysts. The potential link between BFD1 and ROCY1 provides a foundation for the identification of a gene regulatory network utilized by *T. gondii* to transition to the bradyzoite life stage.

The mechanistic role of ROCY1 in bradyzoite development is currently unclear. Our efforts to complement our TgVEGΔ*ROCY1* parasites have not yet been successful, despite numerous attempts. The predicted amino acid sequence of ROCY1 indicates that this protein contains 3 tandem CCCH zinc finger domains (diagramed in Figure 19I). While zinc finger proteins are typically viewed as DNA-binding transcription factors, proteins containing CCCH zinc finger domains are known to bind RNA (*208*, *209*). Interestingly, RNA binding proteins with CCCH zinc finger domains have been implicated in the regulation of growth and stress responses in plants, response to oxidative stress in mammalian cells, and the regulation of immune responses (*209*). CCCH zinc fingers have also been known to promote RNA deadenylation and degradation by binding to AU rich elements in the 3' UTRs of mRNA transcripts (*210*). *T. gondii* RNA binding proteins, such as TgAlba1, and TgAlba2, are involved in bradyzoite development and function in translational control *(138)*. These findings along with the functions of CCCH zinc fingers suggest that ROCY1 could interact with mRNA and regulate transcripts of key developmental genes induced during the alkaline pH stress response in *T. gondii*.

In addition to our transcriptional data, our *in vivo* data from mice infected with parasites lacking ROCY1 demonstrated that ROCY1 is a poor colonizer of the murine brain. We failed to isolate brain cysts from mice infected with TgVEGΔ*ROCY1* parasites (Figure 21C and Figure 22F). The complete lack of *in vivo* brain tissue cyst formation is not commonly observed when other important bradyzoite genes, such as CST1 (*143*), BAG1 (*211*), AP2XI-4 (*131*), AP2IX-4 (*130*), BPK1 (*145*), LDH2 (*212*), and MAG1 (*213*), are ablated. These findings make the ROCY1 phenotype so striking and suggest that it is a necessary factor for differentiation. A complete loss of *in vivo* brain cyst formation has been previously observed following infection with parasites lacking BFD1 (*132*) and AP2IV-4 (*129*), both an inducer and repressor of tissue cyst formation,

respectively. In addition to the complete loss of tissue cyst formation in the murine brain, we also observed a significant decrease in the number of parasites found in the brains of mice infected with TgVEGΔ*ROCY1* parasites. This significant decrease in the number of parasites in the brain is also found in parasites lacking AP2IV-4 and has been attributed to an increase in inflammatory monocytes in mice infected with these parasites. It is possible that mice infected with parasites lacking ROCY1 have a similar altered immune response and are easier for the mouse to clear during the early stages of infection. Understanding the immune pressures associated with this phenotype will be important for our understanding of the establishment of chronic infection in addition to the generation of novel therapeutics to target these currently untreatable life stages.

Given the importance of the tissue cysts for allowing parasites to reside in host tissue without being continually subjected to immune pressures during chronic infection (*17*, *26*), we were surprised that parasites lacking ROCY1, in addition to parasites lacking BFD1, were able to reactivated and cause a systemic infection following immune suppression with dexamethasone. To our knowledge, no other reactivation studies have been performed with parasites lacking critical bradyzoite factors. However, host immunity is thought to kill the majority of tachyzoites during the acute phases of infection and is hypothesized to promote the survival of bradyzoites by either eliminating tachyzoites or by inducing bradyzoite development (*77*). If the majority of tachyzoites are killed by host immunity, the ability of TgVEGΔ*ROCY1* and TgVEGΔ*BFD1* to reactivate when treated with dexamethasone after 30 days of infection suggests that either 1) some tissue cyst formation is occurring in the infected mice at levels below the detection threshold in the brain, 2) tissue cysts are forming in other tissues (such as muscle, spleen, or liver) instead of forming in the brain, or 3) these parasites can survive in the mouse despite being unable to form

tissue cysts, potentially as a transitional life stage that can survive immune pressure without forming a tissue cysts.

Our data also showed that mice infected with parasites lacking BFD1 reactivate faster and die sooner than mice infected with parasites lacking ROCY1 (Figure 22B-C). This difference in reactivation could be explained by increased parasite burden in the brains of mice infected with parasites lacking BFD1 compared to parasites lacking ROCY1 at 3 weeks post infection (Figure 21B). For these experiments, we started dexamethasone treatment at day 30 post infection (~4 weeks), which should allow adequate time for tissue cyst formation to occur (*214*, *215*). However, 30 days may not have been an adequate amount of time for TgVEGΔ*BFD1* parasites to be cleared from the brain, especially since the brain parasite burden of mice infected with TgVEGΔ*ROCY1* and TgVEGΔ*BFD1* were similar at 9 weeks post infection (Figure 22E). It would be interesting to profile the parasite and host transcriptome from infected brains at various time points to determine how/if these parasites differentiate during *in vivo* infection to determine if there is a biological reason attributed to the parasite or the host that allows for faster reactivation in mice infected with TgVEGΔ*BFD1* parasites as compared to infection with TgVEGΔ*ROCY1*.

Taken together, these findings demonstrate that ROCY1 is an important parasite factor for bradyzoite development in *T. gondii* and contributes to the development of a gene regulatory network used by these parasites to initiate the changes required for effective stage conversion. Future studies investigating the role of these factors in bradyzoite development in other parasite species, such as *H. hammondi*, that also rely on bradyzoite development for success, will help compare the strategies used by each species to progress to the bradyzoite life stage. Understanding the complexities of bradyzoite development associated between species has the potential to shed light on the fundamental differences attributed to each parasite's unique life cycle.

3.4 Materials and methods

3.4.1 Host cell and parasite strains

Toxoplasma gondii strain VEG (TgVEG) (*162*) and *Hammondi hammondi* strain HhCatAmer (HhAmer) (*5*) were isolated from oocysts from experimentally infected cats provided by J.P Dubey as previously describe (*44*, *216*). The *Toxoplasma gondii* strain CEPΔHXGRPT-GFP-LUC (TgCEP) (*217*)was also used. All *T. gondii* parasites were maintained through passage in Human foreskin fibroblasts (HFFs) cultivated with DMEM supplemented with 100U/mL penicillin, 100µg/mL streptomycin, 2mM L-glutamine, and 10% FBS (cDMEM) and maintained at 37 degrees C, 5% CO2.

3.4.2 Oocyst excystation

Sporozoites were harvested from oocysts as previously described (*44*, *216*). Following excystation, sporozoites were used to infected confluent monolayers of HFFs grown in T-25 tissue culture flasks and incubated at 37 degrees C, 5% CO2 for 24 hours. Following the initial 24-hour incubation, the infected monolayers were scrape, syringe lysed with a 25G needle, and filtered through a 5µm syringe driven filter. Zoites were then pelleted and counted to set up subsequent infections.

3.4.3 RNAseq of *H. hammondi* (HhAmer) and *T. gondii* (TgVEG) in control and bradyzoite induction conditions

HFFs were infected with 24 hour "zoites" at an MOI of 0.5 for *T. gondii* and 8.5 for *H. hammondi*. After 48 hours (3DPE), infected host cells were exposed to either bradyzoite induction media, pH 8.2, (*119*) or control media, cDMEM pH 7.2, for 48 hours. At 48 hours, the infected host cells were washed with PBS and RNA was harvested using the RNeasy Mini Kit 9(Qiagen). Total isolated RNA was processed for next generation sequencing as previously described (*44*). CLC Genomics Workbench was used to map all fastq reads to either the *T. gondii* genome or the *H. hammondi* genome as previously described (*44*). Total gene counts were exported from CLC and filtered so that only genes with a total of 10 reads across all parasite-specific samples were used for differential expression analysis using DESeq2 (*193*). A total of 7,182/8,920 genes were analyzed for *T. gondii* and 6106/7266 for *H. hammondi*. Venn diagrams were created with BioVenn (*218*) and Venn Diagram Plotter software (*219*). Heat maps were generated with MeV 4.9.0 (*220*).

3.4.4 Disruption of candidate gene loci

The CRISPR/Cas9 gene editing strategy was used to disrupt loci of candidate genes. For each candidate gene specific guide RNAs (gRNAs) were designed using the E-CRISP design tool (*Toxoplasma gondii* genome, medium setting). The gene specific gRNAs were incorporated into a version of the the pSAG1::CAS9-U6::sgUPRT plasmid provided by the Sibley lab (*172*) that was engineered to so that the UPRT gRNA was replaced with an PseI and FseI restriction site (*221*) (pCRISPR_ENZ) using Q5 mutagenesis (NEB) and verified with Sanger sequencing. Linear

repair constructs encoding either the HXGPRT and DHFR-TS selectable markers under the control of the DHFR 5' and 3' UTR were amplified from either the pGRA_HA_HPT (*69*) or pLIC-3HA-DHFR (*112*) using Platinum® *Taq* DNA Polymerase High Fidelity with High Fidelity PCR buffer and 110ng of template per reaction according to the manufacturer's reaction conditions. Approximately $10x10^6$ parasites were transfected with 25µg of the NheI-HF linearized CRISPR plasmid and 2.5µg of the appropriate linear repair cassette in 800µL of Cytomix (10mM KPO_4, 120mM KCL, 5mM $MgCl_2$, 25mM HEPES, 2mM EDTA) supplemented with 2mM ATP and 5mM glutathione using a BTX electroporation system – Electro Cell Manipulator 600 (2.4kV Set Charging Voltage, R3 Resistance timing). Transfection reactions were incubated at room temperature for 5 minutes before infecting confluent monolayers of HFFs. After ~24 hours, the infected host cells were grown in selection media containing cDMEM supplemented with mycophenolic acid (25µg/mL) and xanthine (50µg/mL) for TgCEP or cDMEM with 1µM pyrimethamine for TgVEG to select for parasites that incorporated the repair cassettes containing the selectable markers. After a stable population of parasites capable of growing in selection media was obtained, clonal population were obtained through serial dilution. Genomic DNA was isolated from the clonal populations and used to verify disruption of the candidate gene locus with the selectable marker with PCR (2x Bio^{TM}Mix Red used according to manufacturer's specifications, 25-50ng of genomic DNA per reaction) Amplified products were visualized with 1% agarose gels run at 90 volts for 25-40 minutes. The GeneRuler 1kb Plus DNA Ladder was used to estimate the size of the amplified products.

3.4.5 Alkaline pH-stress-induced tissue cyst formation assays

Confluent monolayers of HFFs grown on acid-etched coverslips in 24-well plates were infected with *T. gondii* at an MOI ranging from 0.25 to 1 depending on experiment. MOIs were the same for all tissue cyst formation assays performed on the same day. Parasites were grown for 48 hours and then their media was replaced with either control media (cDMEM pH 7.2) or bradyzoite induction media, pH 8.2, (*119*). Parasites grown in control conditions were incubated at 37 degrees C, 5% CO_2 and parasites grown in alkaline pH stress conditions were incubate at 37 degrees C with ambient CO_2 (0.03%). Control or bradyzoite induction media was replaced every 24 hours. After 48 hours of alkaline pH stress, infected coverslips were washed 2X with PBS, fixed with 4% paraformaldehyde in PBS, washed 2x with PBS, and stored in PBS at 4 degrees C until immunostaining was performed.

3.4.6 Immunofluorescence assays

Fixed coverslips were blocked with 5% BSA in PBS with 0.15% Triton-X 100 for 1 hour at room temperature. Coverslips infected with TgVEG WT, TgVEGΔ311100 (ROCY1), TgVEGΔ200385 (BFD1), TgVEGΔ207210, and TgCEPΔ221840 were stained with a primary polyclonal anti-MAF1b from mouse serum (1:1,000 dilution). After primary staining, the coverslips washed with PBS, stained with secondary goat anti-mouse Alexa-fluor 488 antibody and Rhodamine-labeled *Dolihos Biflourus* Agglutin (1:250) and washed with PBS. GFP-LUC parasite strains were only stained with Rhodamine-labeled *Dolihos Biflourus* Agglutin (1:250). Coverslips were then mounted using ProLong Diamond Antifade mountant with DAPI and allowed to cure overnight at room temperature. Coverslips were blindly observed with a 100X

objective on an Olympus IX83 microscope with cellSens software. The percentage of DBA-positive vacuoles was determined by counting vacuoles from 15 randomly chosen, parasite containing fields of view. Images were exported as .tiff files and average fluorescence intensity per pixel was quantified using ImageJ software and corrected for background fluorescence intensity.

3.4.7 RNAseq of TgVEGΔ*ROCY1* and TgVEGΔ*BFD1* in control and bradyzoite induction conditions

Confluent monolayers of HFFs grown in 24-well plates were infected with TgVEG WT, TgVEGΔ*ROCY1*, and TgVEGΔ*BFD1* parasites at an MOI of 0.5. Parasites were grown in control conditions (cDMEM pH 7.2, 37 degrees C, 5% CO_2) for 48 hours. After 48 hours the media was replaced with either control media (cDMEM pH 7.2) or bradyzoite induction media, pH 8.2, (*119*). Infected host cells grown in control conditions were incubated at 37 degrees C, 5% CO_2 and infected host cells grown in bradyzoite induction media were incubated at 37 degrees C with ambient CO_2 (0.03%). Control or bradyzoite induction media was replaced every 24 hours. After 48 hours of growth in bradyzoite induction conditions, all infected host cells were washed with PBS and total RNA was harvested using the RNeasy Mini Kit 9 (Qiagen). This RNA was then processed for next generation sequencing as previously described (*44*). Fastq files were first mapped to the human genome to remove host transcripts, Hg38 using CLC Genomics Workbench (default mapping settings for reverse strand sequencing, similarity fraction adjusted to 0.95) and a file of unmapped reads was generated for each sample. Unmapped reads were then mapped to the *T. gondii* genome (TgME49 v38) (default mapping settings for reverse stand sequencing). Total gene counts were exported from CLC and filtered so that a gene was only included for differential

expression analysis using DESeq2 (*193*) if there were a total of 30 or more reads across all samples. A total of 5,970/8,920 genes were analyzed. Venn diagrams were created with BioVenn (*218*) and Venn Diagram Plotter software (*219*).

3.4.8 Generation of GFP luciferase parasites

TgVEG WT, TgVEGΔ*ROCY1,* and TgVEGΔ*BFD1* parasites were modified to contain GPF and click beetle luciferase using the pClickLUC-GFP plasmid (*222*). A gRNA targeting the SNR1 gene in *T. gondii* (TgVEG_290860) was designed using the E-CRISP design tool (*Toxoplasma gondii* genome, medium setting) and incorporated into the pCRISPR_ENZ plasmid using Q5 mutagenesis and verified with Sanger sequencing (pCRISPR_SNR1). Homology arms corresponding to the 20bp sequencing flanking the Cas9 cut site were inserted to the pClickLUC-GFP plasmid (pClickLUC-GFP_SNR1-HA) using Q5 mutagenesis and verified with Sanger sequencing. Approximately $10x10^6$ TgVEG WT, TgVEGΔ*ROCY1,* and TgVEGΔ*BFD1* parasites were transfected with 25µg of the (pCRISPR_SNR1) and 25µg of the pClickLUC-GFP_SNR1-HA as described above. After ~24 hours, the infected host cells were grown in selection media containing cDMEM and $3x10^{-7}$M sinefungin. After a stable population of sinefungin resistant parasites were obtain, parasites were cloned using limiting dilution and screened for expression of GFP using an Olympus IX83 inverted fluorescent microscope. To screen GFP positive parasite clones for luciferase expression, parasites were scraped, syringe lysed with a 25- and 27-gauge needle, pelleted, and resuspended in PBS at a concentration of 500,000 parasites/mL, 250,000 parasites/mL, and 125,000 parasites/mL. For each concentration of parasites, 200µL was added to each well of a black 96 well plate (100,000, 50,000, and 25,000 parasites per well) in triplicate and 50µL of d-Luciferin potassium salt was added to each well. Parasites were incubated with d-

Luciferin at room temperature for 10 minutes and the luciferase signal was measure using an IVIS Lumina II *in vivo* bioluminescence imaging system. Non-luciferase expressing parasites and PBS were also used as controls for this experiment. To determine if the addition of GFP and luciferase altered tissue cyst formation, tissue cyst formation assays and immunofluorescence assays were performed as described above except parasites were only maintained in control conditions (cDMEM, pH 7.2) for 24 hours before the alkaline pH induction was performed.

3.4.9 Murine TgVEG WT-GFP-LUC, TgVEGΔ*ROCY1*-GFP-LUC, and TgVEGΔ*BFD1*-GFP-LUC infections

For *in vivo* infections, 5-week-old CBA/J female mice (Jackson Laboratories) were infected with 250,000 TgVEG WT-GFP-LUC, TgVEGΔ*ROCY1*-GFP-LUC, and TgVEGΔ*BFD1*-GFP-LUC parasites (N=6) in 200 µL of PBS via intraperitoneal injection. Mice were imaged ventrally using a 4 minute exposure and large binning at 3 hours post infection and on days 1-5, 7-8, 10, and 12 post infection 10 minutes following intraperitoneal injection with 200 µL of d-Luciferin potassium salt as previously described (*165*). After 21 days of infection, mice were sacrificed and whole brains were removed. A brain homogenate was prepared by passing whole brains through a 100 µm cell strainer using 5mLs of PBS. An additional 20 mLs of PBS was added to the homogenate and it was pelleted by spinning at 1,000 xg for 5 minutes. The supernatant was discarded, and the pellet was resuspending in 1mL of PBS, which produced a final volume of 1.2 mLs of brain homogenate.

To quantify the number of parasite genomes in the brain homogenate, genomic DNA was extracted from 100 µL of brain homogenate using the GeneJET genomic DNA isolation kit according to manufacturer's instructions. qPCR was used to quantify the total number of genomes

using primers targeting the *T. gondii* B1 gene and primers targeting mouse GAPDH as a control gene. All reactions were performed in duplicate using a QuantStudio 3 Real-Time PCR System. Samples were analyzed in 10 µL reactions consisting of 5 µL of 2X SYBR Green 2X master mix, 1 µL of 5 µM forward and 5 µM reverse primers, 2 µL of ddH2O, and 2 µL of genomic DNA. Cycling and melt curves were performed as previously (*44*) . To determine the total number of parasite genomes per brain, a standard curve of known parasite numbers was also performed using *T. gondii* B1 primers. Statistical significance was determine using ΔC_T (TgB1 C_T - mGAPDH C_T) values.

To quantify *in vivo* tissue cyst formation, 100 µL of brain homogenate was fixed with 900 µL of 4% paraformaldehyde in PBS for 20 minutes. Fixed samples were pelleted at 5,200xg for 5 minutes, washed with 1mL of PBS, resuspended in 1 mL of PBS, and stored at 4 degrees C. Fixed brain homogenate was stained with Rhodamine-labeled *Dolichos Bifluorus* Agglutinin (1:150) overnight at 4 degrees C with rotation. The following day, samples were pelleted (5,200 xg for 5 minutes) washed with 1 mL of PBS, pelleted, and resuspending in 1mL of PBS. For each sample, 50µL of stained homogenate (total of 300 µL) was added to 6 wells of a flat-bottomed 96 well plate and tissue cysts were blindly counted using an Olympus IX83 fluorescent microscope using the 10X objective. Cyst burdens were calculated by multiplying the total number of tissue cyst observed in the 300 µL of brain homogenate by the dilution factor.

3.4.10 Reactivation of chronic murine infections with TgVEG WT, TgVEGΔ*ROCY1*, and TgVEGΔ*BFD1*

For *in vivo* infections, 6-week-old CBA/J female mice (Jackson Laboratories) were infected with 250,000 TgVEG WT-GFP-LUC, TgVEGΔ*ROCY1*-GFP-LUC, and TgVEGΔ*BFD1*-

GFP-LUC parasites (N=12) in 200 µL of PBS via intraperitoneal injection. For each parasite, 6 mice were assigned to either the control group or the reactivation group. The reactivation group was given dexamethasone (20 mg/L) in their drinking water beginning at day 30 post infection. Mice were imaged (as described above) prior to dexamethasone treatment (0 days post dexamethasone) on days 4, 6, 7, 8, 10, 12, and 14 post-dexamethasone treatment. Peritoneal cells were collected from moribund mice and used to infect HFFs grown in T-25s. The mice belonging to the control group were sacrificed at 9 weeks post infection. Whole brains were removed, and a brain homogenate was generated as described above.

To quantify *in vivo* tissue cyst formation at 9 weeks post infection, 300 µL of brain homogenate was fixed with 1,200 µL of 4% paraformaldehyde in PBS for 20 minutes. Fixed samples were stained with Rhodamine-labeled *Dolichos Bifluorus* Agglutinin as described above. For each sample, the total number of tissue cysts present in 600 µL was blindly counted by adding 50 µL of stained homogenate to 12 wells in flat-bottomed 96 well plate. Total cyst burdens were calculated by multiplying the total number of tissue cyst observed by the dilution factor.

To quantify the number of parasite genomes in the brain homogenate at 9 weeks post infection, genomic DNA was extracted from 100 µL of brain homogenate as described above. qPCR was also performed as described above.

4.0 Discussion and conclusions

The success of eukaryotic parasites with multi-host life cycles relies on their ability to transition to various developmental life stages that allow for the survival and persistence in a given host. These life stages are fundamentally important in allowing for survival in a variety of different hosts environment in addition to the transmission of these parasites. *Toxoplasma gondii* and *Hammondia hammondi,* Apicomplexan parasites which both follow a heteroxenous two-host life cycle, each have their unique strategies for transitioning to their varying developmental life stages that are critical for the success of both parasites. Understanding these life stages and the transitions that give rise to them is fundamentally important for the understanding of how pathogens like *T. gondii* cause disease.

In chapter 2, I conducted a thorough head-to-head comparison and characterization of *H. hammondi* and *T. gondii* as they progress through their developmental program following oocyst/sporozoite-derived infection. This characterization has allowed me to precisely define the short but predictable replicative window of *H. hammondi,* which I, along with other lab members, was then able to exploit to generate the first ever transgeneic *H. hammondi* line. In addition to pioneering methods to allow for genetic manipulation in *H. hammondi,* we also demonstrated that 1) *H. hammondi* possesses unique life stages that differ transcriptionally from the canonical tachyzoite and bradyzoite life stages attributed to *T. gondii,* and 2) that these unique life stages in *H. hammondi* fail to respond to a potent stressor that robustly induces bradyzoite and tissue cyst development in *T. gondii.* These fundamental differences in the *H. hammondi* developmental program likely contribute to the stark life cycle differences observed between *T. gondii* and *H.*

hammondi and position the *T. gondii/H. hammondi* comparative system as a promising approach to uncover the molecular mechanisms that underlie these life cycle differences.

While the species distinction between *T. gondii* and *H. hammondi* has previously been questioned based on the extensive similarities between these two parasites (*53*), prior work comparing *H. hammondi* and *T. gondii* tachyzoites and bradyzoites/tissue cysts at the ultrastructural and genomic levels and during murine infection has demonstrated that while similar, these parasites are indeed distinct species (*42*, *68*). Our transcriptional analysis of replicating *H. hammondi* during spontaneous development further supports this distinction as we have demonstrated the existence of unique *H. hammondi* life stages. Specifically, *H. hammondi* has increased transcriptional abundance of genes that are typically attributed to bradyzoite life stages and sexual stages in *T. gondii.* Furthermore, our finding that these life stages of *H. hammondi* are refractory to stressors that induce bradyzoite development in *T. gondii* also support this distinction, as *H. hammondi's* inability to respond to this type of stress prematurely is a critical deviation between the *T. gondii* and *H. hammondi* developmental programs.

I speculate that these unique *H. hammondi* life stages are a consequence of the strict developmental program and strict obligate life cycle followed by *H. hammondi*. The increase in transcriptional abundance of genes typically restricted to the bradyzoite and sexual stages of *T. gondii* identified in *H. hammondi* life stages support the idea that *H. hammondi* follows a predetermined developmental program where its expression of genes required either for transition to a specific life stage or for maintenance of that life stages are preprogramed. It is interesting to postulate that the strategy used by *H. hammondi* to persist in the environment is linked to the confines of this predetermined developmental program. Since *H. hammondi* is incapable of horizontal transmission between intermediate hosts in nature (*3*, *42*), its persistence relies on its

ability to make it back to its definitive feline host and undergo sexual reproduction. Therefore, the *H. hammondi* developmental program could be such that it automatically transitions to the tissue cyst life stages following initial infection so that these parasites can easily exist in rodent hosts until they are consumed by feline predators, thus transmitting live *H. hammondi* bradyzoites to the definitive host resulting in sexual reproduction. This type of automatic transition leading to tissue cyst persistence in an intermediate host would not be as critical for *T. gondii* as its persistence within the environment does not solely rely on sexual reproduction. The flexibility exhibited by the *T. gondii* life cycle along with its multiple modes of transmission could have evolved and been selected for in *T. gondii,* as this trait would enhance the overall success of this parasite species.

The existence of a predetermined developmental program controlling cyst formation in *H. hammondi* to promote persistence could also be supported by the parasites' inability to respond to bradyzoite inducing stress. If the developmental program of *H. hammondi* was already predefined to result in tissue cyst formation after a brief period of dissemination, it would not make sense for these parasites to respond to stressors that induce development because they would already be transitioning to those life stages. However, being able to respond to stressors or environmental changes would be important for a parasite like *T. gondii* that can transition back and forth between life stages so that it can exist in a life form that is most likely to support its survival. Given that the flexibility exhibited by *T. gondii* is atypical among Apicomplexans (*42*, *161*), it is possible that the life cycle and developmental program followed by *H. hammondi* best resembles the ancestral life cycle and that the ability to respond to stress and deviate from a predetermined developmental program was acquired by *T. gondii.* This acquisition could have occurred through differential regulation of sensor, that could sense stress or host cell differentiation state, that drives the transition between life stages in *T. gondii* based on environmental cues allowing for *T. gondii* to

transition between life stages. It is possible that the asexual life stages of *T. gondii* always express this type of sensor protein, yet its expression occurs later in the *H. hammondi* developmental program when the parasites are ready to form tissue cysts. This acquisition of a stress sensor in *T. gondii* could have also possibly occurred through gene expansion-driven diversification, a common phenomenon that has been extensively demonstrated in *T. gondii (223)*. It would be intriguing if through gene expansion-driven diversification, this stress sensor evolved through either an alteration in gene dosage or neofunctionalization (*224–226*). Alternatively, it is possible that the ancestral state of this response included this type of sensor and *H. hammondi* lost its ability to respond, and its stringent, predetermined life cycle emerged as a way for the parasites to compensate for its inability to sense and/or respond to the environment. Investigating these hypotheses could reveal the mechanism of sensing using the *T. gondii/H. hammondi* comparative system by genetically manipulating genes with transmembrane domains that could function as membrane bound sensors that fit and appropriate transcriptional profile in spontaneously developing *T. gondii* an *H. hammondi* or genes that have an expanded locus. These types of experiments would be foundational for our understanding of life stage progression in *T. gondii* and could aid in the development of antiparasitics for the currently untreatable bradyzoite/tissue cyst life stage.

In chapter 3, we used the *T. gondii/H. hammondi* comparative system along with insights gleaned through the experiments in chapter 2 to identify genes that we hypothesized would be critical for driving the tachyzoite-to-bradyzoite transition. To do this we performed the most thorough transcriptional comparison to date between *T. gondii* and *H. hammondi* during both natural and stress-induced stage conversion. Using differences in transcript abundance of putative DNA-binding gene products at critical developmental time points, we identified a small list of

candidate genes that we hypothesized may play a critical role in cyst formation in *T. gondii* and *H. hammondi.* After testing multiple candidates in cyst formation assays, we identified ROCY1, a gene that encodes a CCCH zinc finger motif containing protein, as a critical regulator of tissue cyst formation. We found that ROCY1 plays a fundamental role in shaping the transcriptional response to bradyzoite-inducing alkaline pH stress in *T. gondii* and is absolutely required for tissue cyst formation in mice. ROCY1 is only the third factor identified that is necessary for brain tissue cysts formation in mice. This finding demonstrates the strength of the *T. gondii/H. hammondi* comparative system for identifying mechanisms of stage conversion in Apicomplexan parasites.

Our primary objective with the work described in chapter 3 was to identify genes that may function as transcription factors and drive the global changes in gene expression that occur during stage conversion. The validity of our candidate approach was demonstrated by the inclusion of the gene encoding BFD1, a regulator of stage conversion that was previously identified in *T. gondii (132)*, on our candidate gene list along with what we would soon name ROCY1. Our data suggests that ROCY1 is likely very close to BFD1 in the gene regulatory network responsible for regulating the parasites' response to stress and that the transcriptional abundance of ROCY1 may be regulated by BFD1. Further analysis of the predicted amino acid sequence of ROCY1 suggest that ROCY1 may function as an RNA binding protein due to the CCCH type zinc finger motifs found in the predicted protein. These types of zinc fingers are known to interact with RNA and regulate RNA metabolism (*208*) and interact with AU rich elements in 3' UTRs of mRNA transcripts to regulate mRNA stability. Given that parasites lacking ROCY1 exposed to stress fail to express >80% of transcripts typically induced in response to stress, it is possible that ROCY1 plays a role in stabilization of these transcripts. It is exciting to speculate that BFD1 and ROCY1 may be directly linked in the gene regulatory network underlying stage conversion in *T. gondii*. Future experiments

directly testing this hypothesis are needed to better understand how these factors contribute to stage conversion associated gene expression. Such experiments could include overexpressing ROCY1 in parasites lacking BFD1 and determining the effects on tissue cyst formation in response to stress, quantifying the activity of the ROCY1 promoter in parasites expressing or lacking BFD1, or purifying recombinant BFD1 proteins and determining if they bind the regions of the ROCY1 promoter that contain the predicted binding motif. These types of experiments would allow us to determine if there is an interaction between ROCY1 and BFD1 and how such an interaction alters cystogenesis.

While we primarily focused on finding factors that function as transcription factors in chapter 3, additional factors involved in the mechanisms of stage conversion can be gleaned using the *T. gondii/H. hammondi* comparative approach. One such factor that would be interesting to try to identify would be the sensing component(s) (described above) that allow(s) *T. gondii* to initiate the bradyzoite transition in response to changes in the environment. Prior to our work the fact that *H. hammondi* fails to respond to pH-induced stress was not known, but this fact makes our comparative approach a unique way to begin to identify this factor based on a predicted pattern of transcript abundance during natural and pH-induced development in *T. gondii* and *H. hammondi.* Identification of this mechanism would be a critical addition to our understanding of how *T. gondii* causes disease and could lead to the development of new strategies for treating toxoplasmosis.

Overall, this work demonstrates the power of the *T. gondii*/*H. hammondi* comparative system. These comparisons have improved our understanding of the strategies and developmental life stages employed by these parasites and have led to the identification of novel factors involved in life stage development in *T. gondii*. With our now thorough understanding of the limits of the *H. hammondi* developmental program, we can genetically manipulate this parasite which will

enable us to further identify the genetic factors contributing to the molecular mechanism underlying the critical differences in life cycle and life stage development between *T. gondii* and *H. hammondi.*

Appendix A Development of a serology-based assay for the differential detection between *H. hammondi* and *T. gondii*

Appendix A.1 Introduction

One critical difference between *Toxoplasma gondii* and *Hammondia hammondi* is that *H. hammondi* has a more restricted host range and is not known to naturally infect humans (*42*). Despite this difference, *H. hammondi* is capable of infecting human cells *in vitro* (*55*) and *H. hammondi* oocysts are found similarly to *T. gondii* oocysts in the environment (*52*, *227*), suggesting that human infection could potentially occur. Human infection with *T. gondii* is most typically measured via seroprevalence, where serum samples are screened for *T. gondii* specific immunoglobulins that react with a variety of *T. gondii* antigens (*64*, *228*). Numerous studies have shown that *H. hammondi* is capable of cross-reacting with several *T. gondii* antibodies (*42*, *57–61*, *229*), suggesting that it is possible that some *T. gondii* infections could actually be *H. hammondi* infections. While *H. hammondi* and *T. gondii* infection can be distinguished using PCR based assays to analyze genomic DNA (*62*, *63*), these methods of detection for *T. gondii* are not used as frequently as serology because they require isolation of parasite genomic DNA from samples such as amniotic fluid, cerebrospinal fluid, placental or brain tissue, or fluid derived from the eye (*64*). Furthermore, no *H. hammondi* serology-based detection assay exists to date.

To create a *H. hammondi*-specific test, we exploited the polymorphic C-terminal regions of *T. gondii* and *H. hammondi* dense granule proteins GRA6 and GRA7 that had previously been used to distinguish infections between closely-related *T. gondii* strains (*230*). We identified a *H.*

hammondi peptide that could be used in a serological assay to detect *H. hammondi* infection and distinguish it from *T. gondii* type II, but not type III, infection in mice.

Appendix A.2 Analysis of reactivity of peptides designed from the C-terminus of Gra6 and Gra7 to serum from mice chronically infected with *T. gondii* and *H. hammondi*

The C-termini of the *T. gondii* dense granule proteins GRA6 and GRA7 are highly polymorphic between *T. gondii* strains (Type I, Type II, and Type III). Synthetic peptides designed based on these differences have previously been used to develop serotyping enzyme-linked immunosorbent (ELISA) assays that allow for the identification with Type I, II, or III *T. gondii* from serum samples (*230*). We hypothesized that synthetic peptides corresponding to the C-terminal sequences of *H. hammondi* GRA6 and GRA7 could be used to distinguish between *T. gondii* and *H. hammondi* infection from serum samples. To test our hypothesis, we had several peptides synthesized and conjugated to the carrier protein keyhole limpet hemocyanin that corresponded to *H. hammondi* or *T. gondii* sequences in the C-termini of GRA6 (Appendix Figure 2A-B) and GRA7 (Appendix Figure 1A-B), including 2 previously identified peptides that distinguished between *T. gondii* strains for both GRA6 and GRA7 (*230*). We also synthesized control peptides to a random amino acid sequence as well as a scrambled version of one of our *H. hammondi* peptides (Appendix Table 1). We then tested the reactivity of these peptides to serum from mice chronically infected (at least 4 weeks post infection) with *T. gondii* ME49 (Type II) and *H. hammondi* in an ELISA assay. We found that for peptides designed from GRA7, we saw strong reactivity (Optical density (OD) >1) for the previously designed TgGRA7 II peptide to *T. gondii* serum, but we did not observe any strong reactivity to *H. hammondi* GRA7 peptides (Appendix

Figure 1C). When we tested the peptides that we designed for GRA6 (Appendix Figure 2A-B), we observed strong reactivity (OD > 1) for the previously identified TgGRA6 II peptide to *T. gondii* ME49 serum as well as strong reactivity for the HhGRA6_1 peptide to *H. hammondi* serum (Appendix Figure 2C-D), suggesting that the HhGRA6_1 peptide could be used to identify *H. hammondi*-specific infection. Prior work has identified the final 10 amino acids of *T. gondii* GRA6 is a dominant antigen that functions as a CD8 T cell epitope (*231*, *232*). It is possible that the 10 C-terminal amino acids in *H. hammondi* GRA6 function as a dominant antigen as well, which could explain why serum from *H. hammondi*-infected mice reacted so strongly with only the HhGRA6_1 peptide, which contains the last 11 C-terminal amino acids of GRA6. Future work that identifies dominant *H. hammondi* antigens, such as a phage immunoprecipitation sequencing screen (*233*, *234*), could also be useful for identifying additional *H. hammondi* peptides.

Appendix Table 1. Synthetic peptides used to distiguish between *T. gondii* and *H. hammondi* infection.

Name	Sequence	Target/Description
TgGRA7 I/II	CKNRSRQPALE	Tg Type I/II C-terminus
TgGRA7 II	CVPESGKDGEDARQ	Tg Type II GRA7 (*230*)
TgGRA7III	CVPESGEDREDARQ	Tg Type III GRA7 (*230*)
HhGRA7_1	CVPEAVETGEEAS	Hh GRA7 C-terminus
HhGRA7_2	CKESRRPRRPAL	Hh GRA7 C-terminus
HhGRA7_3	CLQDTGANKRD	Hh GRA7 C-terminus
TgGRA6 I/II	CLHPERVNVFDY	Tg Type I & III GRA6 (*230*)
TgGRA6 II	CLHPGSVNEFDF	Tg Type II GRA6 (*230*)
TgGRA6 II-2	CRRPLHPGSVNE	Tg Type II GRA6 C-terminus - FDF
HhGRA6_1	CDPPRNVNPFDF	Hh GRA6 C-terminus

HhGRA6_2	CGVPDPPRNVNP	Hh GRA6 C-terminus - FDF
HhGRA6_3	CGAGGEGDDGGDG	Hh GRA6 C-terminus
HhGRA6_4	CDGGGVPDPPRN	Hh GRA6 C-terminus
Scramble (HhGRA7_1)	CPVEEETSVEGAA	Control peptide
Random Sequence	CDKHEFGRFGQN	Control peptide

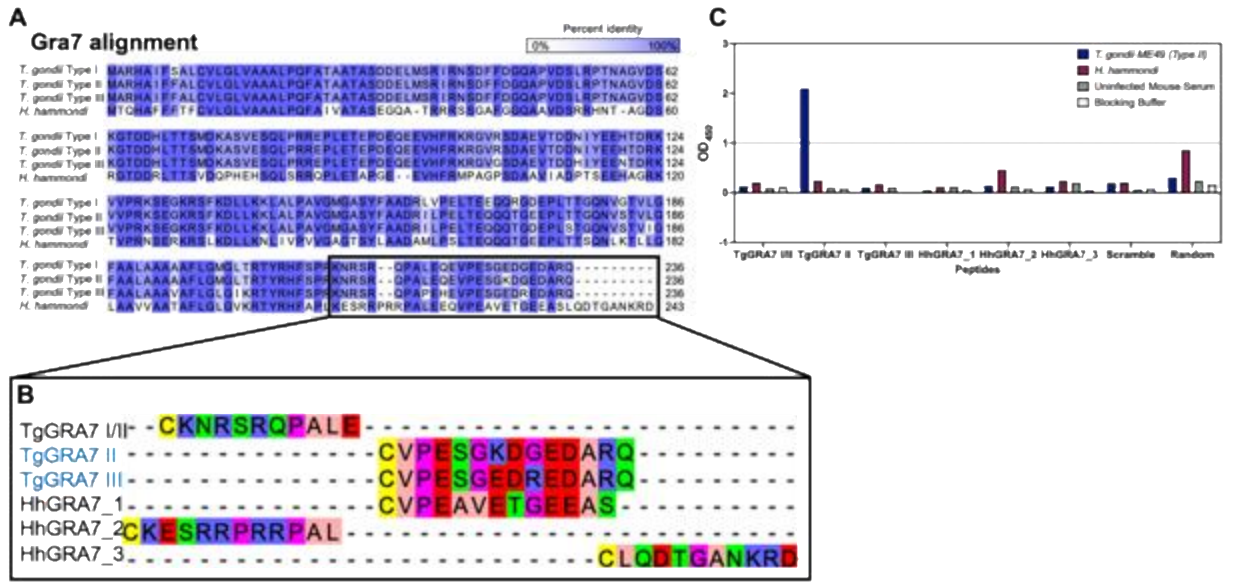

Appendix Figure 1. Validation of differential detection peptides targeting polymorphic c-terminus of GRA7.

A) Alignment of amino acid sequence from type I, II, and III *T. gondii* and *H. hammondi.* Blue coloring represents percent identity. B) Alignment of peptides used for differential detection assays to the c-terminus of GRA7. Colored according to Zappo color scheme. Peptides labeled in blue were previously identified (citation). C) Reactivity of each peptide with serum from a *T. gondii* ME49 (Type II) infected mouse (N=1), a *H. hammondi* infected mouse (N=1), and an uninfected mouse (N=1), and blocking buffer (N=1).

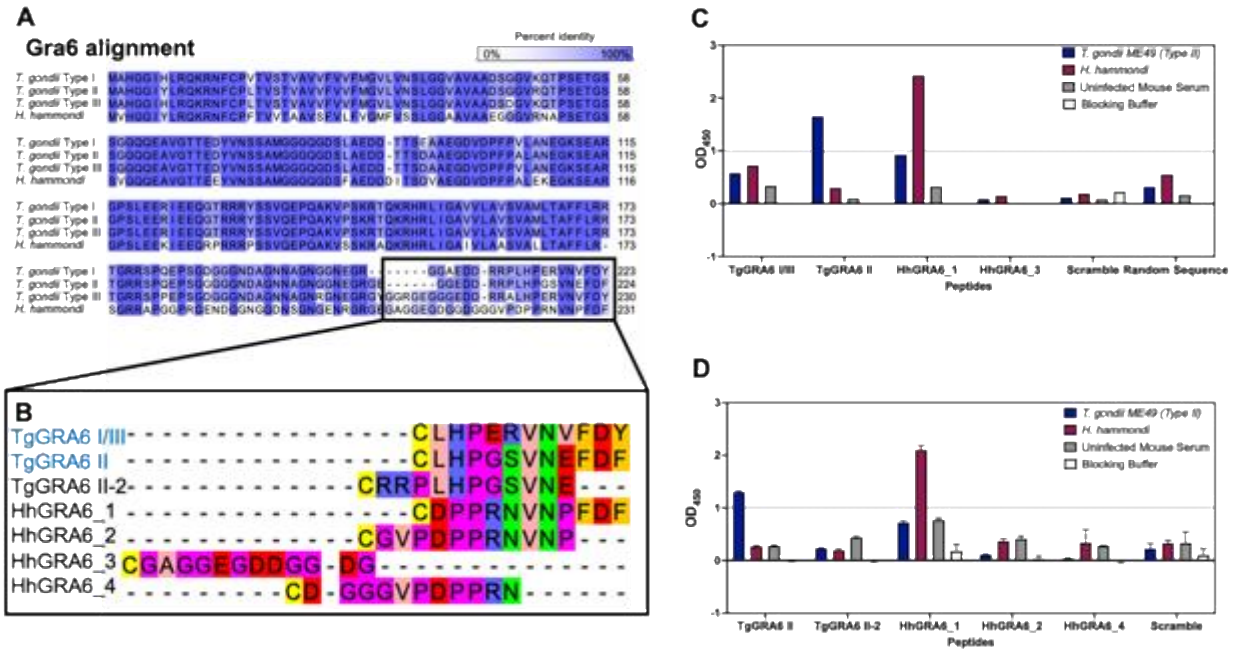

Appendix Figure 2. Validation of differential detection peptides targeting polymorphic c-terminus of GRA6.

A) Alignment of amino acid sequence from type I, II, and III *T. gondii* and *H. hammondi.* Blue coloring represents percent identity. B) Alignment of peptides used for differential detection assays to the c-terminus of GRA6. Colored according to Zappo color scheme. Peptides labeled in blue were previously identified (citation). C) Reactivity of peptides TgGRA6 I/II, TgGRA6 II, HhGRA6_1, HhGRA6_3, and control peptides with serum from a *T. gondii* ME49 (Type II) infected mouse (N=1), a *H. hammondi* infected mouse (N=1), and an uninfected mouse (N=1), and blocking buffer (N=1). D) reactivity of peptides TgGRA6 II, TgGRA6II-2, HhGRA6_1, HhGRA6_2, HhGRA6_4, and scramble control with serum from a *T. gondii* ME49 (Type II) infected mouse (N=1), a *H. hammondi* infected mouse (N=1), and an uninfected mouse (N=1), and blocking buffer (N=1) Peptides were analyzed in technical triplicate.

To further test the specificity of our peptides, we obtained serum from additional mice chronically infected with *T. gondii* ME49 (Type II) (WT and ΔGRA28) (*221*), *T. gondii* VEG (Type III), and *H. hammondi*. We attempted to obtain serum from mice infected with *T. gondii* GT1 (Type I), but we were unable to get the mice to survive to chronic infection (at least 4 weeks post infection). We then tested the reactivity of our most promising *H. hammondi* peptide (HhGRA6_1) and previously identified T. *gondii* specific peptides (TgGRA6 I/III, TgGRA6 II,

TgGRA7 II, and TgGRA7 III) with this panel of chronically infected mouse serum. We again found that the TgGRA7 II peptide reacted strongly with serum from mice infected with Type II *T. gondii* but did not see as strong of a reaction with the TgGRA6 II peptide (Appendix Figure 3). We also observed strong reactivity of *H. hammondi* samples with the HhGRA6_1 peptide, but this peptide also reacted with serum from *T. gondii* VEG (Type III) infected mice (one sample with OD > 1). Yet, this reaction was not as strong as the reaction with serum from *H. hammondi* infected mice (Appendix Figure 3). These results suggest that while the HhGRA6_1 peptide could be used to identify infection with *H. hammondi*, it may also cross-react with a Type III *T. gondii* infection. Future work to further characterize the reactivity of the HhGRA6_1 peptide with serum from mice infected with additional strains for *T. gondii*, specifically Type III strains, is needed to understand if the minor reactivity seen with serum from mice infected with *T. gondii* VEG is a concern for cross-reactivity.

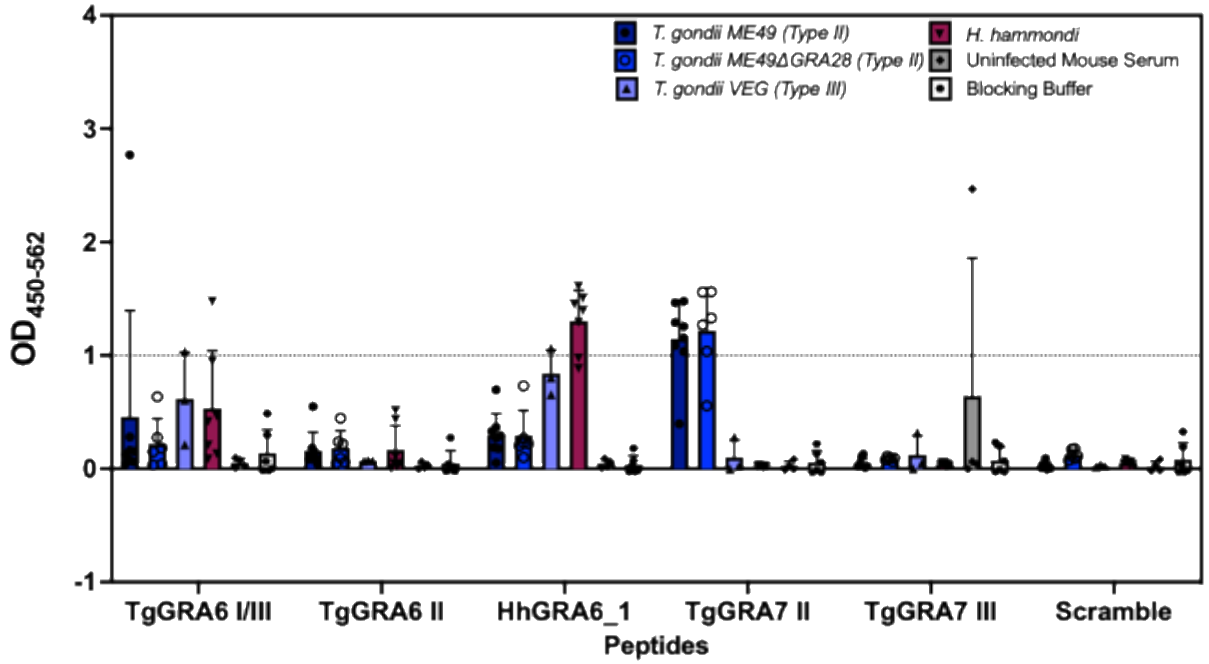

Appendix Figure 3. *H. hammondi* specific peptide (HhGRA6_1) reacts with serum from Type III *T. gondii* VEG infection in addition to serum from *H. hammondi* infected mice.

Reactivity of TgGRA6 I/III, TgGRA6 II, HhGRA6_1, TgGRA7 II, TgGRA7 III, and scramble peptides with serum from *T. gondii* ME49 (Type II) infected mice (N= 8), *T. gondii* ME49ΔGRA28 (Type II) infected mice (N=6), *T. gondii* VEG (Type III) infected mice (M=3), *H. hammondi* infected mice (N=7), uninfected mice (N=4), and blocking buffer.

Appendix A.3 Identification of human samples that react with *H. hammondi* peptide

We next wanted to determine if our *H. hammondi*-specific peptide could be used to identify human samples that could be due to *H. hammondi* human infection. To do this, we obtained serum samples from a cohort of pregnant women in France that first tested positive for *T. gondii* using an IgG based assay during their pregnancy and serum samples from French females and males that tested positive for *T. gondii* and males that tested negative for *T. gondii*. We then tested the samples reactivity of these samples to previously identified *T. gondii* peptides and our *H. hammondi* peptide in an ELISA assay. We found 1 sample (Sample 38) that specifically reacted strongly to the HhGRA6_1 peptide (HhGRA6_1 peptide only peptide with OD>1) from the serum from the pregnant women cohort (Appendix Figure 4A) and 2 samples (Sample 15 – *T. gondii* infected male and Sample 25- *T. gondii* negative male) from French female and male serum samples (Appendix Figure 4B). Overall, these results suggest that infection with *H. hammondi* could be possible in these individuals, however additional *H. hammondi* specific peptides are needed to further support this hypothesis.

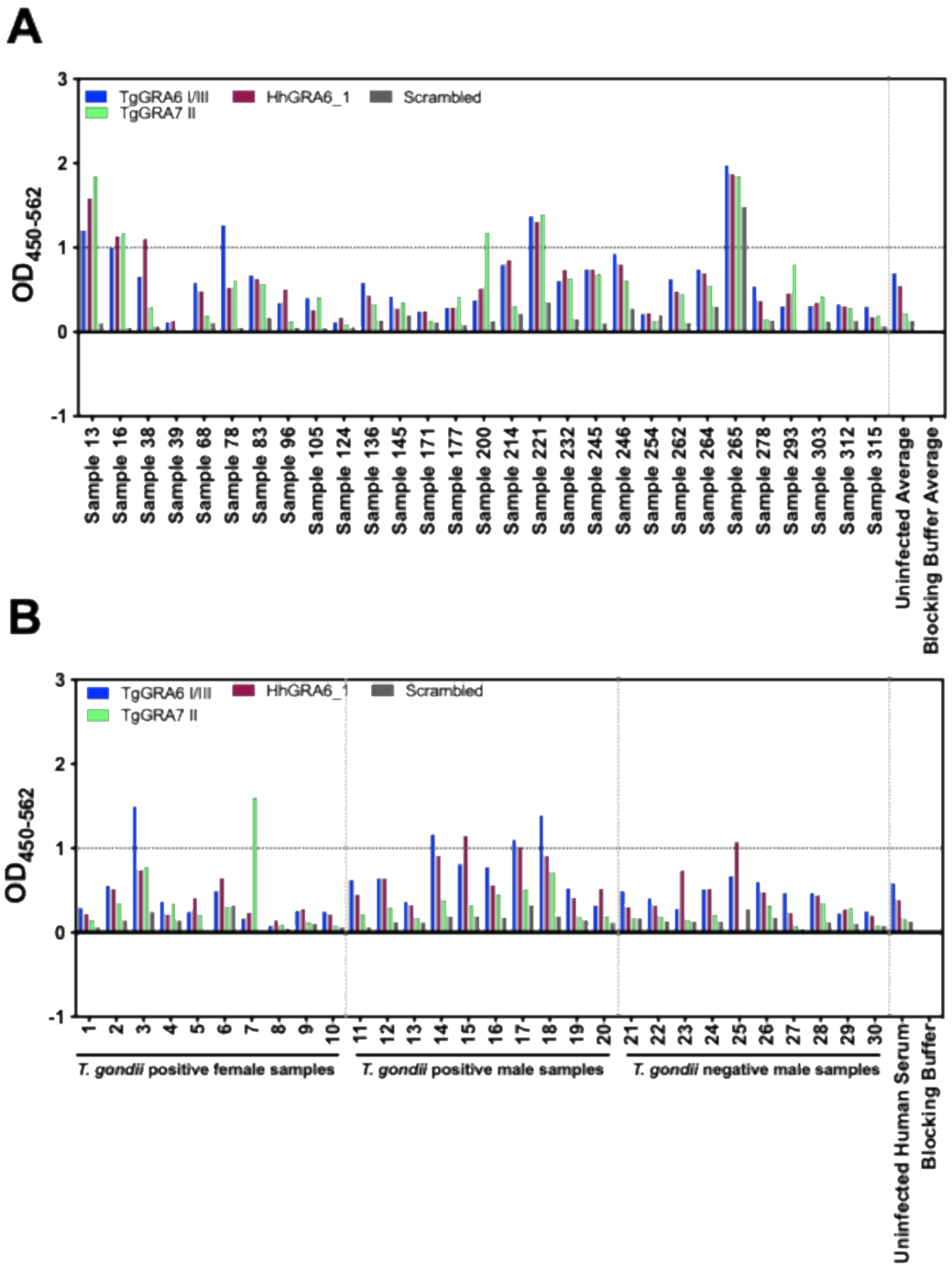

Appendix Figure 4. *H. hammondi* specific peptide (HhGRA6_1) reacts with some human serum samples.

A) Reactivity of *T. gondii* peptides TgGRA6 I/III (blue) and TgGRA7 II (green), *H. hammondi* peptide (maroon), and scramble peptide (gray) with human samples from pregnant women in France in obtained in 2012-2016 B) Reactivity of *T. gondii* peptides TgGRA6 I/III (blue) and TgGRA7 II (green), *H. hammondi* peptide (maroon), and scramble

peptide (gray) with human samples from *T. gondii* positive female and male samples and *T. gondii* negative male samples from France.

Appendix A.4 Material and methods

Appendix A.4.1 Murine infection and serum collection

Swiss webster or BALB/C mice were infected intraperitonially with a non-lethal dose of *T. gondii* tachyzoites (TgME49, TgME49ΔGRA28, TgVEG), intraperitoneally with *H. hammondi* (HhCatAmer or HhEth1) sporozoites or orally with oocysts. Serum was collected after the mice reached chronic infection (a least 4 weeks post infection) and stored at -80 degrees C.

Appendix A.4.2 Human samples

Deidentified human samples were obtained from the lab of Rima McLeod. Samples were aliquoted and stored at -80 degrees C until analyzed in ELISA assays.

Appendix A.4.3 Peptide design and synthesis

H. hammondi and *T. gondii* peptide were designed based on the polymorphic C-terminal sequences of GRA6 and GRA7 or obtained from prior work. A cysteine reside was added to the N-terminus of each peptide to allow for conjugation of the carrier protein keyhole limpet hemocyanin (KLH). Peptides were synthesized and coupled to KLH at the N-terminus by New

England Peptide. All peptides were received at a concentration of 1mg with > 75% purity and stored at -20 degrees C.

Appendix A.4.4 ELISA assays

Synthesized and KLH coupled peptides were thawed on ice and diluted to a concentration of 10 µg/mL in 0.1 M carbonate buffer, pH 8.5. An Immulon ® 4HFB flat-bottomed 96-well plate was coated with 50 µL of each diluted peptide and incubated at 4 degrees C overnight. Each well was block with 200 µL of blocking buffer (2% casein in PBS, pH 7.4) at room temperature for 2 hours. After the 2-hour infection, blocking buffer was aspirated using a BioTek405 LS microplate washer. During the 2-hour blocking incubation, serum from murine or human infections was thawed on ice and diluted 1:50 in blocking buffer and stored on ice until it was added to the 96-well plate. After the blocking buffer was aspirated, 50 µL of the diluted serum was added to a well of the 96-well plate and the plate was incubated at room temperature for 3 hours. After the serum incubation, the plate was washed 4 times with 200 µL of wash buffer (0.1% Tween-20 in PBS) prior to addition of 200 µL of a secondary detection antibody (Invitrogen goat anti-hu IgG or goat anti-mouse IgG) conjugated to horseradish peroxidase and diluted 1:3,000. Samples were incubated with the secondary antibody for 1 hour at room temperature. After incubation with the secondary antibody, the plate was washed 4 times with 200 cµL of wash buffer and 2 times with PBS. A TMB substrate solution (Bd Biosciences) was prepared 15 minutes prior to use by combining equal volumes of solution A (hydrogen peroxide) and solution B (3,3',5,5' tetramethylbenzidine). After washing, 100 µL of the TMB substrate solution was added to each well of the 96-well plate and the plates was incubated at room temperature for 30 minutes. Then 50 µL of stop solution (2N H_2SO_4) was added to each well and the plate was incubated at room

temperature for 10 minutes. The optical density of the each well at either 450 nm or 450 nm with a background measurement at 562 nm was determined using a BioTek EL800 universal microplate reader.

Appendix B A differential interferon-gamma dependent transcriptional difference in host cells infected with *T. gondii* and *H. hammondi*

The figure and methods for this section have been previously published: Wong Z.S., Sokol-Borrelli S.L., Olias P., Dubey J.P., Boyle J.P. 2020. Head-to-head comparisons of Toxoplasma gondii and its near relative Hammondia hammondi reveal dramatic differences in the host response and effectors with species-specific functions. PLoS Pathog. 16, e1008528. I am responsible for the experiments detailed in Appendix figure 5, which was designed by both JPB and myself. I have added a brief introduction and results section to provide clarity.

Appendix B.1 Introduction

In addition to its life cycle flexibility, another characteristic of *T. gondii* that contributes to its success is that it can manipulate several biological processes in the hosts that it infects. Importantly, *T. gondii* encodes several secreted effector proteins that can manipulate host transcriptional machinery to reprogram host cell gene expression (*177*) likely with the goal of promoting the creation of an environment that is amenable to the parasites. *H. hammondi* is also capable of altering the overall host transcriptome. Remarkably, *H. hammondi* induces a more potent transcriptional response when compared to *T. gondii (235)*, which suggest that species-specific differences could exist in the *H. hammondi* version of *T. gondii* secreted effector proteins that are known to alter host transcription. Prior work investigating the *H. hammondi* orthologs of

ROP16 and GRA15, both *T. gondii* secreted effectors that activate transcription in infected host cells, found that these effectors are functionally conserved and can alter host cell transcription when expressed in *T. gondii*. However, the *H. hammondi* ROP16 promoter was less effective than the *T. gondii* ROP16 promoter and the *H. hammondi* version of GRA15 was found to induce a more potent activation of NF-κB which is needed to activate NF-κB-mediated transcription *(72)*. However, these data do not completely explain the stark differences in the host transcription response upon *T. gondii* or *H. hammondi* infection.

Another *T. gondii* secreted effector protein that could contribute to the differential host response between *T. gondii* and *H. hammondi* infection is the *T. gondii* secreted effector protein toxoplasma inhibitor of STAT1-dependent transcription (TgIST). TgIST is known to interact with dimerized STAT1 and recruit the repressive chromatin remodeling complex Mi-2/NuRD that suppresses host cell transcription of interferon-γ dependent transcription, an important primary defense in the host immune response to *T. gondii* infection (*176*, *179*, *236*). Here we investigate the function of the *H. hammondi* IST ortholog, HhIST, on interferon-γ dependent transcription and how it compares to TgIST.

Appendix B.2 Results

To begin to understand if there was a functional difference between HhIST and TgIST, we analyzed how parasite infection alters interferon-γ dependent transcription by quantifying nuclear interferon regulatory factor 1 (IRF1) staining in human foreskin fibroblasts (HFFs), which is activated in response to treatment with interferon-γ (*237*). We found IRF1 expression (measured as normalized IRF1 fluorescence intensity) was significantly reduced in host cells that were

infected with *T. gondii* (either RH88 tachyzoites of TgVEG sporozoites) prior to interferon-γ treatment as compared to uninfected host cells ($P<0.05$) yet there was no significant difference in IFR1 expression in host cells pre-infected with *H. hammondi* or *N. caninum* (*N. caninum* lacks a clear ortholog of TgIST) (Appendix Figure 5 A-B). We next compared the sequence of HhIST (HHA_240060) and TgIST (TgME49_240060) to determine if we could identify any difference that would explain the species-specific difference in interferon-γ dependent IRF1 expression. We identified a sequence assembly gap in the C-terminus of HhIST (*126*) and through analysis of the predicted protein sequence using BLASTP, we identified multiple alignment gaps, a difference in the predicted size of the proteins, and a low level of identity between regions of HhIST and TgIST that align (68%, compared to the predicted proteome-wide average of ~89%). Furthermore, TgIST contains 4 predicted nuclear localization signals while HhIST lacks any predicted NLSs and contains extensive polymorphisms in NLS1 and NLS2 when compared to TgIST (Appendix Figure 5C). These sequence differences suggest that the functional difference between TgIST and HhIST could be due to the lack of functional NLSs in HhIST. To test this possibility, we expressed a Ty-tagged version of TgIST, HhIST, and HhIST with a C-terminal NLS in U2OS cells. We found that TgIST is primarily expressed in the nucleus of the transfected cells, while HhIST can be found in both the nucleus and cytoplasm (Appendix Figure 5D). When we quantified IRF1expression in transfected cells with Ty staining we found that IRF1 expression was significantly decreased in cells expressing TgIST as compared to transfected cells in the same field of view ($P=0.01$) while cells expressing HhIST were not as effective at reducing IRF1 expression. However, addition of a C-terminal NLS to HhIST partially restored the suppression of IRF1 expression, which was not significantly different than cells expressing TgIST ($P=0.9$). Together, these data suggest that sequence differences in HhIST as compared to TgIST are important for the suppression of

interferon-γ dependent transcription and that nuclear localization of IST plays a role in the species-specific difference in suppression of an infected host cell's transcriptional response.

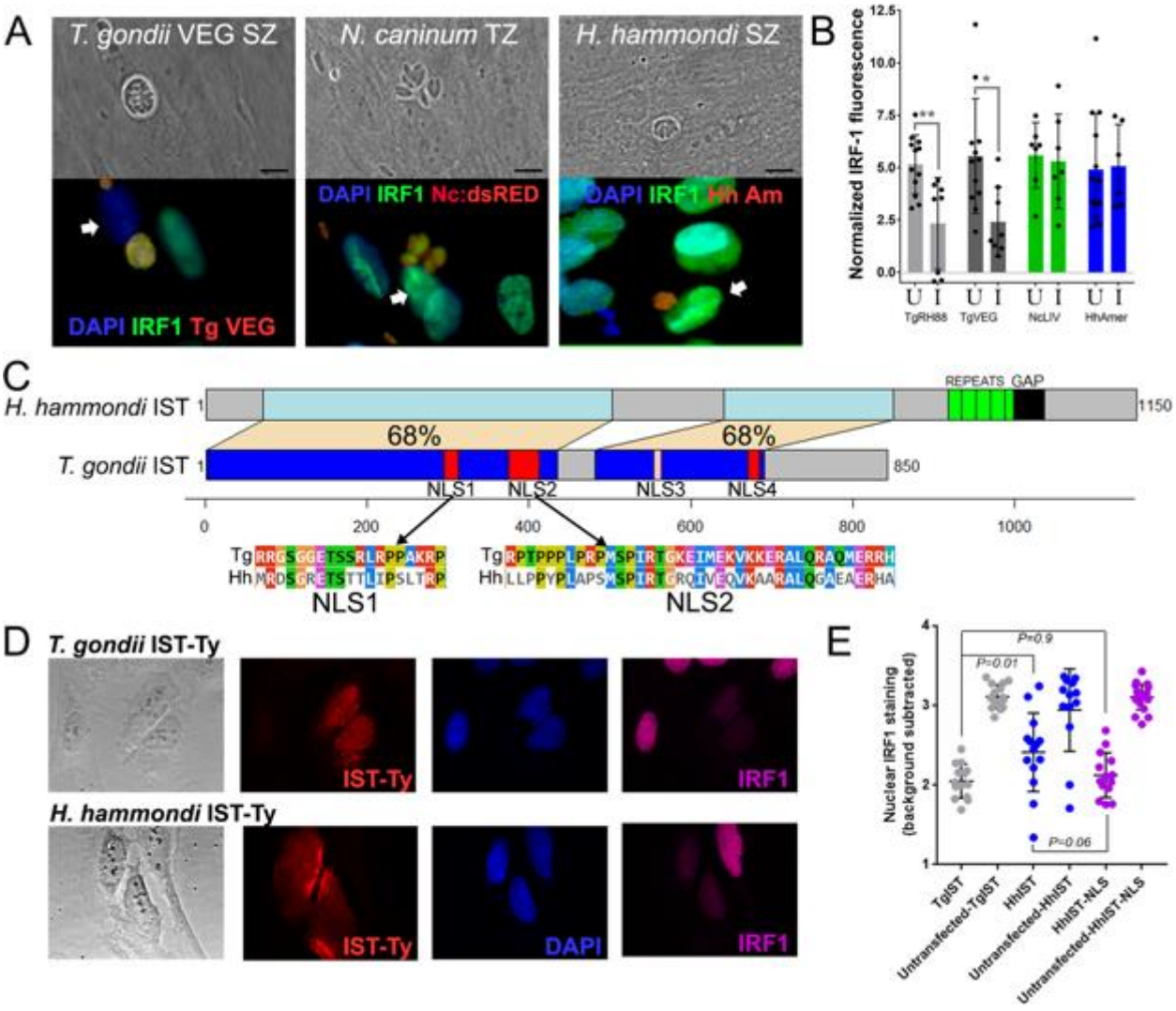

Appendix Figure 5. *H. hammondi* IST lacks suppressive activity compared to *T. gondii* IST due to differences in putative NLS sequences and localization in the host cell.

A) In contrast to *T. gondii*, *H. hammondi* and *N. caninum* infection fails to suppress IFNγ-induced IRF1 activation. Representative images are shown for each species, and the white arrowhead indicates the likely nucleus of the infected cell. As expected *T. gondii* infected cells have reduced IRF1 staining compared to uninfected neighboring cells while cells infected with *N. caninum* or *H. hammondi* have similar IRF1 nuclear staining as uninfected bystander cells. B) Quantification of IRF nuclear staining in cells infected with each indicated species (I) and uninfected bystander cells

(U). *T. gondii* infection (strains RH88 and TgVEG) significantly reduced IFNγ-induced IRF1 nuclear staining while infection with *N. caninum* and *H. hammondi* did not. C) Schematic of the predicted IST protein coding sequence gene from *T. gondii* and *H. hammondi*, showing conserved (blue and light blue connected by tan) and non-conserved (grey) regions of the predicted proteins. Putative NLS sites are indicated in red or pink, and were only found in *T. gondii* IST (not *H. hammondi* IST). *H. hammondi* has a longer predicted protein that includes repetitive sequence (green) and a sequence assembly gap (black). D) Ectopic expression of Ty-tagged *T. gondii* and *H. hammondi* IST in U20S cells showing primarily nuclear staining for TgIST-Ty in contrast to cytoplasmic and nuclear staining for HhIST-Ty. Cell expressing TgIST and HhIST show reduced IRF1 staining in the nucleus after IFNγ treatment. E) Quantification of nuclear IRF1 staining in IST-expressing cells and neighboring bystanders lacking IST expression. Constructs were TgIST-Ty, HhIST-Ty and HhIST-NLS-Ty (Ty-tagged WT HhIST with a C-terminal NLS). Inclusion of an NLS on the C-terminus of *H. hammondi* IST increased its ability to suppress IRF1 induction by IFNγ treatment compared to HhIST-Ty.

Appendix B.3 Materials and methods

Appendix B.3.1 IFNγ-induced IRF1 expression derived from parasite infection

HFFs grown on coverslips were infected with TgVEG and *H. hammondi* sporozoites (MOI 0.5) for 72 hours and with RH88 and *N. caninum* (NC-1) (MOI 0.5) for 3 hours prior to treatment with IFNγ. Infected cells were treated with IFNγ recombinant human protein (1 µL/mL of cDMEM, approximately 165-1000 U per well) (Gibco PHC4031) for 15 hours. Infected host cells were fixed with 4% paraformaldehyde. Coverslips were stored in blocking buffer (5% BSA, 0.1% Triton X-100) at 4 degrees C until staining was performed. Coverslips were stained with goat *Toxoplasma gondii* Polyclonal Antibody (1:500) (Invitrogen PA1-7256) and rabbit IRF1 (1:200) (Cell Signaling Technology, 8478S) primary antibodies for 1 hour at room temperature. Coverslips

were washed 3X with PBS and stained with Goat-anti Rabbit IgG Alexa Fluor 488 (1:1000) (Invitrogen A-11008) and Donkey anti-Goat IgG Alexa Fluor 594 (1:1000) (Invitrogen A-11058) secondary antibodies for 1 hour at room temperature. Coverslips were washed 3X with PBS and mounted with Prolong ™ Diamond antifade mountant with DAPI (Invitrogen P36962).

Appendix B.3.2 IFNγ-induced IRF1 expression derived from mammalian expression

U2OS cells were grown on coverslips in cDMEM supplemented with 10% FBS and 2mM L-glutamine. For transfections, cells were maintained in cDMEM supplemented with only 2mM L-glutamine. Cells were transfected with 500ng of plasmid DNA using the Lipofectamine ™ 3000 Transfection Reagent (Invitrogen™ L3000001) according to the manufacturer's instructions. Cells were incubated at 37 degrees C, 5% CO_2 for 17 hours. Cells were treated with IFNγ recombinant human protein (1 µL/mL of cDMEM, approximately 165-1000 U per well) (Gibco PHC4031) for 6 hours. Coverslips were fixed with 4% paraformaldehyde and stored in PBS at 4 degrees C until staining was performed. Coverslips were incubated with blocking buffer (5% BSA, 0.15% Triton X-100) for 1 hour and stained with mouse Ty1 Tag monoclonal Ab (BB2) (1:100) (Invitrogen MA5-23513) and rabbit IRF1 (1:200) (Cell Signaling Technology, 8478S) primary antibodies for 1 hour at room temperature. Coverslips were washed 3X with PBS and stained with Goat-anti Rabbit IgG Alexa Fluor 647 (1:1000) (Invitrogen A-21244) and Goat anti-Mouse IGG Alexa Fluor 594 (1:1000) (Invitrogen A-11032) secondary antibodies for 1 hour at room temperature. Coverslips were washed 3X with PBS and mounted with Prolong ™ Diamond antifade mountant with DAPI (Invitrogen P36962).

5.0 Bibliography

1. J. K. Frenkel, J. P. Dubey, N. L. Miller, Toxoplasma gondii in cats: fecal stages identified as coccidian oocysts. *Science*. 167, 893–896 (1970).
2. J. P. Dubey, History of the discovery of the life cycle of Toxoplasma gondii. *Int. J. Parasitol.* **39**, 877–882 (2009).
3. J. P. Dubey, D. J. P. Ferguson, Life Cycle of Hammondia hammondi (Apicomplexa: Sarcocystidae) in Cats. *J Eukaryot Microbiol*. **62**, 346–352 (2015).
4. M. M. McAllister *et al.*, Rapid communication. *Int. J. Parasitol.* **28**, 1473–1479 (1998).
5. J. K. Frenkel, J. P. Dubey, Hammondia hammondi gen. nov., sp.nov., from domestic cats, a new coccidian related to Toxoplasma and Sarcocystis. *Z. Parasitenkd.* **46**, 3–12 (1975).
6. C. Nicolle, L. Manceaux, Sur une infection à corps de Leishman (ou organismes voisins) du gondi. *C. R. Seances Acad. Sci*. **147**, 763–766 (1908).
7. A. Splendore, Un nuovo protozoa parassita de' conigli. incontrato nelle lesioni anatomiche d'une malattia che ricorda in molti punti il Kala-azar dell' uomo. *Rev. Soc. Scient. Sao Paulo*. **3**, 109–112 (1908).
8. C. Nicolle, L. Manceaux, Sur un protozoaire nouveau du gondi. *C. R. Seances Acad. Sci*. **148**, 369–372 (1909).
9. J. P. Dubey, The history of Toxoplasma gondii--the first 100 years. *J Eukaryot Microbiol*. **55**, 467–475 (2008).
10. L. M. Weiss, K. Kim, Eds., *Toxoplasma Gondii: The Model Apicomplexan. Perspectives and Methods* (Elsevier, 2011).

11. J. P. Dubey, Advances in the life cycle of Toxoplasma gondii. *Int. J. Parasitol.* **28**, 1019–1024 (1998).

12. A. M. Tenter, A. R. Heckeroth, L. M. Weiss, Toxoplasma gondii: from animals to humans. *Int. J. Parasitol.* **30**, 1217–1258 (2000).

13. J. B. McAuley, Congenital Toxoplasmosis. *J. Pediatric Infect. Dis. Soc.* **3 Suppl 1**, S30–5 (2014).

14. A. Molan, K. Nosaka, M. Hunter, W. Wang, Global status of Toxoplasma gondii infection: systematic review and prevalence snapshots. *Trop. Biomed.* **36**, 898–925 (2019).

15. J. M. Furtado, J. R. Smith, R. Belfort, D. Gattey, K. L. Winthrop, Toxoplasmosis: a global threat. *J Glob Infect Dis*. **3**, 281–284 (2011).

16. J. P. Dubey, in *Medical Microbiology*, S. Baron, Ed. (University of Texas Medical Branch at Galvesto, Galveston, ed. 4, 1996).

17. J. P. Dubey, D. S. Lindsay, C. A. Speer, Structures of Toxoplasma gondii tachyzoites, bradyzoites, and sporozoites and biology and development of tissue cysts. *Clin. Microbiol. Rev.* **11**, 267–299 (1998).

18. J. P. Dubey, J. K. Frenkel, Cyst-Induced Toxoplasmosis in Cats*. *J Protozool*. **19**, 155–177 (1972).

19. J. K. Frenkel, Besnoitia wallacei of Cats and Rodents: With a Reclassification of Other Cyst-Forming Isosporoid Coccidia. *J. Parasitol.* **63**, 611 (1977).

20. J. S. Remington, E. N. Cavanaugh, Isolation of the encysted form of Toxoplasma gondii from human skeletal muscle and brain. *N. Engl. J. Med.* **273**, 1308–1310 (1965).

21. S. Tomavo, J. C. Boothroyd, Interconnection between organellar functions, development and drug resistance in the protozoan parasite, Toxoplasma gondii. *Int. J. Parasitol.* **25**, 1293–1299 (1995).

22. W. J. Sullivan, V. Jeffers, Mechanisms of Toxoplasma gondii persistence and latency. *FEMS Microbiol. Rev.* **36**, 717–733 (2012).

23. R. McLeod, C. Van Tubbergen, J. Montoya, E. Petersen, in *Toxoplasma gondii The Model Apicomplexan: Perspectives and Methods*, L. Weiss, K. Kim, Eds. (Elsevier, ed. 2nd, 2014), pp. 99–161.

24. S. Rajapakse, M. Chrishan Shivanthan, N. Samaranayake, C. Rodrigo, S. Deepika Fernando, Antibiotics for human toxoplasmosis: a systematic review of randomized trials. *Pathog. Glob. Health*. **107**, 162–169 (2013).

25. S. Rougier, J. G. Montoya, F. Peyron, Lifelong persistence of toxoplasma cysts: A questionable dogma? *Trends Parasitol.* **33**, 93–101 (2017).

26. L. M. Weiss, K. Kim, The development and biology of bradyzoites of Toxoplasma gondii. *Front. Biosci.* **5**, D391–405 (2000).

27. S. K. Halonen, L. M. Weiss, Toxoplasmosis. *Handb Clin Neurol*. **114**, 125–145 (2013).

28. J. L. Jones, G. N. Holland, Annual burden of ocular toxoplasmosis in the US. *Am. J. Trop. Med. Hyg.* **82**, 464–465 (2010).

29. E. Scallan *et al.*, Foodborne illness acquired in the United States-major pathogens. *Emerging Infect. Dis.* **17**, 7–15 (2011).

30. J. G. Montoya, O. Liesenfeld, Toxoplasmosis. *Lancet*. **363**, 1965–1976 (2004).

31. O. Beran *et al.*, The Effect of Latent Toxoplasma gondii Infection on the Immune Response in HIV-Infected Patients. *Biomed Res. Int.* **2015**, 271842 (2015).

32. V. Nissapatorn, Toxoplasma gondii and HIV: a never-ending story. *Lancet HIV*. **4**, e146–e147 (2017).

33. S. Khurana, N. Batra, Toxoplasmosis in organ transplant recipients: Evaluation, implication, and prevention. *Trop. Parasitol.* **6**, 123–128 (2016).

34. N. Fernàndez-Sabé *et al.*, Risk factors, clinical features, and outcomes of toxoplasmosis in solid-organ transplant recipients: a matched case-control study. *Clin. Infect. Dis.* **54**, 355–361 (2012).

35. F. Derouin, H. Pelloux, ESCMID Study Group on Clinical Parasitology, Prevention of toxoplasmosis in transplant patients. *Clin. Microbiol. Infect.* **14**, 1089–1101 (2008).

36. F. Derouin, D. Vittecoq, B. Beauvais, A. Bussel, Toxoplasma parasitaemia associated with serological reactivation of chronic toxoplasmosis in a patient with the acquired immunodeficiency syndrome. *J. Infect.* **14**, 189–190 (1987).

37. C. Ozgonul, C. G. Besirli, Recent developments in the diagnosis and treatment of ocular toxoplasmosis. *Ophthalmic Res*. **57**, 1–12 (2017).

38. G. M. Bhopale, Pathogenesis of toxoplasmosis. *Comp Immunol Microbiol Infect Dis*. **26**, 213–222 (2003).

39. A. B. Sabin, J. Warren, Therapeutic effectiveness of certain sulfonamides on infection by an intracellular protozoon (toxoplasma). *Exp. Biol. Med.* **51**, 19–23 (1942).

40. D. E. Eyles, N. Coleman, Synergistic Effect of Sulfadiazlne and Daraprim against Experimental Toxoplasmosis in the Mouse. *Antibiotics & Chemotherapy* (1953).

41. M. E. Fichera, M. K. Bhopale, D. S. Roos, In vitro assays elucidate peculiar kinetics of clindamycin action against Toxoplasma gondii. *Antimicrob. Agents Chemother*. **39**, 1530–1537 (1995).

42. J. P. Dubey, C. Sreekumar, Redescription of Hammondia hammondi and its differentiation from Toxoplasma gondii. *Int. J. Parasitol.* **33**, 1437–1453 (2003).

43. H. Lorenzi *et al.*, Local admixture of amplified and diversified secreted pathogenesis determinants shapes mosaic Toxoplasma gondii genomes. *Nat. Commun.* **7**, 10147 (2016).

44. S. L. Sokol *et al.*, Dissection of the in vitro developmental program of Hammondia hammondi reveals a link between stress sensitivity and life cycle flexibility in Toxoplasma gondii. *Elife*. **7** (2018), doi:10.7554/eLife.36491.

45. R. W. Mason, The detection of Hammondia hammondi in Australia and the identification of a free-living intermediate host. *Z. Parasitenkd.* **57**, 101–106 (1978).

46. R. Entzeroth, E. Scholtyseck, The roe deer intermediate host of different Coccidia. N*aturwissenschaften.* 6**5,** 395 (1978).

47. K. Shimura, S. Ito, Goats as natural intermediate hosts of Hammondia hammondi. *Zentralblatt für Bakteriologie, Mikrobiologie und Hygiene. Series A: Medical Microbiology, Infectious Diseases, Virology, Parasitology*. **264**, 348–352 (1987).

48. J. P. Dubey, M. Wong, Experimental Hammondia hammondi infection in monkeys. *J. Parasitol.* **64**, 551–552 (1978).

49. J. P. Dubey, Experimental hammondia hammondi infection in dogs. *British Veterinary Journal*. **131**, 741–743 (1975).

50. G. D. Wallace, Observations on a feline coccidium with some characteristics of Toxoplasma and Sarcocystis. *Z. Parasitenkd.* **46**, 167–178 (1975).

51. J. P. Dubey, R. H. Streitel, Further Studies on the Transmission of Hammondia hammondi in Cats. *J. Parasitol.* **62**, 548 (1976).

52. G. Schares *et al.*, Seasonality in the proportions of domestic cats shedding Toxoplasma gondii or Hammondia hammondi oocysts is associated with climatic factors. *Int. J. Parasitol.* **46**, 263–273 (2016).

53. A. O. Heydorn, H. Mehlhorn, Further remarks on Hammondia hammondi and the taxonomic importance of obligate heteroxeny. *Parasitol. Res.* **87**, 573–577 (2001).

54. N. D. Levine, Tazonomy of Toxoplasma. *J Protozool*. **24**, 36–41 (1977).

55. H. G. Sheffield, M. L. Melton, F. A. Neva, Development of Hammondia hammondi in cell cultures. *Proc. Helminthol. Soc. Wash.* (1976).

56. H. Riahi, M. J. Leboutet, F. Labrousse, B. Bouteille, M. L. Dardé, Monoclonal antibodies to Hammondia hammondi allowing immunological differentiation from Toxoplasma gondii. *J. Parasitol.* **86**, 1362–1366 (2000).

57. E. Christie, J. P. Dubey, Cross-immunity between Hammondia and Toxoplasma infections in mice and hamsters. *Infect. Immun.* **18**, 412–415 (1977).

58. G. Weiland, M. Rommel, F. von Seyerl, Serological cross-reactions between toxoplasma and hammondia. *Zentralbl. Bakteriol. Orig. A.* **244**, 391–393 (1979).

59. F. G. Araujo, J. P. Dubey, J. S. Remington, Antigenic similarity between the coccidian parasites Toxoplasma gondii and Hammondia hammondi. *J Protozool*. **31**, 145–147 (1984).

60. H. Riahi, B. Bouteille, M. L. Darde, Antigenic similarity between Hammondia hammondi and Toxoplasma gondii tachyzoites. *J. Parasitol.* **84**, 651–653 (1998).

61. H. Riahi, M. J. Leboutet, B. Bouteille, J. F. Dubremetz, M. L. Dardé, Hammondia hammondi organelle proteins are recognized by monoclonal antibodies directed against organelles of Toxoplasma gondii. *J. Parasitol.* **85**, 580–583 (1999).

62. G. Schares *et al.*, A real-time quantitative polymerase chain reaction for the specific detection of Hammondia hammondi and its differentiation from Toxoplasma gondii. *Parasit. Vectors*. **14**, 78 (2021).

63. C. Sreekumar *et al.*, Differential detection of Hammondia hammondi from Toxoplasma gondii using polymerase chain reaction. *Parasitol. Int.* **54**, 267–269 (2005).

64. A. Rostami, P. Karanis, S. Fallahi, Advances in serological, imaging techniques and molecular diagnosis of Toxoplasma gondii infection. *Infection*. **46**, 303–315 (2018).

65. H. Riahi, M. L. Dardé, B. Bouteille, M. J. Leboutet, M. Pestre-Alexandre, Hammondia hammondi cysts in cell cultures. *J. Parasitol.* **81**, 821–824 (1995).

66. C. Su *et al.*, Recent expansion of Toxoplasma through enhanced oral transmission. *Science*. **299**, 414–416 (2003).

67. J. T. Ellis *et al.*, The genus Hammondia is paraphyletic. *Parasitology*. **118 (Pt 4)**, 357–362 (1999).

68. K. A. Walzer *et al.*, Hammondia hammondi, an avirulent relative of Toxoplasma gondii, has functional orthologs of known T. gondii virulence genes. *Proc. Natl. Acad. Sci. USA*. **110**, 7446–7451 (2013).

69. J. P. J. Saeij *et al.*, Polymorphic secreted kinases are key virulence factors in toxoplasmosis. *Science*. **314**, 1780–1783 (2006).

70. C. A. Hunter, L. D. Sibley, Modulation of innate immunity by Toxoplasma gondii virulence effectors. *Nat. Rev. Microbiol.* **10**, 766–778 (2012).

71. E. E. Rosowski *et al.*, Strain-specific activation of the NF-kappaB pathway by GRA15, a novel Toxoplasma gondii dense granule protein. *J. Exp. Med.* **208**, 195–212 (2011).

72. K. A. Walzer *et al.*, Hammondia hammondi harbors functional orthologs of the host-modulating effectors GRA15 and ROP16 but is distinguished from Toxoplasma gondii by a unique transcriptional profile. *Eukaryotic Cell*. **13**, 1507–1518 (2014).

73. J. Sharma, P. Rodriguez, P. Roy, P. S. Guiton, Transcriptional ups and downs: patterns of gene expression in the life cycle of Toxoplasma gondii. *Microbes Infect.* (2020), doi:10.1016/j.micinf.2020.09.001.

74. L. Jacobs, J. S. Remington, M. L. Melton, The resistance of the encysted form of Toxoplasma gondii. *J. Parasitol.* **46**, 11–21 (1960).

75. K. E. McGovern, C. M. Cabral, H. W. Morrison, A. A. Koshy, Aging with Toxoplasma gondii results in pathogen clearance, resolution of inflammation, and minimal consequences to learning and memory. *Sci. Rep.* **10**, 7979 (2020).

76. V. Jeffers, Z. Tampaki, K. Kim, W. J. Sullivan, A latent ability to persist: differentiation in Toxoplasma gondii. *Cell Mol. Life Sci.* **75**, 2355–2373 (2018).

77. S. Skariah, M. K. McIntyre, D. G. Mordue, Toxoplasma gondii: determinants of tachyzoite to bradyzoite conversion. *Parasitol. Res.* **107**, 253–260 (2010).

78. D. S. Lindsay, J. P. Dubey, B. L. Blagburn, M. Toivio-Kinnucan, Examination of tissue cyst formation by Toxoplasma gondii in cell cultures using bradyzoites, tachyzoites, and sporozoites. *J. Parasitol.* **77**, 126–132 (1991).

79. D. S. Lindsay, M. A. Toivio-Kinnucan, B. L. Blagburn, Ultrastructural Determination of Cystogenesis by Various Toxoplasma gondii Isolates in Cell Culture. *J. Parasitol.* **79**, 289 (1993).

80. M. E. Jerome, J. R. Radke, W. Bohne, D. S. Roos, M. W. White, Toxoplasma gondii bradyzoites form spontaneously during sporozoite-initiated development. *Infect. Immun.* **66**, 4838–4844 (1998).

81. M. da F. Ferreira-da-Silva, A. C. Takács, H. S. Barbosa, U. Gross, C. G. K. Lüder, Primary skeletal muscle cells trigger spontaneous Toxoplasma gondii tachyzoite-to-bradyzoite conversion at higher rates than fibroblasts. *Int. J. Med. Microbiol.* **299**, 381–388 (2009).

82. I. J. Swierzy, C. G. K. Lüder, Withdrawal of skeletal muscle cells from cell cycle progression triggers differentiation of Toxoplasma gondii towards the bradyzoite stage. *Cell Microbiol.* **17**, 2–17 (2015).

83. J. R. Radke *et al.*, Changes in the expression of human cell division autoantigen-1 influence Toxoplasma gondii growth and development. *PLoS Pathog.* **2**, e105 (2006).

84. Z. Chai, B. Sarcevic, A. Mawson, B. H. Toh, SET-related cell division autoantigen-1 (CDA1) arrests cell growth. *J. Biol. Chem.* **276**, 33665–33674 (2001).

85. C. G. Lüder, M. Giraldo-Velásquez, M. Sendtner, U. Gross, Toxoplasma gondii in primary rat CNS cells: differential contribution of neurons, astrocytes, and microglial cells for the intracerebral development and stage differentiation. *Exp Parasitol*. **93**, 23–32 (1999).

86. N. Tanaka, D. Ashour, E. Dratz, S. Halonen, Use of human induced pluripotent stem cell-derived neurons as a model for Cerebral Toxoplasmosis. *Microbes Infect.* **18**, 496–504 (2016).

87. C. G. K. Lüder, T. Rahman, Impact of the host on Toxoplasma stage differentiation. *Microb. Cell*. **4**, 203–211 (2017).

88. M. Soête, D. Camus, J. F. Dubremetz, Experimental induction of bradyzoite-specific antigen expression and cyst formation by the RH strain of Toxoplasma gondii in vitro. *Exp Parasitol.* **78**, 361–370 (1994).

89. L. M. Weiss, Y. F. Ma, P. M. Takvorian, H. B. Tanowitz, M. Wittner, Bradyzoite development in Toxoplasma gondii and the hsp70 stress response. *Infect. Immun.* **66**, 3295–3302 (1998).

90. C. Tobin, A. Pollard, L. Knoll, Toxoplasma gondii cyst wall formation in activated bone marrow-derived macrophages and bradyzoite conditions. *J. Vis. Exp.* (2010), doi:10.3791/2091.

91. Y. W. Zhang, S. K. Halonen, Y. F. Ma, M. Wittner, L. M. Weiss, Initial characterization of CST1, a Toxoplasma gondii cyst wall glycoprotein. *Infect. Immun.* **69**, 501–507 (2001).

92. A. C. Taylor, Responses of cells to pH changes in the medium. *J. Cell Biol.* **15**, 201–209 (1962).

93. A. Lardner, The effects of extracellular pH on immune function. *J. Leukoc. Biol.* (2001).

94. R. L. Mahnensmith, P. S. Aronson, The plasma membrane sodium-hydrogen exchanger and its role in physiological and pathophysiological processes. *Circ. Res.* **56**, 773–788 (1985).

95. L. M. Weiss *et al.*, A cell culture system for study of the development of Toxoplasma gondii bradyzoites. *J Eukaryot Microbiol*. **42**, 150–157 (1995).

96. B. R. Joyce, Z. Tampaki, K. Kim, R. C. Wek, W. J. Sullivan, The unfolded protein response in the protozoan parasite Toxoplasma gondii features translational and transcriptional control. *Eukaryotic Cell*. **12**, 979–989 (2013).

97. W. Bohne, D. S. Roos, Stage-specific expression of a selectable marker in Toxoplasma gondii permits selective inhibition of either tachyzoites or bradyzoites. *Mol. Biochem. Parasitol.* **88**, 115–126 (1997).

98. B. A. Fox, J. P. Gigley, D. J. Bzik, Toxoplasma gondii lacks the enzymes required for de novo arginine biosynthesis and arginine starvation triggers cyst formation. *Int. J. Parasitol.* **34**, 323–331 (2004).

99. F. Ihara, Y. Nishikawa, Starvation of low-density lipoprotein-derived cholesterol induces bradyzoite conversion in Toxoplasma gondii. *Parasit. Vectors*. **7**, 248 (2014).

100. W. Bohne, J. Heesemann, U. Gross, Reduced replication of Toxoplasma gondii is necessary for induction of bradyzoite-specific antigens: a possible role for nitric oxide in triggering stage conversion. *Infect. Immun.* **62**, 1761–1767 (1994).

101. Y. Suzuki, F. K. Conley, J. S. Remington, Importance of endogenous IFN-gamma for prevention of toxoplasmic encephalitis in mice. *J. Immunol.* **143**, 2045–2050 (1989).

102. W. Bohne, J. Heesemann, U. Gross, Induction of bradyzoite-specific Toxoplasma gondii antigens in gamma interferon-treated mouse macrophages. *Infect. Immun.* **61**, 1141–1145 (1993).

103. Y. Suzuki, M. A. Orellana, R. D. Schreiber, J. S. Remington, Interferon-gamma: the major mediator of resistance against Toxoplasma gondii. *Science*. **240**, 516–518 (1988).

104. R. S. Coombs *et al.*, Immediate interferon gamma induction determines murine host compatibility differences between Toxoplasma gondii and Neospora caninum. *Infect. Immun.* (2020), doi:10.1128/IAI.00027-20.

105. G. S. Yap, T. Scharton-Kersten, H. Charest, A. Sher, Decreased resistance of TNF receptor p55- and p75-deficient mice to chronic toxoplasmosis despite normal activation of inducible nitric oxide synthase in vivo. *J. Immunol.* **160**, 1340–1345 (1998).

106. T. M. Scharton-Kersten, G. Yap, J. Magram, A. Sher, Inducible nitric oxide is essential for host control of persistent but not acute infection with the intracellular pathogen Toxoplasma gondii. *J. Exp. Med.* **185**, 1261–1273 (1997).

107. R. Gazzinelli, Y. Xu, S. Hieny, A. Cheever, A. Sher, Simultaneous depletion of CD4+ and CD8+ T lymphocytes is required to reactivace chronich infection with *Toxoplasma gondii* . *J. Immunol.* (1992).

108. L. A. Kirkman, L. M. Weiss, K. Kim, Cyclic nucleotide signaling in Toxoplasma gondii bradyzoite differentiation. *Infect. Immun.* **69**, 148–153 (2001).

109. A. Hartmann *et al.*, Optogenetic modulation of an adenylate cyclase in Toxoplasma gondii demonstrates a requirement of the parasite cAMP for host-cell invasion and stage differentiation. *J. Biol. Chem.* **288**, 13705–13717 (2013).

110. M. S. Eaton, L. M. Weiss, K. Kim, Cyclic nucleotide kinases and tachyzoite-bradyzoite transition in Toxoplasma gondii. *Int. J. Parasitol.* **36**, 107–114 (2006).

111. P. Sassone-Corsi, The cyclic AMP pathway. *Cold Spring Harb. Perspect. Biol.* **4** (2012), doi:10.1101/cshperspect.a011148.

112. T. Sugi *et al.*, Toxoplasma gondii Cyclic AMP-Dependent Protein Kinase Subunit 3 Is Involved in the Switch from Tachyzoite to Bradyzoite Development. *MBio*. **7** (2016), doi:10.1128/mBio.00755-16.

113. C. Gomez, M. Esther Ramirez, M. Calixto-Galvez, O. Medel, M. A. Rodríguez, Regulation of gene expression in protozoa parasites. *J. Biomed. Biotechnol.* **2010**, 726045 (2010).

114. L.-F. Chen *et al.*, Comparative studies of Toxoplasma gondii transcriptomes: insights into stage conversion based on gene expression profiling and alternative splicing. *Parasit. Vectors*. **11**, 402 (2018).

115. N. Saksouk *et al.*, Histone-modifying complexes regulate gene expression pertinent to the differentiation of the protozoan parasite Toxoplasma gondii. *Mol. Cell. Biol.* **25**, 10301–10314 (2005).

116. A. Bougdour *et al.*, Drug inhibition of HDAC3 and epigenetic control of differentiation in Apicomplexa parasites. *J. Exp. Med.* **206**, 953–966 (2009).

117. D. C. Farhat *et al.*, A MORC-driven transcriptional switch controls Toxoplasma developmental trajectories and sexual commitment. *Nat. Microbiol.* **5**, 570–583 (2020).

118. S. Srivastava, M. W. White, W. J. Sullivan, Toxoplasma gondii AP2XII-2 Contributes to Proper Progression through S-Phase of the Cell Cycle. *mSphere*. **5** (2020), doi:10.1128/mSphere.00542-20.

119. A. Naguleswaran, E. V. Elias, J. McClintick, H. J. Edenberg, W. J. Sullivan, Toxoplasma gondii lysine acetyltransferase GCN5-A functions in the cellular response to alkaline stress and expression of cyst genes. *PLoS Pathog.* **6**, e1001232 (2010).

120. W. J. Sullivan *et al.*, Molecular cloning and characterization of an SRCAP chromatin remodeling homologue in Toxoplasma gondii. *Parasitol. Res.* **90**, 1–8 (2003).

121. M. P. J. Craver, P. J. Rooney, L. J. Knoll, Isolation of Toxoplasma gondii development mutants identifies a potential proteophosphogylcan that enhances cyst wall formation. *Mol. Biochem. Parasitol.* **169**, 120–123 (2010).

122. P. J. Rooney, L. M. Neal, L. J. Knoll, Involvement of a Toxoplasma gondii chromatin remodeling complex ortholog in developmental regulation. *PLoS One*. **6**, e19570 (2011).

123. M. C. Dalmasso, D. O. Onyango, A. Naguleswaran, W. J. Sullivan, S. O. Angel, Toxoplasma H2A variants reveal novel insights into nucleosome composition and functions for this histone family. *J. Mol. Biol.* **392**, 33–47 (2009).

124. S. Balaji, M. M. Babu, L. M. Iyer, L. Aravind, Discovery of the principal specific transcription factors of Apicomplexa and their implication for the evolution of the AP2-integrase DNA binding domains. *Nucleic Acids Res.* **33**, 3994–4006 (2005).

125. H. J. Painter, T. L. Campbell, M. Llinás, The Apicomplexan AP2 family: integral factors regulating Plasmodium development. *Mol. Biochem. Parasitol.* **176**, 1–7 (2011).

126. B. Gajria *et al.*, ToxoDB: an integrated Toxoplasma gondii database resource. *Nucleic Acids Res.* **36**, D553–6 (2008).

127. J. B. Radke *et al.*, ApiAP2 transcription factor restricts development of the Toxoplasma tissue cyst. *Proc. Natl. Acad. Sci. USA.* **110**, 6871–6876 (2013).

128. D.-P. Hong, J. B. Radke, M. W. White, Opposing transcriptional mechanisms regulate toxoplasma development. *mSphere*. **2** (2017), doi:10.1128/mSphere.00347-16.

129. J. B. Radke *et al.*, Transcriptional repression by ApiAP2 factors is central to chronic toxoplasmosis. *PLoS Pathog.* **14**, e1007035 (2018).

130. S. Huang *et al.*, Toxoplasma gondii AP2IX-4 Regulates Gene Expression during Bradyzoite Development. *mSphere*. **2** (2017), doi:10.1128/mSphere.00054-17.

131. R. Walker *et al.*, The Toxoplasma nuclear factor TgAP2XI-4 controls bradyzoite gene expression and cyst formation. *Mol. Microbiol.* **87**, 641–655 (2013).

132. B. S. Waldman *et al.*, Identification of a master regulator of differentiation in toxoplasma. *Cell*. **180**, 359–372.e16 (2020).

133. D. J. P. Ferguson, S. F. Parmley, S. Tomavo, Evidence for nuclear localisation of two stage-specific isoenzymes of enolase in Toxoplasma gondii correlates with active parasite replication. *Int. J. Parasitol.* **32**, 1399–1410 (2002).

134. M. K. Kibe *et al.*, Transcriptional regulation of two stage-specifically expressed genes in the protozoan parasite Toxoplasma gondii. *Nucleic Acids Res.* **33**, 1722–1736 (2005).

135. J. Narasimhan *et al.*, Translation regulation by eukaryotic initiation factor-2 kinases in the development of latent cysts in Toxoplasma gondii. *J. Biol. Chem.* **283**, 16591–16601 (2008).

136. W. J. Sullivan, J. Narasimhan, M. M. Bhatti, R. C. Wek, Parasite-specific eIF2 (eukaryotic initiation factor-2) kinase required for stress-induced translation control. *Biochem. J.* **380**, 523–531 (2004).

137. L. Augusto, J. Martynowicz, K. A. Staschke, R. C. Wek, W. J. Sullivan, Effects of PERK eIF2α Kinase Inhibitor against Toxoplasma gondii. *Antimicrob. Agents Chemother.* **62** (2018), doi:10.1128/AAC.01442-18.

138. M. Gissot *et al.*, Toxoplasma gondii Alba proteins are involved in translational control of gene expression. *J. Mol. Biol.* **425**, 1287–1301 (2013).

139. U. Singh, J. L. Brewer, J. C. Boothroyd, Genetic analysis of tachyzoite to bradyzoite differentiation mutants in Toxoplasma gondii reveals a hierarchy of gene induction. *Mol. Microbiol.* **44**, 721–733 (2002).

140. C. Odberg-Ferragut *et al.*, Molecular cloning of the Toxoplasma gondii sag4 gene encoding an 18 kDa bradyzoite specific surface protein. *Mol. Biochem. Parasitol.* **82**, 237–244 (1996).

141. S.-K. Kim, A. Karasov, J. C. Boothroyd, Bradyzoite-specific surface antigen SRS9 plays a role in maintaining Toxoplasma gondii persistence in the brain and in host control of parasite replication in the intestine. *Infect. Immun.* **75**, 1626–1634 (2007).

142. M. D. Cleary, U. Singh, I. J. Blader, J. L. Brewer, J. C. Boothroyd, Toxoplasma gondii asexual development: identification of developmentally regulated genes and distinct patterns of gene expression. *Eukaryotic Cell*. **1**, 329–340 (2002).

143. T. Tomita *et al.*, The Toxoplasma gondii cyst wall protein CST1 is critical for cyst wall integrity and promotes bradyzoite persistence. *PLoS Pathog.* **9**, e1003823 (2013).

144. S. F. Parmley *et al.*, Molecular characterization of a 65-kilodalton Toxoplasma gondii antigen expressed abundantly in the matrix of tissue cysts. *Mol. Biochem. Parasitol.* **66**, 283–296 (1994).

145. K. R. Buchholz, P. W. Bowyer, J. C. Boothroyd, Bradyzoite pseudokinase 1 is crucial for efficient oral infectivity of the Toxoplasma gondii tissue cyst. *Eukaryotic Cell*. **12**, 399–410 (2013).

146. W. Bohne, U. Gross, D. J. Ferguson, J. Heesemann, Cloning and characterization of a bradyzoite-specifically expressed gene (hsp30/bag1) of Toxoplasma gondii, related to genes encoding small heat-shock proteins of plants. *Mol. Microbiol.* **16**, 1221–1230 (1995).

147. C. Toursel, F. Dzierszinski, A. Bernigaud, M. Mortuaire, S. Tomavo, Molecular cloning, organellar targeting and developmental expression of mitochondrial chaperone HSP60 in Toxoplasma gondii. *Mol. Biochem. Parasitol.* **111**, 319–332 (2000).

148. S. Yang, S. F. Parmley, Toxoplasma gondii expresses two distinct lactate dehydrogenase homologous genes during its life cycle in intermediate hosts. *Gene*. **184**, 1–12 (1997).

149. F. Dzierszinski, M. Mortuaire, N. Dendouga, O. Popescu, S. Tomavo, Differential expression of two plant-like enolases with distinct enzymatic and antigenic properties during stage conversion of the protozoan parasite Toxoplasma gondii. *J. Mol. Biol.* **309**, 1017–1027 (2001).

150. T. Sugi, V. Tu, Y. Ma, T. Tomita, L. M. Weiss, Toxoplasma gondii Requires Glycogen Phosphorylase for Balancing Amylopectin Storage and for Efficient Production of Brain Cysts. *MBio*. **8** (2017), doi:10.1128/mBio.01289-17.

151. J. P. Dubey, *Toxoplasmosis Of Animals And Humans* (Crc Press, Boca Raton, ed. 2, 2010).

152. G. Pappas, N. Roussos, M. E. Falagas, Toxoplasmosis snapshots: global status of Toxoplasma gondii seroprevalence and implications for pregnancy and congenital toxoplasmosis. *Int. J. Parasitol.* **39**, 1385–1394 (2009).

153. J. L. Jones *et al.*, Toxoplasma gondii infection in the United States: seroprevalence and risk factors. *Am. J. Epidemiol.* **154**, 357–365 (2001).

154. B. J. Luft *et al.*, Toxoplasmic encephalitis in patients with the acquired immunodeficiency syndrome. Members of the ACTG 077p/ANRS 009 Study Team. *N. Engl. J. Med.* **329**, 995–1000 (1993).

155. B. Carme *et al.*, Severe acquired toxoplasmosis in immunocompetent adult patients in French Guiana. *J. Clin. Microbiol.* **40**, 4037–4044 (2002).

156. J. S. Remington, *Infectiousdiseases of the fetus and newborn infant* (Saunders, Philadelphia, ed. 5th, 2001).

157. M. E. Grigg, J. Ganatra, J. C. Boothroyd, T. P. Margolis, Unusual abundance of atypical strains associated with human ocular toxoplasmosis. *J. Infect. Dis.* **184**, 633–639 (2001).

158. P. Marty *et al.*, Lethal congenital toxoplasmosis resulting from reactivation of toxoplasmosis in a pregnant HIV-positive patient. *Presse Med.* **31**, 1558 (2002).

159. Y. Takashima *et al.*, Detection of the initial site of Toxoplasma gondii reactivation in brain tissue. *Int. J. Parasitol.* **38**, 601–607 (2008).

160. M. M. Conde de Felipe, M. M. Lehmann, M. E. Jerome, M. W. White, Inhibition of Toxoplasma gondii growth by pyrrolidine dithiocarbamate is cell cycle specific and leads to population synchronization. *Mol. Biochem. Parasitol.* **157**, 22–31 (2008).

161. R. Muller, J. R. Baker, *Advances in Parasitology* (New York Academic Press, New York, 1982).

162. J. P. Dubey, Oocyst shedding by cats fed isolated bradyzoites and comparison of infectivity of bradyzoites of the VEG strain Toxoplasma gondii to cats and mice. *J. Parasitol.* **87**, 215–219 (2001).

163. C. A. Speer, J. P. Dubey, J. A. Blixt, K. Prokop, Time lapse video microscopy and ultrastructure of penetrating sporozoites, types 1 and 2 parasitophorous vacuoles, and the transformation of sporozoites to tachyzoites of the VEG strain of Toxoplasma gondii. *J. Parasitol.* **83**, 565–574 (1997).

164. J. P. Dubey *et al.*, Molecular and biological characterization of first isolates of Hammondia hammondi from cats from Ethiopia. *J. Parasitol.* **99**, 614–618 (2013).

165. J. P. J. Saeij, J. P. Boyle, M. E. Grigg, G. Arrizabalaga, J. C. Boothroyd, Bioluminescence imaging of Toxoplasma gondii infection in living mice reveals dramatic differences between strains. *Infect. Immun.* **73**, 695–702 (2005).

166. M. M. Croken *et al.*, Distinct strains of Toxoplasma gondii feature divergent transcriptomes regardless of developmental stage. *PLoS One*. **9**, e111297 (2014).

167. T. C. Paredes-Santos *et al.*, Spontaneous cystogenesis in vitro of a Brazilian strain of Toxoplasma gondii. *Parasitol. Int.* **62**, 181–188 (2013).

168. A. Subramanian *et al.*, Gene set enrichment analysis: a knowledge-based approach for interpreting genome-wide expression profiles. *Proc. Natl. Acad. Sci. USA.* **102**, 15545–15550 (2005).

169. M. M. Croken, W. Qiu, M. W. White, K. Kim, Gene Set Enrichment Analysis (GSEA) of Toxoplasma gondii expression datasets links cell cycle progression and the bradyzoite developmental program. *BMC Genomics*. **15**, 515 (2014).

170. M. S. Behnke, T. P. Zhang, J. P. Dubey, L. D. Sibley, Toxoplasma gondii merozoite gene expression analysis with comparison to the life cycle discloses a unique expression state during enteric development. *BMC Genomics*. **15**, 350 (2014).

171. J. P. Boyle, J. P. J. Saeij, S. Y. Harada, J. W. Ajioka, J. C. Boothroyd, Expression quantitative trait locus mapping of toxoplasma genes reveals multiple mechanisms for strain-specific differences in gene expression. *Eukaryotic Cell*. **7**, 1403–1414 (2008).

172. B. Shen, K. M. Brown, T. D. Lee, L. D. Sibley, Efficient gene disruption in diverse strains of Toxoplasma gondii using CRISPR/CAS9. *MBio*. **5**, e01114–14 (2014).

173. K. Kim, L. M. Weiss, Toxoplasma gondii: the model apicomplexan. *Int. J. Parasitol.* **34**, 423–432 (2004).

174. J. R. Radke, M. N. Guerini, M. Jerome, M. W. White, A change in the premitotic period of the cell cycle is associated with bradyzoite differentiation in Toxoplasma gondii. *Mol. Biochem. Parasitol.* **131**, 119–127 (2003).

175. R. E. Lyons, R. McLeod, C. W. Roberts, Toxoplasma gondii tachyzoite-bradyzoite interconversion. *Trends Parasitol.* **18**, 198–201 (2002).

176. P. Olias, L. D. Sibley, Functional Analysis of the Role of Toxoplasma gondii Nucleoside Triphosphate Hydrolases I and II in Acute Mouse Virulence and Immune Suppression. *Infect. Immun.* **84**, 1994–2001 (2016).

177. M.-A. Hakimi, P. Olias, L. D. Sibley, Toxoplasma effectors targeting host signaling and transcription. *Clin. Microbiol. Rev.* **30**, 615–645 (2017).

178. P. Olias, R. D. Etheridge, Y. Zhang, M. J. Holtzman, L. D. Sibley, Toxoplasma Effector Recruits the Mi-2/NuRD Complex to Repress STAT1 Transcription and Block IFN-γ-Dependent Gene Expression. *Cell Host Microbe*. **20**, 72–82 (2016).

179. G. Gay *et al.*, Toxoplasma gondii TgIST co-opts host chromatin repressors dampening STAT1-dependent gene regulation and IFN-γ-mediated host defenses. *J. Exp. Med.* **213**, 1779–1798 (2016).

180. S.-K. Kim, A. E. Fouts, J. C. Boothroyd, Toxoplasma gondii dysregulates IFN-gamma-inducible gene expression in human fibroblasts: insights from a genome-wide transcriptional profiling. *J. Immunol.* **178**, 5154–5165 (2007).

181. V. Tu, R. Yakubu, L. M. Weiss, Observations on bradyzoite biology. *Microbes Infect.* (2017), doi:10.1016/j.micinf.2017.12.003.

182. P. H. Alday, J. S. Doggett, Drugs in development for toxoplasmosis: advances, challenges, and current status. *Drug Des. Devel. Ther.* **11**, 273–293 (2017).

183. R. H. Powell, M. S. Behnke, WRN conditioned media is sufficient for in vitro propagation of intestinal organoids from large farm and small companion animals. *Biol. Open*. **6**, 698–705 (2017).

184. M. S. Behnke, J. B. Radke, A. T. Smith, W. J. Sullivan, M. W. White, The transcription of bradyzoite genes in Toxoplasma gondii is controlled by autonomous promoter elements. *Mol. Microbiol.* **68**, 1502–1518 (2008).

185. A. B. Hehl *et al.*, Asexual expansion of Toxoplasma gondii merozoites is distinct from tachyzoites and entails expression of non-overlapping gene families to attach, invade, and replicate within feline enterocytes. *BMC Genomics*. **16**, 66 (2015).

186. Z.-X. Wang *et al.*, Proteomic Differences between Developmental Stages of Toxoplasma gondii Revealed by iTRAQ-Based Quantitative Proteomics. *Front. Microbiol.* **8**, 985 (2017).

187. D. Xia *et al.*, The proteome of Toxoplasma gondii: integration with the genome provides novel insights into gene expression and annotation. *Genome Biol.* **9**, R116 (2008).

188. C. Konradt *et al.*, Endothelial cells are a replicative niche for entry of Toxoplasma gondii to the central nervous system. *Nat. Microbiol.* **1**, 16001 (2016).

189. H. Lambert, N. Hitziger, I. Dellacasa, M. Svensson, A. Barragan, Induction of dendritic cell migration upon Toxoplasma gondii infection potentiates parasite dissemination. *Cell Microbiol.* **8**, 1611–1623 (2006).

190. A. Sanecka, E.-M. Frickel, Use and abuse of dendritic cells by Toxoplasma gondii. *Virulence*. **3**, 678–689 (2012).

191. V. Jeffers *et al.*, TgPRELID, a Mitochondrial Protein Linked to Multidrug Resistance in the Parasite Toxoplasma gondii. *mSphere*. **2** (2017), doi:10.1128/mSphere.00229-16.

192. Y. Liao, G. K. Smyth, W. Shi, The Subread aligner: fast, accurate and scalable read mapping by seed-and-vote. *Nucleic Acids Res.* **41**, e108 (2013).

193. H. Varet, L. Brillet-Guéguen, J.-Y. Coppée, M.-A. Dillies, SARTools: A DESeq2- and EdgeR-Based R Pipeline for Comprehensive Differential Analysis of RNA-Seq Data. *PLoS One*. **11**, e0157022 (2016).

194. M. I. Love, W. Huber, S. Anders, Moderated estimation of fold change and' ' dispersion for RNA-seq data with DESeq2. *Genome Biol.* **15**, 550 (2014).

195. K. J. Livak, T. D. Schmittgen, Analysis of relative gene expression data using real-time quantitative PCR and the 2(-Delta Delta C(T)) Method. *Methods*. **25**, 402–408 (2001).

196. J. P. Boyle, X.-J. Wu, C. B. Shoemaker, T. P. Yoshino, Using RNA interference to manipulate endogenous gene expression in Schistosoma mansoni sporocysts. *Mol. Biochem. Parasitol.* **128**, 205–215 (2003).

197. J. R. Radke *et al.*, The transcriptome of Toxoplasma gondii. *BMC Biol.* **3**, 26 (2005).

198. S. Tanaka *et al.*, Transcriptome analysis of mouse brain infected with Toxoplasma gondii. *Infect. Immun.* **81**, 3609–3619 (2013).

199. K. R. Buchholz *et al.*, Identification of tissue cyst wall components by transcriptome analysis of in vivo and in vitro Toxoplasma gondii bradyzoites. *Eukaryotic Cell*. **10**, 1637–1647 (2011).

200. B. F. C. Kafsack *et al.*, A transcriptional switch underlies commitment to sexual development in malaria parasites. *Nature*. **507**, 248–252 (2014).

201. S. Kosugi *et al.*, Six classes of nuclear localization signals specific to different binding grooves of importin alpha. *J. Biol. Chem.* **284**, 478–485 (2009).

202. A. N. Nguyen Ba, A. Pogoutse, N. Provart, A. M. Moses, NLStradamus: a simple Hidden Markov Model for nuclear localization signal prediction. *BMC Bioinformatics*. **10**, 202 (2009).

203. S. M. Sidik *et al.*, A Genome-wide CRISPR Screen in Toxoplasma Identifies Essential Apicomplexan Genes. *Cell*. **166**, 1423–1435.e12 (2016).

204. B. Shen, K. Brown, S. Long, L. D. Sibley, Development of CRISPR/Cas9 for Efficient Genome Editing in Toxoplasma gondii. *Methods Mol. Biol.* **1498**, 79–103 (2017).

205. V. Tu *et al.*, Enrichment and Proteomic Characterization of the Cyst Wall from In Vitro Toxoplasma gondii Cysts. *MBio*. **10** (2019), doi:10.1128/mBio.00469-19.

206. M. S. Behnke, A. Khan, L. D. Sibley, Genetic mapping reveals that sinefungin resistance in Toxoplasma gondii is controlled by a putative amino acid transporter locus that can be used as a negative selectable marker. *Eukaryotic Cell*. **14**, 140–148 (2015).

207. S. Nicoll, S. Wright, S. W. Maley, S. Burns, D. Buxton, A mouse model of recrudescence of Toxoplasma gondii infection. *J. Med. Microbiol.* **46**, 263–266 (1997).

208. T. M. T. Hall, Multiple modes of RNA recognition by zinc finger proteins. *Curr. Opin. Struct. Biol.* **15**, 367–373 (2005).

209. M. Fu, P. J. Blackshear, RNA-binding proteins in immune regulation: a focus on CCCH zinc finger proteins. *Nat. Rev. Immunol.* **17**, 130–143 (2017).

210. W. S. Lai, E. Carballo, J. M. Thorn, E. A. Kennington, P. J. Blackshear, Interactions of CCCH zinc finger proteins with mRNA. Binding of tristetraprolin-related zinc finger proteins to Au-rich elements and destabilization of mRNA. *J. Biol. Chem.* **275**, 17827–17837 (2000).

211. Y. W. Zhang *et al.*, Disruption of the Toxoplasma gondii bradyzoite-specific gene BAG1 decreases in vivo cyst formation. *Mol. Microbiol.* **31**, 691–701 (1999).

212. A. E. Abdelbaset *et al.*, Lactate dehydrogenase in Toxoplasma gondii controls virulence, bradyzoite differentiation, and chronic infection. *PLoS One*. **12**, e0173745 (2017).

213. T. Tomita *et al.*, Toxoplasma gondii Matrix Antigen 1 Is a Secreted Immunomodulatory Effector. *MBio*. **12** (2021), doi:10.1128/mBio.00603-21.

214. W. K. Chew, M. J. Wah, S. Ambu, I. Segarra, Toxoplasma gondii: determination of the onset of chronic infection in mice and the in vitro reactivation of brain cysts. *Exp Parasitol*. **130**, 22–25 (2012).

215. C. E. Pavesio, M. L. Chiappino, P. Y. Setzer, B. A. Nichols, Toxoplasma gondii: differentiation and death of bradyzoites. *Parasitol. Res.* **78**, 1–9 (1992).

216. S. L. Sokol, S. Wong, J. P. Boyle, J. P. Dubey, in *Toxoplasma gondii: Methods and Protocols*, C. J. Tonkin, Ed. (2020), *Methods in Molecular Biology* .

217. E. Kamau *et al.*, A novel benzodioxole-containing inhibitor of Toxoplasma gondii growth alters the parasite cell cycle. *Antimicrob. Agents Chemother.* **55**, 5438–5451 (2011).

218. T. Hulsen, J. de Vlieg, W. Alkema, BioVenn – a web application for the comparison and visualization of biological lists using area-proportional Venn diagrams. *BMC Genomics*. **9**, 488 (2008).

219. Pacific Northwest National Laboratory, *Venn Diagram Plotter* .

220. A. I. Saeed *et al.*, TM4: a free, open-source system for microarray data management and analysis. *BioTechniques*. **34**, 374–378 (2003).

221. E. N. Rudzki *et al.*, Toxoplasma gondii GRA28 is required for specific induction of the regulatory chemokine CCL22 in human and mouse cells. *BioRxiv*. **https://www.biorxiv.org/content/10.1101/2020.10.14.335802v1** (2020), doi:10.1101/2020.10.14.335802.

222. J. P. Boyle, J. P. J. Saeij, J. C. Boothroyd, Toxoplasma gondii: inconsistent dissemination patterns following oral infection in mice. *Exp Parasitol*. **116**, 302–305 (2007).

223. M. L. Blank, J. P. Boyle, Effector variation at tandem gene arrays in tissue-dwelling coccidia: who needs antigenic variation anyway? *Curr. Opin. Microbiol.* **46**, 86–92 (2018).

224. A. Espinosa-Cantú, D. Ascencio, F. Barona-Gómez, A. DeLuna, Gene duplication and the evolution of moonlighting proteins. *Front. Genet.* **6**, 227 (2015).

225. S. Magadum, U. Banerjee, P. Murugan, D. Gangapur, R. Ravikesavan, Gene duplication as a major force in evolution. *J Genet*. **92**, 155–161 (2013).

226. S. Ohno, *Evolution by gene duplication* (Allen & Unwin, London, 1970).

227. G. Schares, M. G. Vrhovec, N. Pantchev, D. C. Herrmann, F. J. Conraths, Occurrence of Toxoplasma gondii and Hammondia hammondi oocysts in the faeces of cats from Germany and other European countries. *Vet. Parasitol.* **152**, 34–45 (2008).

228. K. Zhang, G. Lin, Y. Han, J. Li, Serological diagnosis of toxoplasmosis and standardization. *Clin. Chim. Acta*. **461**, 83–89 (2016).

229. M. Koethe *et al.*, Prevalence of specific IgG-antibodies against Toxoplasma gondii in domestic turkeys determined by kinetic ELISA based on recombinant GRA7 and GRA8. *Vet. Parasitol.* **180**, 179–190 (2011).

230. J.-T. Kong, M. E. Grigg, L. Uyetake, S. Parmley, J. C. Boothroyd, Serotyping of Toxoplasma gondii infections in humans using synthetic peptides. *J. Infect. Dis.* **187**, 1484–1495 (2003).

231. N. Blanchard *et al.*, Immunodominant, protective response to the parasite Toxoplasma gondii requires antigen processing in the endoplasmic reticulum. *Nat. Immunol.* **9**, 937–944 (2008).

232. V. Feliu *et al.*, Location of the CD8 T cell epitope within the antigenic precursor determines immunogenicity and protection against the Toxoplasma gondii parasite. *PLoS Pathog.* **9**, e1003449 (2013).

233. H. B. Larman *et al.*, Autoantigen discovery with a synthetic human peptidome. *Nat. Biotechnol.* **29**, 535–541 (2011).

234. H. B. Larman *et al.*, PhIP-Seq characterization of autoantibodies from patients with multiple sclerosis, type 1 diabetes and rheumatoid arthritis. *J. Autoimmun.* **43**, 1–9 (2013).

235. Z. S. Wong, S. L. Sokol-Borrelli, P. Olias, J. P. Dubey, J. P. Boyle, Head-to-head comparisons of Toxoplasma gondii and its near relative Hammondia hammondi reveal dramatic differences in the host response and effectors with species-specific functions. *PLoS Pathog.* **16**, e1008528 (2020).

236. S. K. Matta *et al.*, Toxoplasma gondii effector TgIST blocks type I interferon signaling to promote infection. *Proc. Natl. Acad. Sci. USA.* **116**, 17480–17491 (2019).

237. A. Kröger, M. Köster, K. Schroeder, H. Hauser, P. P. Mueller, Activities of IRF-1. *J. Interferon Cytokine Res.* **22**, 5–14 (2002).